



Hydraulics Research
Wallingford

Hydraulic Performance of Breakwater
Crown Walls

A P Bradbury, N W H Allsop & R V Stephens

Report No SR 146
March 1988

**Registered Office: Hydraulics Research Limited,
Wallingford, Oxfordshire OX10 8BA.
Telephone: 0491 35381. Telex: 848552**

This report describes work funded jointly by the Department of the Environment and the Ministry of Agriculture Fisheries and Food.

The Department of the Environment contract number was PFCD 7/6/52 for which the nominated officer was Dr R P Thorogood.

The Ministry of Agriculture Fisheries and Food contribution was within the Research Commission (Marine Flooding) CSA 557 for which the nominated officer was Mr A J Allison.

The work was carried out in the Maritime Engineering Department of Hydraulics Research, Wallingford under the management of Dr S W Huntington.

The report is published on behalf of both DoE and MAFF, but any opinions expressed in this report are not necessarily those of the funding Departments.

© Crown copyright 1988

Published by permission of the Controller of Her Majesty's Stationery Office.

Hydraulic performance of breakwater crown walls

A P Bradbury, N W H Allsop & R V Stephens

Report SR 146, March 1988

Hydraulics Research, Wallingford

Abstract

A breakwater crown wall can increase the overall effectiveness of the structure in limiting wave overtopping. In so doing, it will contribute to a reduction in the volumes of material required and hence the cost to achieve a given level of performance. Current design methods are unreliable in their prediction of the effectiveness of different crown wall armour crest configurations in reducing overtopping. Similarly very little information is available to support the estimation of wave forces on the front face of the crown wall.

This study has addressed two of the major aspects of the design of breakwater crown walls: the efficiency with which such walls deal with wave overtopping; and the forces imparted to the front face of the crown wall.

This report draws together information from previous studies, together with results from a series of random wave model tests. The overtopping discharge and the impact force have been quantified for a range of wave conditions and crown wall configurations. The effects of the main wave and structure variables have been described by dimensionless parameters. Empirical formulae have been derived allowing the data presented to be used for design purposes for a wide range of conditions. A series of recommendations for good practice are made based upon the results of the review and model tests.

The results of this study will allow the designer of many configurations of crown wall to determine the overtopping performance, and to quantify the factor of safety against sliding failure, with a much higher level of certainty than hitherto.

CONTENTS

	Page
1 INTRODUCTION	1
1.1 Background	1
1.2 Outline of this study	1
1.3 Outline of this report	2
2 PERFORMANCE OF CROWN WALLS	3
2.1 Previous experience	3
2.2 Wave overtopping	4
2.3 Wave forces on crown walls	11
2.4 Physical modelling of crown wall stability	12
2.5 Summary of factors influencing crown wall performance	13
3 DESIGN OF MODEL TEST PROGRAMME	14
3.1 Aims of the model tests	14
3.2 Selection of model test parameters	14
4 TEST PROCEDURE AND MEASUREMENTS	16
4.1 Test facility	16
4.2 Wave calibration	17
4.3 Construction of model test section	17
4.4 Overtopping measurements	18
4.5 Pressure measurements	19
4.6 Force measurements	20
5 ANALYSIS OF RESULTS	22
5.1 Overtopping	22
5.1.1 Empirical relationships	22
5.1.2 Effectiveness of crest geometry	26
5.2 Forces	29
5.2.1 Analysis procedure for random wave tests	29
5.2.2 Results	30
5.2.3 Calculation of horizontal wave forces on the crown wall	33
6 RECOMMENDATIONS	34
6.1 Design calculations	34
6.1.1 Overtopping	34
6.1.2 Wave forces on a crown wall	34
6.1.3 Sliding	35
6.2 Recommendations for good practice	35

CONTENTS (CONT/D)

	Page
7	ACKNOWLEDGEMENTS
	36
8	REFERENCES
	37

TABLES

1. Test conditions
2. Test section construction
3. Summary of empirical coefficients for various crown wall configurations
4. Results of comparative wave loading

FIGURES

1. Geometry of breakwater cross sections
2. Overtopping of breakwater crown walls - after Gravesen & Sorensen
3. Deep random wave flume
4. Test section 1, 2, 3 and 14 (smooth slopes)
5. Test sections 4-7 & 11
6. Test sections 8,10,12, comparison of armour configuration at crest
7. Test section 13 - recurved wall
8. Force table
9. Test section 3 R^* vs $-\ln Q^*$
10. Test section 4 R^* vs $-\ln Q^*$
11. Test section 8 R^* vs $-\ln Q^*$
12. Test section 9 R^* vs $-\ln Q^*$
13. Test section 3 F' vs \bar{Q}
14. Test section 4 F' vs \bar{Q}
15. Test section 8 F' vs \bar{Q}
16. Test section 9 F' vs \bar{Q}
17. Test section 1 $-\ln F^*$ vs $-\ln O^*$
18. Test section 2 $-\ln F^*$ vs $-\ln Q^*$
19. Test section 3 $-\ln F^*$ vs $-\ln O^*$
20. Test section 4 $-\ln F^*$ vs $-\ln Q^*$
21. Test section 5 $-\ln F^*$ vs $-\ln O^*$
22. Test section 6 $-\ln F^*$ vs $-\ln Q^*$
23. Test section 7 $-\ln F^*$ vs $-\ln Q^*$
24. Test section 8 $-\ln F^*$ vs $-\ln Q^*$
25. Test section 9 $-\ln F^*$ vs $-\ln Q^*$
26. Test section 10 $-\ln F^*$ vs $-\ln Q^*$
27. Test section 11 $-\ln F^*$ vs $-\ln O^*$
28. Test section 12 $-\ln F^*$ vs $-\ln Q^*$
29. Test section 13 $-\ln F^*$ vs $-\ln Q^*$
30. Comparison of measured and predicted discharges
31. Example of force table output signals
32. Example of derived total force time series
33. Example of multiple threshold crossing with raw data
34. Influence of section geometry on impact ratio

CONTENTS (CONT/D)

FIGURES (CONT/D)

35. Influence of section geometry on impact ratio
36. Influence of section geometry on filtered 5% exceedence force
37. Influence of section geometry on filtered 5% exceedence force
38. Influence of section geometry on filtered maximum force
39. Influence of section geometry on filtered maximum force
40. Influence of T_m on filtered maximum force - constant H_s
41. Influence of T_m on impact ratio - constant H_s
42. Influence of H_s on filtered maximum force - constant T_m
43. Influence of H_s on impact ratio - constant T_m
44. Influence of T_m on filtered maximum force - constant s
45. Influence of T_m on impact ratio - constant s
46. Comparison between measured forces and those predicted
47. Measured forces presented in the form proposed by Jensen
48. Comparison between measured forces and predicted forces using Jensen's best fit line
49. Force data presented by Jensen (Ref 28)
50. Spatial distribution of maximum wave pressure on crownwall
- after Jensen

PLATES

1. Force table showing proof ring details

NOTATION

A, B	Empirical coefficients
a, b	"
A_c	Elevation of armour crest relative to static water level
B_c	Structure width, in direction normal to face, see Figure 1
C, C_1 , C_2 , C_i	Empirical or shape coefficients
C_r	Coefficient of reflection
d_p	Typical dimension of prototype structure
d_m	Typical dimension of model structure
D	Particle size or typical dimension
D_n	Nominal particle diameter
E	Elastic modulus
E_i	Incident wave energy
F_c	Projection of crown wall above armour crest, see Figure 1
F_H	Total depth-integrated horizontal force on crown wall per unit width
F_{H5}	Horizontal force exceeded by 5% of force peaks
F_{Hmax}	Maximum horizontal force
F^*	Dimensionless freeboard parameter, defined in Equation 5.4
G_c	Width of horizontal armour crest berm, see Figure 1
g	Gravitational acceleration
H	Wave height, from trough to crest
H_o	Offshore wave height, unaffected by shallow water processes
H_s	Significant wave height, average of highest one-third of wave heights
H_{max}	Maximum wave height in a record
h	Water depth
h_f	Height of front face of crown wall, over which wave forces may act
h_s	Water depth in front of structure
J	Geometric parameter, rear face, see Figure 1
Ir	Iribarren or surf similarity number
Ir'	Modified Iribarren number
IR	Ratio between wave impact period and mean wave period, T_{imp}/T_m
K	Geometric parameter, rear face, see Figure 1

K_D	Damage coefficient in Hudson formula
k	Wave number, $2\pi/L$, also armour layer packing coefficient
L	Wave length
L_o	Deep water or offshore wave length, $gT^2/2\pi$
L_p	Deep water wave length of peak wave period
L_{ps}	Wave length of peak period in water depth in front of structure
M	Armour unit mass
N_a	Number of armour units, on the slope, or in an area of the (test) section
N_d	Number of armour units displaced
N_r	Number of armour units rocking
N_w	Number of waves in a storm, record or test
n	Porosity, usually taken as n_v
n_v	Volumetric porosity, volume of voids expressed as proportion of total volume
n_a	Area porosity
Q	Overtopping discharge, per unit length of sea wall
Q^*	Dimensionless overtopping discharge, defined in equation 2.2
q_o	Volume of overtopping, per wave, per unit length of structure
q_s	Superficial velocity, or specific discharge, discharge per unit area, usually through a porous matrix
R	Run-up level, relative to static water level
\bar{R}	Mean run-up level
R_c	Crown wall freeboard, relative to static water level
R^*	Dimensionless freeboard, defined in Equation 2.3
R_s	Run-up level of significant wave
R_2	Run-up level exceeded by only 2% of run-up crests
R_{d98}	Run-down level, below which only 2% pass
r	Roughness value, usually relative to smooth slopes
S_i	Incident spectral energy density
S_r	Reflected spectral energy density
s	Wave steepness, H/L
s_m	Steepness of mean period $2\pi H_s/g T_m^2$
s_p	Steepness of peak period, $2\pi H_s/g T_p^2$
T	Wave period
T_m	Mean wave period

T_p	Spectral peak period, inverse of peak frequency
T_R	Duration of storm, sea state or test
T_{imp}	Mean period between wave impacts on crown walls
u, v	Flow velocities, often orthogonal components of velocity
α	Structure front slope angle
β	Angle of wave attack
ρ	Mass density, usually of fresh water
ρ_w	Mass density of sea water
ρ_r	Mass density of rock
ρ_c	Mass density of concrete
Δ	Relative density, $(\frac{\rho_c}{\rho_w} - 1)$
λ	Prototype to model ratio of a characteristic structural dimension

1 INTRODUCTION

1.1 Background

Rubble mound breakwaters or sea walls usually incorporate a crown or parapet wall to reduce the severity and limit the effects, of any waves overtopping the structure. This contributes to the overall effectiveness of a breakwater in reducing the transmission of wave energy, and of a sea wall in reducing erosion and flooding. By increasing the performance of the structure, a crown wall will allow a reduction in the volume of rubble required, and hence the cost, to achieve a given standard of protection. Crown walls are often also designed to carry and protect pipelines and other services from berths in the lee of the breakwater; to provide access along, and to the outer end of the structure; and to contain and direct any overtopping to avoid damage or flooding of vulnerable areas.

Two main uncertainties affect the design of a crown wall in the calculation of:

- a) the effect of the crown wall on wave overtopping;
- b) the forces applied to the wall.

Present design methods do not allow the description of wave-induced flow over the front face and at the crest of a rubble structure with acceptable certainty. The design of crown walls generally relies on the results of a few, site specific, hydraulic model studies; together with the local knowledge and experience of the designer. The consequence may be over-design and hence increased cost, or under-design with the attendant risk of failure. There have been many examples of damage to breakwater crown walls by storm action. In several instances this has contributed to the failure of lengths of the structure. Some notable examples of crown wall failure have been at Sines, Diablo Canyon, Arzew, Tripoli and Antalya. Despite these failures there has been very little research effort directed to the design of crown walls, and their response to wave flows and forces has been little understood.

1.2 Outline of this study

A study of wave overtopping and wave forces on crown walls was instituted as part of an overall programme of research on the design and performance of rubble mound structures. The study was conducted in three stages.

The literature available on hydraulic performance of crown walls and design practice was reviewed to identify the data and methods available, and the major areas of uncertainty. The results of this review were then used to set the parameters to be determined, design the model test procedures, and to identify possible empirical methods for the analysis of test results.

A comprehensive series of model tests were conducted in the large random wave flume at Hydraulics Research. A base test section with a 1:2 front slope was modified to give 13 different test sections. The main structural parameters to be varied were the crown wall height and freeboard, and the relative armour crest level. The tests were conducted at 2 different water levels using 10 wave conditions. During testing, measurements were made of wave overtopping discharges, wave pressures and wave forces on the front face of the wall. Video recordings were made of wave flows over the wall, and an attempt was made to quantify overtopping velocities using video image processing techniques.

The results of these measurements, and of the other studies reviewed, were then analysed to give appropriate design guidance. A number of empirical formulae were used to describe the data, and to allow the generalisation of the test results for use in design.

It may be useful to the reader concerned with the design and performance of rubble mound structures to note that the project, of which this study was a part, has also addressed:-

- a) the hydro-geotechnical performance of large rubble mounds (Ref 1);
- b) the design and performance of concrete armour units for coastal structures (Ref 2);
- c) the design, performance and durability of rock armour (Refs 3-5).

1.3 Outline of this report

This report may be considered in three parts. The review of information on the performance of crown walls in Chapter 2 draws together the results of site and laboratory experience to identify the main variables, and suggests possible design methods. The design and execution of model studies conducted in this project are reported in Chapters 3 and 4. The results of the test measurements are analysed and discussed in Chapter 5. Conclusions and

recommendations drawn from both the review and the model tests are described in Chapter 6.

2 PERFORMANCE OF CROWN WALLS

2.1 Previous experience

Much may be learnt of the performance of breakwater crown walls from examples of their failure. The principal modes of failure may be divided into two categories: functional and/or structural failure. Functional failure occurs when the breakwater, or the element considered, fails to perform its main task. A structural failure occurs when an element is broken, or significantly displaced, such that it no longer serves its original purpose.

At Diablo Canyon, California, the two breakwaters protecting the cooling water basin were armoured with large Tribars and surmounted by a very simple crown wall slab (Ref 6). During a storm peaking on 27-28 January 1981 the outer section of the west breakwater was severely damaged, and 4 of the 300 ton capping blocks slid into the sea. Model tests conducted to study the reasons for the failure suggest that the loss of the crown wall sections was precipitated by a local failure of the armour, followed by a progressive failure of armour up to the crown wall. Direct wave attack on the crown wall sections caused sufficient movement to release its weight from underlayer stone beneath. Continuing wave attack progressively removed the underlayer support, allowing the wall to fail in 8.7m long sections.

In December 1971 the new breakwater at Antalya harbour Turkey was very near completion, lacking only the placement of some rock armour behind the crown wall sections. A severe storm on 10-11 December led to the failure of the outer 600m of the breakwater. Gunbak & Ergin (Ref 7) describe details of the construction and damage. They describe calculations of wave force on the crown wall, and conclude that sliding of the 250 tonne crown wall sections was the primary failure mode. As at Diablo Canyon, the crown wall had been cast directly onto the 2-6 tonne underlayer, rather than onto the less permeable core material. In their calculations, Gunbak & Ergin note that a mean value for the coefficient of friction $\mu = 0.7$ between the crown wall and the underlayer allowed crown wall failure at the wave conditions estimated for the storm, $H_s = 6m$, $T_m = 10s$.

Allsop & Steele (Ref 8) report the results of tests on alternative breakwater cross-sections in a water depth of $h = 23\text{m}$ with a 1:100 year design offshore storm of $H_s = 8.7\text{m}$. One cross-section was armoured with 16m^3 Tetrapods at a front slope of 1:1.5 to a crest level around 7.8m above static water level. The other used 16m^3 Antifer cubes at a slope of 1:2.0. The upstand on the crown wall reached around 6.7m above water level. For both cross-sections, the first design for the crown wall, weighing around 1000 tonnes in 15m lengths, and laid with a small key onto 3-6 tonne underlayer, started to slide backwards under waves of $H_s = 8.0\text{m}$. The final, stable, crown wall section was approximately 30% heavier.

The failure of the north west main breakwater to Tripoli harbour, Libya, also involved the failure of the crown wall (Refs 9, 10). In this instance structural failure of lengths of the wall was precipitated by breakage and removal of the Tetrapod armour, and the consequent impact forces. Many sections of the crown wall upstand sheared or were bent backwards from the base plate. Gunbak (Ref 9) estimates a number of alternative combinations of wave conditions and sliding coefficients, between $\mu = 0.5-0.9$, that would lead to crown wall movement. At Tripoli the crown wall was cast in 10m lengths, each weighing around 500 tonnes, onto 2-4 tonne underlayer. The upstand of the crown wall projected approximately 3 metres above the crest of the armour layer.

At Arzew and Sines the main cause of failure appears to have been the relative fragility of 48 tonne Tetrapods and 42 tonne Dolosse respectively (Refs 2, 11,12). As a consequence of the removal of the primary armour the crown wall was severely damaged on both structures. At Sines the upstand of the crown wall projected 3 metres above the original crest of the Dolosse armour. The crown wall was cast in 15m long sections weighing around 4000-5000 tonnes (Ref 13,14).

The crown wall at Akranes, Iceland, survived a severe storm which removed much of the rock armour in front (Ref 15). In this instance the crown wall was constructed as part of a caisson used to form the rear part of the breakwater.

2.2 Wave overtopping

The main purpose of a breakwater crown wall is to allow a saving in materials by reducing the wave overtopping. It will be noted that the stochastic

nature of storm waves implies that a crown wall would have to be uneconomically large to prevent all overtopping. It is therefore well accepted that some probability of overtopping should be allowed for in design, perhaps by limiting the mean expected discharge for a given return period event to an acceptable level. The level of overtopping permitted will vary widely, depending upon the crest and rear slope protection; the frequency of use of berths in the lee of the breakwater; and the construction and use of any other structures closely behind the breakwater. The design overtopping should be much less if the area behind the breakwater is to be reclaimed, than if open water is to be maintained.

Relatively little guidance is available to the designer on the level of discharge that may be permitted. It will be influenced by the importance of three different aspects:

- a) Inconvenience or danger to persons or vehicles using the crown wall;
- b) Damage to elements of the crown wall structure, or leeward protection;
- c) Wave disturbance in the lee of the breakwater.

The limiting discharges for use of the area behind an overtopping sea wall have been studied by Japanese researchers Fukuda, Uno & Irie (Ref 36). Their work has been discussed by Owen (Ref 16) and Jensen & Juhl (Ref 34). Owen has summarised their recommendations:

- 1) For a person to walk immediately behind the seawall with a little discomfort,
 $Q < 4 \times 10^{-6} \text{m}^3/\text{s.m}$
- 2) For a person to walk immediately behind the seawall with little danger
 $Q < 3 \times 10^{-5} \text{m}^3/\text{s.m}$
- 3) For an automobile to pass immediately behind the seawall at high speed
 $Q < 1 \times 10^{-6} \text{m}^3/\text{s.m}$
- 4) For an automobile to pass immediately behind the seawall at low speed
 $Q < 2 \times 10^{-5} \text{m}^3/\text{s.m}$

- 5) For a house located immediately behind the seawall to suffer no damage,

$$0 < 1 \times 10^{-6} \text{m}^3/\text{s.m}$$

- 6) For a house located immediately behind the seawall to suffer no substantial flooding or damage, although experiencing partial damage to windows and glazed doors,

$$0 < 3 \times 10^{-5} \text{m}^3/\text{s.m}$$

It may be noted that these suggested limits are, as yet, not supported by tests or field measurements elsewhere. It is recommended that the reader should consult the original reference before using the values in design.

Again, relatively little information is available on the effect of overtopping discharge on crest and rear slope protection. In general, proposed solutions should be model tested to give acceptable certainty. Goda (Ref 37) has suggested limits for certain levels of protection to crest or rear slopes of sea walls:-

Structure	Max value of \bar{Q} :m ³ /s.m
Paved (concrete) crest	0.2
unpaved (grassed) crest	0.05
Crest and rear slope paved	0.05
Crest, paved and rear slope unprotected	0.02
Crest and rear slope grassed only	0.005

It may be noted that the last value compares well with the historical Dutch limit for grassed sea walls of $0.002 \text{m}^3/\text{s.m}$.

No information is available on the limiting overtopping conditions that may be tolerated by vessels against or close to the leeward face of the breakwater. The assessment of this, and of the degree of wave disturbance caused by overtopping that may be tolerated, are generally treated as site specific problems using physical model tests.

The calculation of overtopping discharge under random waves has been addressed by relatively few researchers, and the general application of those results available to breakwater crown walls is somewhat uncertain.

Owen (Ref 16-18) has developed an empirical method for the calculation of overtopping discharges for simple seawalls, based on a series of hydraulic model tests under random waves. The test used plain and bermed sea wall sections with smooth faces and no crown wall. Owen derived an empirical equation relating a dimensionless discharge, Q^* , to a dimensionless freeboard, R^* :

$$Q^* = A \exp (-B R^*/r) \quad (2.1)$$

where

$$Q^* = \bar{O}/T_m \text{ } g H_s \quad (2.2)$$

$$R^* = \frac{R_c}{H_s} \left(\frac{s_m}{2\pi} \right)^{\frac{1}{2}} = R_c/T_m (g H_s)^{\frac{1}{2}} \quad (2.3)$$

Owen presents values of the empirical coefficients A & B for a range of slope angles and berm configurations. This method was not developed for walls with complex crest details. However, two modifications have been considered. They involve the definition of an efficiency factor to describe the effect of the crown wall element in relation to the simple slope. In defining an efficiency factor for a given crown wall detail, a hypothetical discharge may be useful. This is defined as the discharge that would occur for the same wave conditions over a simple slope to the crest level considered. Steele & Owen (Ref 19) have defined an efficiency factor E_f :

$$E_f = 1 - \frac{O_2}{O_1} \quad (2.4)$$

where O_1 is the predicted discharge at the crest of the armour, without the crown wall, and O_2 is that with the crown wall. The efficiency factor will depend upon the crown wall geometry, principally F_c , G_c and A_c (see Fig 1), as well as the incident wave conditions, H_s and T_m . In use, values of the discharge needed, O_2 , might be calculated using a modified version of Owen's expression:

$$\frac{O_2}{T_m g H_s} = (1-E_f)A \exp (-B R_c^*/r) \quad (2.5)$$

where

$$R_c^* = \frac{A_c}{H_s} \left(\frac{s}{2\pi} \right)^{\frac{1}{2}} \quad (2.6)$$

It should be noted that the freeboard used to calculate R_c^* is that of the crest of the armoured slope, not of the crown wall. F_f will therefore depend strongly on the projection of the crown wall $R_c - A_c$.

An alternative efficiency factor, W_f , may be defined in terms of a discharge, Q_1^* , predicted at the crest of the equivalent simple slope continued up to the level of the crown wall crest:

$$W_f = \frac{Q_2^*}{Q_1^*} \quad (2.7)$$

Again, if using Owen's general form of expression:

$$\frac{Q_2}{T_m g H_s} = A W_f \exp(-B R^*/r) \quad (2.8)$$

where R^* is defined as before in equation 2.3. It may be noted that W_f may in turn depend upon R^* .

Ahrens & Heimbaugh (Ref 20) discuss a series of random wave tests for a sea wall in relatively shallow water. The sea wall incorporates a rip-rap armoured revetment slope, and a crown wall with various geometries. They derive an expression that appears similar to Owen's:

$$Q = Q_o \exp(C_1 F') \quad (2.9)$$

where Q_o is a coefficient having the dimensions of discharge rate per metre run; C_1 is a dimensionless coefficient; and the dimensionless freeboard parameter, F' , is defined in terms of the local wave height, H_{si} , and wave length, L_{ps} :

$$F' = R_c / (H_{si}^2 L_{ps})^{1/3} \quad (2.10)$$

In their work, Ahrens & Heimbaugh, define H_{si} in terms of spectral energy, $H_{si} = 4m_o^{1/2}$. In deep water $L_p = g T_p^2 / 2\pi$, but in shallower water the following approximation may be used:

$$L_{ps} = \frac{g T_p^2}{2\pi} \left[\tanh(4\pi^2 h / T_p^2 g) \right]^{1/2} \quad (2.11)$$

Generally the remaining information on breakwater overtopping either relates to structures without crown walls, or is based on regular wave testing only. Allsop (Ref 21) measured wave transmission over rock-armoured low crest breakwaters without crown walls. A good description of the coefficient of wave

transmission was given by the dimensionless freeboard, R^* . Jensen & Sorensen (Ref 22) present a set of equations, based on site specific model tests allowing the calculation of the intensity of overtopping water as a function of distance behind the breakwater:

$$0 = q_0 b / \ln 10 \quad (2.12)$$

and

$$q(x) = q_0 10^{-x/b} \quad (2.13)$$

Where : Q is the total overtopping discharge (m³/s per m)
 b is a constant equal to the distance behind the breakwater, in metres, for which the overtopping decreases by a factor of 10
 $q(x)$ is the overtopping intensity at a distance x along a normal to the rear of the breakwater (m²/s per m)
 q_0 is the overtopping intensity immediately behind the breakwater (ie at $x = 0$) (m²/s per m)

These equations give an indication of the decrease in overtopping intensity with distance behind the structure. It is likely however that these spatial variations will be significantly less important than the variations of discharge wave by wave, where peak discharges may be orders of magnitude greater than the mean value. Unfortunately little data is available on the temporal variations of overtopping discharges under random waves. Jensen & Juhl (Ref 34) report results of the measurement of discharge over the 5 - 10 waves giving the highest overtopping. They present results of their measurements graphically, fitting a line of general equation:

$$(q_w / \bar{Q})^{\frac{1}{2}} = A (\ln p) + B \quad (2.14)$$

Where : \bar{Q} is the average discharge over N waves
 q_w is the discharge for the single largest overtopping wave in N waves
 p is the probability of occurrence, $1/N$
 A and B are empirical coefficients

Example values that may be deduced from the graph as shown below:

N	P	q_w/\bar{O}
25	0.040	1.5
100	0.010	33
200	0.005	87
500	0.002	243

The effect of the shape of the front face of the crown wall has been addressed by Vera-Cruz (Ref 23). Using regular waves only, Vera-Cruz defined an effectiveness parameter for a curved wall in terms of the ratio of wave heights at the onset of overtopping for the curved wall relative to a simple vertical wall. Values of this effectiveness parameter of around 80-85% were determined, suggesting that under random waves any small change in wall shape will have relatively little influence.

Generally little data is available to describe the effects of different crown wall configurations on the overtopping performance. Some experience from the measurement of wave run-up levels, and of overtopping of simple sea walls, may still be helpful.

In predicting overtopping discharges of simple sea walls using Owen's method, a simple relative run-up or roughness factor, r , is used to describe the influence of roughness and permeability of the front face. Values of r were assumed from the results of previous investigations of run-up under regular waves. It was implicitly assumed that values of r were constant for a given structures. More recently Allsop et al (Refs 24,25) have examined wave run-up on smooth and rubble slopes under random waves. From these tests it may be concluded that the value of the roughness coefficient r , varies with the Iribarren number, I_r .

The effect of the angle of incidence, β , on run-up and overtopping has been studied by Owen (Refs 16-18) and Tautenhaim et al (Ref 26). In both instances increases in the response measured, overtopping discharge and run-up levels respectively, were noted for angles of incidence around $\beta = 10-20^\circ$, over those for $\beta = 0^\circ$. Whilst noticeable, these increases were not sufficiently severe to outweigh many of the other uncertainties. A more complete review of the effect of wave obliquity has been given previously by Allsop (Ref 27).

In the design of a crown wall the velocity and path of waves overtopping the structure will be of concern.

Often the parapet wall will be positioned so as to throw overtopping water clear of the rear face armour. An example of such a design is shown by Jensen (Ref 28), citing earlier work by Gravesen & Sorensen (Ref 29), and is illustrated by Figure 2.

2.3 Wave forces on crown walls

Wave forces acting on a crown wall section will principally act on the front face, and on the underneath causing uplift. In both instances hydraulic model test results are liable to scale effects. Wave impact pressure against a wall may reach very large values for very short durations. These short duration impact pressures are unlikely to excite any significant response in crown wall sections weighing hundreds, or thousands, of tonnes. This is fortunate as it is the brief impact pressure that is most affected by scale effects in the entrainment of air. Momentum and quasi-hydrostatic forces generally scale correctly in well designed hydraulic models, so the wave forces on the front face causing sliding or overturning will be expected to be reproduced by model tests. Uplift pressures on the underside of the crown wall are less easy to reproduce correctly due to the uncertainty in the scaling of viscous flow effects, particularly under conditions of air entrainment.

The scaling of steady state flows to correct for any viscous effects has been discussed previously by Allsop & Wood (Ref 1) and by Jensen (Ref 28). In such circumstances flow velocities can be corrected by using a distorted scale for the modelling of the porous layers. Very little data is available to cover conditions of reversing flow with high levels of entrained air. In design work the pressure distribution is generally assumed to be rectangular, trapezoidal, or triangular, with the maximum pressure on the underside equal to that acting at the bottom of the front face.

In one of the more comprehensive pieces of analysis of forces on crown walls, Jensen presents results of wave force measurements, and discusses the main design assumptions (Refs 28,30). The maximum horizontal force in 1000 waves, per metre run, F_H , is made dimensionless by dividing by $\rho g h_f L_p$, where h_f is the height of the front face of the crown wall. This dimensionless force is then plotted against a relative wave height, H_s/A_c , and a straight line drawn through the results for each structure, implying

$$F_H = \rho g h_f L_p \left(a \frac{H_s}{A_c} + b \right) \quad (2.15)$$

where the dimensionless coefficients a and b are specific to a particular crown wall configuration. Jensen argues that the influences of water level and wave period are given by A_c and L_p respectively. The effect of wave obliquity was examined by tests at $\beta = 0^\circ, 22^\circ$ and 45° . Over this range the force decreased with angle. The decrease was most marked at the shorter wave periods, being equivalent to a reduction factor, k_β , of around 0.33 at $\beta = 45^\circ$. For the longer wave period the reduction factor was nearer 0.5 at $\beta = 45^\circ$.

Jensen notes that wave forces are often calculated by determining the conditions for sliding, and suggests that for concrete on quarry stone, a coefficient of friction $\mu = 0.50-0.55$ is appropriate. Where a downward key, or heel is incorporated into the crown wall, values for μ up to 1.0 might be used.

Other analyses of wave pressures and forces on crown walls have been reported by Gunbak & Gokce (Ref 31), and Gunbak & Ergin (Ref 7). A triangular pressure distribution on the front face is postulated by Gunbak & Gokce, but this relates primarily to the brief duration impact pressures. The worst case for sliding or overturning of the wall will occur when the wave has reached, or is near, its full run-up height. Gunbak & Ergin use a very simplistic calculation of run-up to estimate a maximum depth of water over the armour. A total force is calculated by summing an impact force derived from the local wave celerity, and the hydro-static force. This approach appears to be considerably less certain than one based on test results, as described by Jensen (Refs 28, 30).

2.4 Physical modelling of crown wall stability

A rigorous mathematical model of the wave processes involved is not yet attainable. Thus in any investigation of these phenomena for design purposes, it is necessary to rely on physical modelling. The scaling laws for wave forces acting directly on vertical wall breakwaters have been discussed by Lundgren (Ref 32). However the situation considered in this study is a little different in that the wave may break onto a rubble mound slope and then subsequently run up the slope to impact with the crown wall. This process may produce a shock loading, comparable with the ventilated shock profile described

by Lundgren, whereby all, or nearly all, of the air between the run-up front and the parapet is able to escape upwards. For this ventilated shock, Lundgren concluded that both the pressures and the resulting impulse forces could be scaled using Froude's law. However, it should be noted that the concentration of entrained air within the run-up front will be much greater in prototype than in the model; thus the model will have a relatively higher fluid density. This may result in local pressures derived from the model being a little conservative, although the impulse forces will be substantially unaffected.

2.5 Summary of factors influencing crown wall performance

The primary variables affecting the overtopping performance of a breakwater crown wall are:

- a) incident wave conditions, given by H_s , T_m and/or T_p ;
- b) total structure freeboard, R_c ;
- c) armour slope, α , armour unit size, D_n , and layer thickness, t_a ;
- d) geometry of crown wall/armour crest detail, given by A_c , F_c , and G_c .

A number of empirical expressions have been suggested to relate the mean overtopping discharge, Q , to some of the primary variables. Those based on random waves by Owen and by Ahrens & Heimbaugh use exponential expressions and dimensionless freeboard parameters R^* or F' . It may be noted however that values of the empirical coefficients for these expressions have only been derived for a very limited set of configurations, none directly appropriate to breakwater crown walls.

Previous work suggests that run-up levels and overtopping discharges on simple slopes may increase at angles of wave attack $\beta = 10-20^\circ$. The relative increase is not great, and no data is available to predict the effect of a crown wall. Test results reported by Jensen suggests that the wave forces decrease significantly at angles of $\beta > 20^\circ$.

Wave forces on a crown wall section depend primarily on the velocity and volume of the wave arriving at the wall. Very high impact pressures of very short duration may be measured in hydraulic models, but such measurements will usually suffer from scale effects. Short duration impact pressures are unlikely to have any structural significance for the design of large concrete crown wall sections, often weighing many

hundreds of tonnes. Those forces that may cause sliding failure of the wall must persist for long enough to overcome the overall sliding resistance. These forces are generally correctly scaled in a well designed hydraulic model. The review has identified a simple empirical relationship from previous measurements which may allow the description of the horizontal wave force, F_H , in terms of parameters describing the incident wave conditions and crown wall/armour configuration.

3 DESIGN OF MODEL TEST PROGRAMME

3.1 Aims of the model tests

The literature review identified a number of areas of hydrodynamic design of crown walls presently subject to uncertainty which can be reduced by the present research. The main areas of performance selected for detailed study in these tests were:

- a) Overtopping discharges;
- b) Wave forces.

It was intended that the study should permit development of methods of prediction of overtopping discharges and forces on crown walls, using empirical frameworks derived from model testing. In both cases, the emphasis on the model tests would be on geometric variation of the crest detail, both to armouring and to the shape and height of the crown wall.

3.2 Selection of model test parameters

The hydraulic efficiency of the breakwater is often assessed on its performance under a given design storm, defined in terms of wave and water level conditions. These two parameters, along with wave direction, structure geometry, construction type, and foreshore gradient, are the most important factors affecting the level of overtopping and the wave forces acting on a structure.

A study of the hydraulic performance and stability of breakwater crown walls should therefore take account of as wide a range of these parameters as possible. A wide range of wave conditions were selected for use in this study, thus allowing a good description to be made of the hydraulic performance of the structure. The following effects have all been considered:

- a) Constant wave period and varying significant wave height;

- b) Constant significant wave height and varying wave period;
- c) Constant wave steepness - various values of H_s , and T_p for a sea steepness of 0.04.

Since a breakwater with a crown wall superstructure is of relatively complex geometry, it might reasonably be expected that the overtopping discharge would be given by a more complex function than that suggested by Owen for simple sloping seawalls (Ref 16). The effects of water level relative to the crest of the seaward slope of the breakwater and the crest of the breakwater superstructure were therefore examined.

The effects of foreshore gradient have not been investigated in this study and a single foreshore gradient of 1:52 was used throughout this study. Effects of any uncertainties in the wave transformations near the structure, caused by wave breaking, shoaling and refraction, were minimised by measurement of wave conditions at the site of the structure in the calibration stage of testing.

Whilst it is acknowledged that the effects of oblique wave attack on wave forces and overtopping of the structure may be important, the effect of this parameter was not investigated in this study.

The structure geometry and construction type of breakwaters and their crown walls varies quite considerably. Factors such as seaward slope of the breakwater; porosity, permeability, and roughness of the front slope armouring; positioning of the armouring relative to the crown wall; elevation and geometry of the wall; all have significant effects on the hydraulic performance. The test sections were designed to incorporate as many of these parameters as practicable. The effects of slope roughness were examined by comparing rock armoured structures with smooth slopes. In all cases the core was impermeable, representing a worst case for wave run-up. A single seaward slope of 1:2 was used throughout the study. Whilst the slope will affect the form of the wave striking the crown wall, it was felt that a 1:2 slope was reasonably typical, and also generally represents the most severe case for wave run-up (Refs 24, 25).

Geometric changes to the structure were concentrated around the crest area, at the interface between the crown wall and the armouring, and at the crest of the crown wall. The following geometric parameters were varied:

- a) Freeboard;
- b) Height of crown wall;
- c) Level of armouring and berm width of armouring relative to crown wall;
- d) Profile of crown wall.

A detailed description of the wave conditions, water levels, and test sections used in the model tests is given in Chapter 4.

It will be noted that the test programme was not designed to measure uplift pressures on the underside of the crown wall. The flow of air and water in the region below a crown wall will depend critically upon the detailing of the local geometry and on the effective permeability of the rock layers in this region of the structure. Problems in the scaling of these flows have been discussed previously, by Allsop & Wood (Ref 1) and elsewhere. It was clear that it would not be possible to reduce present uncertainties in the calculation of uplift pressures until results of another research project on the hydro-geotechnical behaviour of rubble mounds were available. Uplift forces were not therefore addressed further in this study.

4 TEST PROCEDURES AND MEASUREMENTS

4.1 Test facility

The model tests were conducted in the deep random wave flume at Hydraulics Research, Wallingford. This flume, shown in Figure 3 is 52m long, and is divided for much of its length into a central test channel, ending in a finger flume, and two side absorption channels. Splitter walls of graduated porosity are designed to minimise the level of re-reflected waves. The flume has a range of working water depths between 1.3-1.7m. Two water depths at the paddle, of 1.5m and 1.4m, were used for this project. The wave paddle is a buoyant sliding wedge, driven by a double acting hydraulic ram. The random wave control signal is supplied by a BBC micro computer using software written at Hydraulic Research.

An approach beach, at a slope of 1:52, was moulded in cement mortar, in the central channel of the flume. The slope extended offshore from the test section around 18 metres into deep water, where it was truncated by a smooth curved transition slope into a 1:10 slope to the floor of the flume.

4.2 Wave calibrations

Before testing of the various crown wall sections commenced, a series of wave calibrations were carried out with the moulded seabed in place, but with no test section. A wave absorbing beach was installed landward of the site of the test section to limit wave reflections from the end wall of the flume. Wave conditions were measured in deep water offshore and at the site of the structure.

Waves were recorded using twin wire resistance type wave probes. The analogue signal was digitized and analysed on line using a PDP11/73 minicomputer. Wave data was analysed using a spectral analysis program and the significant wave height defined using the approximation $H_s = 4m_o^{\frac{2}{3}}$. Results of the wave calibrations are given in Table 1. JONSWAP wave spectra were used throughout the study.

4.3 Construction of Model Test Sections

The test section was constructed on a flat floor in the glazed section of the finger flume, with the toe of the structure approximately 46m from the wave paddle. An impermeable core section was constructed in plywood, with a seaward slope of 1:2.

A total of 13 test sections, with different crest geometries, were constructed for the overtopping tests. The test sections are described below and are shown in Figures 4-7.

All test sections were constructed using the same impermeable core section. Test sections 1-3 were not armoured, whilst sections 4-13 were all armoured with rock. The rock armoring was designed to be statically stable under the most severe test conditions and was not rebuilt during testing.

The level of the slope break at the top of the smooth 1:2 slope was fixed for all tests except for test 3. For this test the smooth plain slope was extended upwards to the same level as the vertical crown walls on sections 1 & 2, thus allowing directly comparative measurements of structures with and without crown walls. The effect of a narrow berm at the base of the crown wall was tested in sections 1 and 2. These sections had the same crest elevation and a smooth slope, with and without a berm at the toe of the wall. Sections 4-13 were rock armoured. Sections 4-7 had a narrow berm at the toe of the vertical face of the crown wall. The height of the vertical crown wall was

varied in these test sections, to examine the effect of freeboard, F_c , of a vertical wall on overtopping. Test sections 6,8,9,10 and 12 were all constructed with the vertical faced crown wall at the same level. The effect of varying the level of rock armour relative to the crest of the crown wall, A_c , was investigated in these tests. The effect of a wider armour berm was tested in section 11, where the crown wall level was comparable with test section 6. A recurve wall was used in section 13. Details of the geometry of all test sections are given in Table 2.

Following tests to measure overtopping discharges, test sections 1,4,8,10 and 12 were modified by removing the crown wall section. This was replaced by a force table, to allow force measurements to be recorded, using the same rock armour configurations. These tests are described in detail in section 4.6.

4.4 Overtopping measurements

A calibrated volumetric tank was installed landwards of the model test section. The tank was fitted with a hinged chute which could be lifted and lowered onto the rear of the crown wall section thus allowing water discharged over the crown wall to be collected and measured when required. The tank was of rectangular plan shape. It was subdivided into sections of different plan area, to allow accurate measurement of low discharge. Baffles were incorporated to reduce wave movement in the tanks. Water levels in the tank were recorded using a magnetostrictive float transducer, which produced a voltage signal proportional to the level, and hence volume of water, in the tank. The minimum volume that could be measured accurately was 0.15 litres. Water was directed into a tank of small plan area, which overspilled successively into each of the three larger tanks when full.

A standard procedure for measurement of overtopping discharges, was used throughout this study. This procedure is outlined below.

	No. of waves(T_m)	Operation
a)	0	Remove overtopping chute from rear of crown wall and set wave generator running for required wave conditions.
b)	300	Lower water collection chute onto rear of crown wall, start to

		collect overtopping discharge (sample 1).
c)	400	Remove overtopping chute from rear of crown wall, record level in calibrated tanks.
d)	600	Sample 2 as b.
e)	700	As c.
f)	900	Sample 3 as b.
g)	1000	As c.
h)	1200	Sample 4 as b.
i)	1300	As c.
j)	1500	Sample 5 as b.
k)	1600	End of test.

This procedure allows a statistical description of the variation of discharge, over 5 batches of 100 waves. The overtopping tests were run with the wave generator set to produce very long sequence of waves without repetition of the sequence, thereby reproducing correctly the Rayleigh probability of wave heights found in natural sea waves.

An extensive series of tests for various combinations of wave height, period and water level were run on each of the 13 test sections described in section 4.3. A total of 247 overtopping tests were carried out. The full range of wave and water level conditions tested are described in Table 1. The full range of structure parameters are given in Table 2.

4.5 Pressure measurements

It was intended initially that the horizontal component of force acting on the breakwater should be calculated from the output of a series of pressure transducers mounted into the seaward face of the crown wall. By using transducers with an appropriate frequency response, it would be possible to calculate both high frequency wave impact pressures and also quasi-hydrostatic inertial wave pressures. The pressure distribution over the vertical face of the crown wall could be described, and the total force and moment calculated from the transducer analogue time series output. A set of six pressure transducers, were purchased. The transducers had a ceramic diaphragm of 40mm diameter. It was noted that they might therefore be subject to erroneous output due to partial immersion of the relatively large pressure sensor head. The pressure transducers were calibrated by measuring the output voltages for a range of constant depths of immersion.

A test programme was commenced with the intention of measuring pressure distributions on the crown wall,

for a wide range of wave conditions and crest geometries. Initially, very short tests were run, to identify the most appropriate digitization rate for the output from the pressure transducers. As this study was primarily designed to measure inertial wave forces, which might result in backward sliding of the crown wall, as opposed to impact forces causing deformation of the materials, it was not necessary to measure the peak of the very fast edge of the signal resulting from the initial impact on the wall. Spectral analysis of the pressure signals, digitized at 500Hz identified little energy above frequencies of about 50Hz. It was therefore decided to digitize the signal at a rate of 100Hz. It was accepted that the measured peak impact force might be rather lower than if a higher digitization rate had been used.

On starting testing however, a large zero signal drift occurred from all of the pressure transducers. In many cases the drift was greater than the full range of peak to zero impact measurements. This was attributed to the heating and rapid cooling, at the air/water interface, of the electronic elements attached to the diaphragm, causing variable output from the transducers. As the drift was not linear, it was not possible to filter the data for further analysis. Additionally, the transducers were operating over a very narrow range of their initial calibration range, thus reducing accuracy of measurements and requiring very large amplifier gains, which resulted in further heating of the transducers. Prior to testing however, the range of pressures to be measured was not known, therefore selection of a transducer with an appropriate range was extremely difficult. These problems resulted in significant changes to this part of the study. The use of pressure transducers was abandoned in favour of force measurements recorded by a simple force table, discussed below.

4.6 Force measurements

The force table was designed to measure horizontal wave loadings. Details of the instrument are shown in Figure 8 and Plate 1. The force table element was a rigid lightweight aluminium channel section, cantilevered from a supporting plate by four proof rings. A clearance of approximately 1mm was allowed between the bottom flange of the channel section and the wooden test section base. A similar clearance was allowed between the end of the force table and the flume walls. In this way, the force table element was free to move under wave loading and to deform elastically the supporting proof rings. The proof

rings, each of diameter 70mm, were constructed from 1.5mm thick aluminium tube. Foil strain gauges were resin-bonded to the outer face of each ring at the points at maximum flexure. Each pair of strain gauges were connected in a full bridge circuit to produce an output voltage proportional to the applied force. A precision strain gauge amplifier unit was used to power the gauges and to amplify the output signal.

The calibration procedure was to clamp the supporting plate such that the force table element was horizontal. Loads were applied incrementally to the point of attachment to the force table element for each proof ring in turn. For each applied load, the output voltage was recorded. Output voltage was found to vary linearly with applied load over the calibration range.

The force table was not expected to respond well to very high frequency forces induced by wave impact. This was due in part to the natural damping of the system and also to the difficulty of effectively depth-averaging a wave pressure signal, the phase of which varies with height up the crown wall. The instrument described here is therefore considered most suited to assessing the total depth-integrated horizontal force imparted on a crown wall by the wave. It is this parameter which has been considered in the subsequent data analysis.

Maximum expected loading on the force table, calculated using a simplistic design procedure for wave forces on a vertical caisson (Ref 33), was approximately 500N, under the most severe test conditions. Each proof ring was therefore designed to withstand a 140N load and remain within its elastic limit.

No attempt was made to measure uplift forces on the crown wall. There are substantial problems associated with the accurate model scaling of flow through permeable underlayers and such uplift forces cannot be simulated reliably in a small scale flume model.

The test programme was designed to assess the influence of the following parameters on wave-induced crown wall loadings:

- a) Incident wave climate. Influence of wave height, wave period and wave steepness;
- b) Water level;
- c) Armour geometry.

The wave conditions applied to each test section were identical to those used for overtopping measurements, presented in section 4.2 and Table 1. Tests were conducted at two water depths, $h = 0.4\text{m}$ and $h = 0.5\text{m}$ respectively, at the toe of the slope.

The various armour geometries tested are described in Figures 4 to 6. These sections were designed to be representative of those commonly used on coastal structures. In all cases, the model armour was angular rock. In all of the force tests, the height of the crown wall, h_f , remained constant at 110mm. It should be noted that the crown wall element used for overtopping tests on sections 6, 8-12 was slightly smaller at 85mm high.

For each test the amplified analogue voltage signal from each proof ring of the force table was digitised and the four data channels were logged simultaneously onto a PDP11/73 minicomputer. A trial wave sequence was imposed on the test rig and the force table output was logged. This procedure was repeated several times using the same wave sequence but varying the digitisation rate in order to determine that most appropriate for the tests. A rate of 100Hz was chosen; this gave adequate representation of the output signal without significant loss of details. A higher frequency would be required to describe wave impact forces but these were not reliably measured by the force table.

Each random wave test was of duration $1000T_m$ where T_m is the nominal mean wave zero-crossing period.

5 ANALYSIS OF RESULTS

5.1 Overtopping

5.1.1 Empirical relationships

The mean and standard deviation of the overtopping discharge was calculated from the five samples each for 100 waves, collected during each test. This data, together with the other input parameters, was analysed using a number of dimensionless parameters derived from earlier work. These methods are discussed briefly below.

Owen (Ref 16) has used an equation of the form:

$$O^* = A \exp(-BR^*/r) \quad (5.1)$$

A and B are coefficients for different slope angles $\cot\alpha$ and r is a relative run-up or roughness

coefficient. The study from which the above formula is derived was conducted on smooth faced seawalls with a roughness coefficient $r = 1$. A large proportion of this study was however conducted using permeable rock armour, with an impermeable core. It is reasonable to expect therefore, that the roughness coefficient r will be significantly less for the structures in this study. A roughness coefficient of $r = 0.5-0.6$ has been suggested (Ref 16) for two or more layers of rock armour. The relative roughness for smooth and rough slopes, measured in this study is discussed in Section 5.1.2.

The data collected in this study was fitted to the dimensionless parameters suggested by Owen. The coefficient of regression for the fit of the data to this relationship was not particularly good, even for structures of the simplest geometry. Results from the present study have been compared using this method and examples are shown in Figures 9-12.

Ahrens & Heimhaugh (Ref 20) present overtopping data for a number of structures in a different form. They suggest that discharge is not well described by dimensionless parameters, but describe a dimensionless freeboard parameter that takes account of the local wave length. This allows a better description of structure performance in relatively shallow water, and is appropriate to the shallow water tests in Ahrens & Heimhaugh's study. Whilst this method does appear to indicate some improvement on Owen's method, it has the disadvantage of not being truly dimensionless. Ahrens & Heimhaugh derived equations of the form given below:

$$Q = Q_0 \exp (C_1 F') \quad (5.2)$$

Where Q_0 is a coefficient with the same units as Q (volume/unit time per metre run of wall), C_1 is a dimensionless coefficient, and Ahrens' dimensionless freeboard is defined in terms of the local wave length of the peak period, L_{ps} :

$$F' = \frac{R_c}{(H_s^2 L_{ps})^{1/3}} \quad (5.3)$$

Comparison of the results of this study with a simplified version of the above equations (using the shallow water wave wavelength $L_p = T_m \sqrt{gh}$), suggest a better relationship than that discussed by Owen. The measured data has been presented, for selected test sections as $-\ln Q$ against F' in Figures 13-16.

On careful examinations of graphs of R^* against O^* , for values measured in this study, it was noted that there was a stronger dependence on dimensionless freeboard R_c/H_s than on wave steepness. A dimensionless relationship incorporating this function was derived and an equation for dimensionless freeboard developed:

$$F^* = R^* \left(\frac{R_c}{H_s} \right) = \left(\frac{R_c}{H_s} \right)^2 \left(\frac{s_p}{2\pi} \right)^{\frac{1}{2}} \quad (5.4)$$

It is also suggested that an equation of the form:

$$Q^* = A F^{*B} \quad (5.5)$$

gives a slightly better description of the relationship of Q^* to F^* than does an equation of exponential form. Coefficients A and B have been calculated for each test section. These are given in Table 3. The effect of increasing the weighting of the function R_c/H_s draws the data closer to a regression line, improving the correlation coefficient significantly, particularly for higher discharge events.

The relationship between $\ln Q^*$ and $\ln F^*$ is demonstrated in Figures 17-29. It should be noted that the results of this study were derived in relatively deep water conditions. Ahrens' prediction method, which was based largely on results in shallow water, may be more appropriate at lower water levels, because of the local wave length effects considered by the inclusion of L_{ps} in the equation for F' .

None of the analysis methods described above, explicitly take account of the structure geometry. The use of empirically derived coefficients involves a significant simplification of the description of the overtopping processes. The effects of berm width, armour crest position and vertical wall freeboard must each have an effect on discharge, inside of certain threshold levels. It seems likely that the geometric variations described above will have the most significant effect for a limited range of dimensionless freeboard values. When the freeboard is such that the crown wall is inundated, relatively small geometric variations at the crest are less significant and will have no noticeable effect on discharge. For very high discharge events, it seems likely that the relatively simple relationship of dimensionless freeboard, F^* , to dimensionless overtopping, Q^* , does provide an adequate description of the overtopping performance of the structure. The

threshold for which this relationship holds is however not easily defined. The results from this study suggest that an equation of the form $AF^{*B} = Q^*$ is valid where $Q^* > 2 \times 10^{-5}$. This argument is described in more detail below.

Similarly the crown wall geometry is less significant for low discharge conditions, when the freeboard is very large. There is however a range of events for which the crest geometry plays a significant part in the overtopping performance of the structure. The graphs of $-\ln Q^*$ against $-\ln F^*$, shown in Figures 17-29 suggest that the relationship between F^* and Q^* becomes weaker for values of $Q^* < 2 \times 10^{-5}$. This may be due to two factors. Firstly, the crown wall geometry may have sufficient effect on overtopping to distort the relationship. Secondly, when Q^* is small, the mean overtopping discharge will generally be low and therefore subject to significant variation by occasional large waves. The confidence in the use of measured discharges of relatively small samples of waves, for prediction of overtopping, is therefore much reduced. The large coefficient of variation of the five samples measured in each test in this study, for low mean discharge conditions, bears out this point. This effect can be compensated for in one of two ways. Either a weighting factor, proportional to discharge, can be applied to the data, or values of \bar{Q} below a certain limit can be discounted in analysis. In this study, discharge events resulting in values of \bar{Q} less than 0.05 litres per second per metre (model) have not been included in the calculation of coefficients A & B, as such low mean discharges are subject to large random variations. The importance of exclusion of invalid data from a data set is demonstrated in Figure 30, which shows measured Q^* against predicted Q^* , using the whole data set for a single test section. Elimination of the low discharge values results in a stronger correlation between predicted and measured discharge. More importantly though, the slope of the prediction line and thus the coefficients of A and B can be altered quite significantly by changing the range. Coefficients A and B, for the restricted data set, are given in Table 3.

The scatter in the data set, $Q^* < 2 \times 10^{-5}$, may however result from the geometry of the crown wall and armour. It is possible that the relationship $Q^* = AF^{*B}$ is too simple to describe the overtopping of a structure over the range $Q^* < 2 \times 10^{-5}$. The following ratios might be considered to have an effect on overtopping performance of a structure. The ratio F_c/A_c describes

the freeboard in terms of the ratio of the projection of the crown wall above the armour crest, against the elevation of the armour crest relative to static water level. This ratio may help to describe the relative effect of various combinations of wall geometry and armour on discharge. Similarly the ratio F_c/G_c may be used to describe the effect of the projection of the crown wall above the armour crest, against the width of the horizontal armour crest berm. The geometry of the seaward face of the crown wall is also likely to have a significant effect on the discharge for a range of dimensionless freeboards.

5.1.2 Effectiveness of crest geometry

An additional method, for the comparison of structures with a crown wall with a smooth plain slope, has also been used to describe the relative performance of crown wall sections. Comparisons of the relative performance of different crest geometries are described below.

The influence of the geometry of the test sections can be described by a relationship of the form:

$$W_f = \frac{O_{*2}}{O_{*1}} = \frac{A_2 F_*^{B_2}}{A_1 F_*^{B_1}}$$

$$W_f = A_3 F_*^{B_3} \quad (5.6)$$

where, W_f is the efficiency factor; A_1, B_1 , are coefficients for the performance of a smooth plain slope and A_2, B_2 are coefficients describing the performance of a structure of more complex geometry. The performance of each test section can therefore be related to a smooth plain slope, by substitution of the coefficients given for each structure in Table 3, for any value of dimensionless freeboard.

The relative performance of each of the test sections is described below, and the effects of geometric variations of the crest detail on overtopping performance discussed.

Comparison of the performance of test sections 1, 2 & 3 allows the relative performance of impermeable structures, of the same height, to be described. The presence of a narrow berm at the toe of the crown wall in section 1, compared with section 2 which has no berm, appears to reduce the discharge when F^* is larger than about 0.135. Discharge is however slightly increased when F^* is smaller than 0.135.

This may be explained by examining the effective vertical height of the crown wall. The ratio F_c/G_c is very close to 1. This ratio combined with the slope angle, $\cot\alpha = 2$, reduces the effective vertical height of the wall, by 50% by extending the slope trajectory to the wall. When inundation occurs the angle between the wall and the slope will fill with water thus causing a ramping effect, and increasing discharge. The vertical wall with no berm however returns wave action over a larger vertical range, thus reducing overtopping at higher discharge levels.

The smooth slope with no crown wall, test section 3, performs significantly worse than both test sections 1 and 2, for all wave conditions, indicating that the crest geometry does have a significant effect on discharge, for structures with the same crest level.

The performance of a rock armoured structure with the same profile as a smooth impermeable structure was compared, by relating sections 4 and 1, which had the same cross-section geometry. The rock armouring has a marked effect on the discharge. Section 1 has an efficiency factor of $W_f = 3.6 \times 10^{-2} F_*^{-1.25}$ whilst section 4 has an efficiency factor of $W_f = 4.8 \times 10^{-4} F_*^{-1.61}$. This difference represents the effect of the roughness coefficient (r) in Owen's equation (Ref 16).

The effect of extension of the crown wall above the armouring, increasing both R_c and the ratio F_c/A_c was examined by comparing test sections 4,5,6,7 and 9 (shown in Fig 5). As expected, a reduction in discharge results from increasing freeboard. In addition however there is a general trend indicating a slight reduction in discharge as a result of increasing the ratio F_c/A_c . This is shown by comparison of Figures 20,21,22,23 and 25. This indicates that a vertical crown wall at the crest of a 1:2 slope is more efficient at reducing overtopping than a plain 1:2 slope of the same crest level, for the range tested, confirming the conclusion drawn by comparison of sections 1,2 and 3.

The effect of widening the armour berm at the toe of the crown wall reducing the ratio F_c/G_c is quite marked, resulting in a considerable reduction in discharge for all events measured. This is illustrated by comparison of Figures 23 and 25 with 27.

Variation of both A_c and F_c was investigated by

comparison of test sections 6,8,10 and 12 (Fig 6). A constant berm width was maintained in each test section, as was the crown wall level, but the level of the crest of the armour was varied. The trend observed on test sections 6,8 and 10, shown by comparing Figures 22, 24 and 26, suggests that the higher berms reduce the discharge for R^* values greater than about 0.06. Higher discharges were however noted for values of R^* less than about 0.06, as the berm level increased. This may be explained by the fact that the permeable mound becomes fully saturated under severe conditions, causing the rock mound to act as a ramp, over which the waves run. This once again suggests that the crest freeboard parameter A_c/F_c may be a significant factor in the analysis of crown wall overtopping.

The effect of altering the geometry of the crown wall, whilst maintaining the same freeboard parameters, was investigated by comparing a vertical wall with a recurved wall. The reduction in discharge brought about by introducing a wave return recurve on the crown wall is quite dramatic, as is shown by comparison of Figure 29 with Figures 22 & 25. It should however be noted that the fit of the data to the regression line is not particularly good, suggesting strongly that a more complex relationship may be required to describe the performance of recurved crown walls.

The repeatability of the testing procedure was investigated by comparison of tests 6 and 9 which were carried out on an identical test section. The results of these tests are shown in Figures 22 and 25, and suggest that the procedure adopted provides repeatable results over the high discharge range. The regression lines are quite closely aligned for both tests. There was however some considerable scatter observed over the low discharge range, where the results are very sensitive to individual discharge events. This has resulted in a significant variation in correlation coefficients for these two tests.

The results of overtopping coefficients for all test sections, are given in Table 3. These may be used to estimate the overtopping performance for structures of the geometry tested, for a wide range of values of R^* .

5.2 Forces

5.2.1 Analysis procedure for random wave tests

Typical signal outputs from each of the proof ring channels are shown in Figure 31. The locations of each proof ring are described in Figure 8. It is interesting to note that the upper rings experienced less loading than the lower ones. Some lateral variation in loading was also evident; this was attributed to local differences in rock armour placement detail. For each test, the four resultant force time series were simply summed and divided by the test section width to give an equivalent total horizontal force per unit width of crown wall, F_H . Typical raw total force time series are presented in Figure 32(a). It can be seen from this example that there is a certain amount of noise superimposed on the signal. Although the signal to noise ratio is relatively high, the signal perturbations complicate any threshold crossing type analysis, particularly when the peak force level is coincident with the selected event threshold level. This can be seen clearly in Figure 33(a) where multiple threshold-crossings would be predicted from the raw data. Additionally, it is difficult to define a peak load from the raw data. On many of the force peaks, there exist high frequency components which would not be of great structural significance because of their very short durations. The inability of the force table to resolve high frequency wave impact loadings has been discussed previously in section 4.6.

It was decided to filter the total force data prior to statistical analysis, in order to remove unwanted high frequency components. The selection of an appropriate low pass filter was somewhat subjective. If the frequency cut-off was too high, the signal could not be smoothed adequately. If the cut-off was too low, the inherent characteristics of the signal would be modified. The filter selected was a low pass Butterworth time domain filter with cut-off frequency 5Hz, applied over 5 passes. Examples of the resulting filtered time series are presented in Figures 32(b), and 33(b). It should be noted that application of the filter induces an effective delay of 0.1 seconds in the resultant time series; but does not affect the statistical validity of the resultant data.

For the crossing analysis, an event threshold level of 9N/m was selected. The selection of this level again required a somewhat subjective judgement. The level chosen was just above the peak of zero level fluctuations.

The following parameters were derived from the data:

a) UNFILTERED TIME SERIES:

- i) Maximum recorded force (N/m run)
- ii) 1% exceedance force from entire dataset (N/m run)

b) FILTERED TIME SERIES:

- iii) Maximum filtered force F_{Hmax} (N/m run)
- iv) 5% exceedance force from threshold-crossing peak dataset F_{H5} (N/m run)
- v) Mean threshold up-crossing period T_{imp} (seconds)
- vi) Mean impact ratio $IR = T_{imp}/T_m$ where T_m is the mean inshore zero up-crossing period in seconds.

In some tests, for the largest incident wave conditions, the force table exhibited a zero level instability. Particularly large incident waves would induce a permanent offset to the recorded zero force level. This might be attributed to a small plastic deformation of the proof rings; relative movements between the resin bonded strain gauges and the proof rings; or some relative movement between the proof rings and their fixing blocks. The third explanation was considered to be most likely. Despite the induced zero level offsets, the calibration coefficients for each proof ring remained quite constant throughout the test programme. Where severe zero level instabilities were experienced, a low pass filtered time series with frequency cut-off 0.2Hz was subtracted from the raw data prior to further analysis. This procedure improved significantly the quality of the measured forces, but was time-consuming to apply and did not completely resolve individual zero offsets. It was therefore only applied to badly corrupted data.

5.2.2 Results

The test results were assessed in three ways. Firstly, for each of the test sections, subjected to a common random wave sequence, the derived parameters for wave loading on the crown wall were compared. This procedure was carried out for two of the most severe test wave conditions; in each case relative performances of the various rock armour configurations were derived. Secondly, for a single armour geometry, a more intensive study was made of the influence of various wave parameters on crown wall loading. Finally, where possible, test results were compared with those presented by other workers.

The results of the comparative wave loading analysis for each of the test sections are presented in Figures 34 to 39 and Table 4. The impact ratio, IR, describes the mean period between successive wave impacts on the crown wall, relative to the wave zero-crossing period. The greater the value of IR, the less frequently waves hit the wall. The two force parameters considered both relate to the filtered total horizontal peak wave forces on the wall, respectively as a 5% exceedence level, and a maximum recorded level. The 5% exceedence value would be expected to be more stable than the singular maximum point. Both the impact ratio and the two force parameters have been used to assess the relative severity of wave attack on the crown wall to allow comparison between the performance of each test section. In Table 4 the parameters IR, F_{H5} and F_{Hmax} are also presented as proportions of the equivalent parameter for test section 8f. This enables a simplistic extension of the information derived for section 8f, concerning the influence of incident wave conditions on crown wall loading. Section 8f is similar to the structure for which Jensen presents data (Refs 28, 30). The use of the force ratios, $F_{H5}/F_{H5\ 8f}$ and $F_{Hmax}/F_{Hmax\ 8f}$, presented in this study may be used to extend the scope of Jensen's work.

In each of the comparative wave loading tests, the least severe wave loading, in terms both of IR and F_H , occurred for section 12f. The second least severe loading occurred consistently for section 10f. These results would be expected intuitively as the rock armour completely protected the crown wall face in each case. Section 8f, with rock armour extending half way up the crown wall, was considered to provide the next most effective armour protection. Section 11f had a wide rock berm with its crest at the base of the crown wall. This was found to be equivalent to section 8f in terms of wave impact occurrence on the crown wall, but induced force magnitudes were between 20% and 30% greater. The two most severely loaded test sections were 4f, with a narrow rock berm at the base of the crown wall, and 14f with a narrow impermeable berm at the base of the wall. As might be expected, section 14f, with a smooth impermeable slope, experienced the highest incidence of wave impact on the crown wall. However, magnitudes of wave forces acting on section 4f were approximately twice those for section 14f.

The results of the study of wave parameter influence on crown wall loadings, for test section 8f, are presented in Figures 40 to 45. The results are considered in terms of filtered peak force, F_{Hmax} , and

mean impact period ratio, IR, with respect to wave height, wave period and wave steepness, respectively. The results presented relate to a single water depth at the toe of the armour slope, $h_s = 0.5\text{m}$. It is suggested from Figures 40 and 41 that there is an approximately linear dependence of peak force on both wave height and wave period. However, further data would be required to substantiate this assertion. A detailed analysis of the results shown in Figures 40-45 is presented and discussed in Appendix A. An alternative technique to that of Jensen for the estimation of wave forces on crown walls is suggested. However, further work is required to resolve limitations of the method and to extend its range of applicability.

The threshold wave conditions below which no waves hit the crown wall is not clearly defined from the data analysed in this study. The threshold is not of great significance in the structural design of the crown wall but if required, is perhaps better assessed using wave run-up relationships such as those which appear in Reference 25.

The mean wave impact period T_{imp} gives information about the frequency with which the crown wall is hit by waves. It does not, however, define the durations of quasi-hydrostatic loading. Further analysis would be required to study the loading duration parameter.

The maximum wave forces measured in each of the tests on section 8f have been plotted in the non-dimensional format proposed by Jensen in References 28 and 30. The parameter $F_{Hmax}/\rho g h_s L_p$ is plotted against H_s/A_c in Figure 47. The best fit line from Jensen's results (Figure 49) is also compared with data from this study in Figure 47. There is reasonable agreement between the data sets, in terms of the slope of the best fit lines. The scatter of data from this study, about the best fit line, suggests that the relationship may be more complex than is suggested by Jensen. Closer examination of the cluster of points in the centre of the graph reveal that these scattered points have a common significant wave height but varied mean wave period. A strong linear dependence of force on wave period is suggested by the trend shown in Figure 40. This dependence is not shown in the relationship suggested by Jensen. A comparison between measured and predicted forces (using Jensen's predicted line from Figure 49) is shown in Figure 48. This indicates that Jensen's prediction is within $\pm 30\%$ of the results given in this study.

5.2.3 Calculation of horizontal wave forces on the crown wall

In order to assess horizontal wave loadings on a crown wall it is necessary to make use of results from hydraulic physical model tests, conducted for structures of similar geometrical configuration to those of interest. No prototype measurements have been reported in the literature. In general, the hydrodynamics of the problem, for an armoured structures, are too complex to model reliably using numerical or analytical techniques.

Dimensionless empirical relationships are presented by Jensen (Refs 28 & 30) for the prediction of maximum wave forces on three different types of coastal structure. Jensen suggested that, for a given structural form, there exists a linear relationship of the form:

$$\frac{F_{Hmax}}{\rho g h_f L_p} = a + b \left[\frac{H_s}{A_c} \right] \quad (5.6)$$

Where a and b are empirical coefficients and F_{Hmax} is the predicted maximum horizontal force per metre which might be expected to act on a crown wall during a random sequence of 1000 incident waves of given significant wave height H_s and mean wave period T_m .

This method provides a valuable first estimate of wave force. However, it appears that the method by which the relevant parameters have been non-dimensionalised is not completely valid, and that the influence of wave period on crown wall force is not represented adequately. It is suggested that wave forces, F_H , predicted using Jensen's best fit lines are generally accurate to $\pm 30\%$. Furthermore, the influence of armour geometry in reducing wave loadings has not been addressed.

The present study has addressed the influence of armour geometry on crown wall loading. The armour coefficients H_{max}/H_{max} g_f quoted in Table 4 may be used to extend the H_{max} values predicted by Jensen's relationship to structures of different crest armour detail.

An alternative approach is suggested in Appendix A, but this is still under development. Further work is required to resolve some of the limitations and to extend the range of applicability before it can be used with confidence.

6 RECOMMENDATIONS

6.1 Recommendations for design calculations

6.1.1 Overtopping

The overtopping performance of a breakwater crown wall can be described by an equation of the form

$$Q_{*} = A F_{*}^B \quad (6.1)$$

Coefficients for A and B for the crown wall configurations tested are given in Table 3. This method of prediction provides a better description of overtopping than equations of the form suggested by Owen for simple slopes (Ref 16) and Ahrens & Heimbaugh (Ref 20) for a revetment and wave wall.

Coefficients of $A = 7 \times 10^4$ and $B = -1.85$ are suggested for a smooth slope in equation 6.1.

The model test confirms that the following factors will reduce wave overtopping:

- a) Increasing the freeboard of the vertical wall (F_c);
- b) Increasing the rock armour berm width (G_c);
- c) Concave seaward faces of the crown wall will give a better performance than vertical crown walls of the same height;
- d) Increasing the freeboard of the rock armour (A_c) and reducing the ratio F_c/A_c , will reduce overtopping for most conditions, except for conditions that lead to particularly high discharges.

6.1.2 Wave forces on a crown wall

The method of Jensen (Ref 28 and 30) to assess wave forces on crown walls is described in section 2.3. For a selection of structural geometries Jensen presents relationships of the form:

$$\frac{F_{Hmax}}{\rho g h_1 L_p} = a + b \left[\frac{H_s}{A_c} \right] \quad (6.3)$$

where a and b are empirical coefficients.

The F_{Hmax} values predicted using Jensen's method may

now be extended to structures with different crest armour geometries using the armour coefficients presented in Table 4.

6.1.3 Sliding

In determining the weight of a crown wall to resist sliding a value for the coefficient of friction $\mu = 0.5$ should generally be used unless:

- a) the crown wall slab is keyed down into the layers below, when μ up to 0.7 may be appropriate; and/or
- b) tests have confirmed a different value.

Where the crown wall sits on underlayer or secondary armour, the pressure distribution on the underside of the crown wall slab may generally be assumed to be triangular, varying from a maximum at the front to zero at the rear, drained, face.

6.2 Recommendations for good practice

A series of basic guidelines have been derived from the physical model studies and from the other studies discussed in this report. These guidelines are general in nature and may be inappropriate in certain circumstances. They do however provide the reader with some basic guideline on preliminary considerations for the design of crown walls.

Where possible the design of the crown wall cross-section should ensure that:

- a) the shape of the crown wall will throw any overtopping water clear of vulnerable parts of the rear slope;
- b) the upstand is kept as low as possible commensurate with performance;
- c) the crown wall slab should be cast on the least permeable material where possible, to prevent the transmission of large volumes of water and entrapped air through to the lee-side; and/or
- d) the crown wall should be keyed in to the material below by a 'heel' or 'downstand' at the seaward side;
- e) the crown wall should be cast at a sufficient level above static water level, to allow construction without casting operations being hampered by water ingress.
- f) pre-cast parapet sections should generally be avoided owing to their low coefficient of friction against sliding.

7 ACKNOWLEDGEMENTS

The work at Hydraulics Research covered by this report was conducted by members of the Coastal Structures Section in the Maritime Engineering Department. The authors are grateful to Dr K A Powell for his work on the literature review, Mr A R Channel for assistance in the tests; and to their colleagues in technical and support services for assistance in the analysis and production of this report. The authors are also grateful for the advice and comments of O J Jensen of the Danish Hydraulic Institute.

8 REFERENCES

1. Allsop N W H & Wood L A. "Hydro-geotechnical performance of rubble mound breakwaters". Report SR 98, Hydraulics Research, Wallingford, March 1987.
2. Allsop N W H. "Concrete armour units for rubble mound breakwaters and sea walls: recent progress". Report SR 100, Hydraulics Research, Wallingford, March 1988.
3. Bradbury A P, Allsop N W H, Latham J-P, Mannion M & Poole A B. "Rock armour for rubble mound breakwaters, sea walls, and revetments: recent progress". Report SR 150, Hydraulics Research, Wallingford, March 1988.
4. Bradbury A P & Allsop N W H. "Durability of rock on coastal structures". Proc 20th Coastal Eng Conf, Taipei, November 1986. (Also as Hydraulics Research Conference Paper No 1.)
5. Allsop N W H & Latham J-P. "Rock armouring to unconventional breakwaters: the design implications for rock durability". Proc. Seminar on unconventional rubble mound breakwaters. NRCC, Ottawa, September 1987. (Also as Hydraulics Research Conference Paper No 2.)
6. Lillevang O J, Raichlen F R, Cox J C & Behnke D L. "A detailed model study of damage to a large breakwater, and model verification of concepts for repair and upgraded strength". Proc 19th Coastal Eng Conf, Houston, September 1984.
7. Gunbak A R & Ergin A. "Damage and repair of Antalya Harbour breakwater". In Design and Construction of mounds for breakwaters and coast protection, Elsevier, Amsterdam, 1985.
8. Allsop N W H & Steele A A J. "Ashdod port development-north breakwater stability studies". Report EX 1158 (Restricted), Hydraulics Research, Wallingford, May 1985.
9. Gunbak A R. "Damage to Tripoli harbour north west breakwater". In Design and construction of mounds for breakwaters and coastal protection, Elsevier 1985.
10. Barony Y S, Malick V D, Gusby M & Seherly F. "Tripoli harbour north west breakwater, and its problems". Proc 1st COPEDEC Conf, Columbo, March 1983.

11. Abdelbaki A & Jensen O J. "Study of provisional repair of the breakwater in Port d'Arzew El Djedid". Proc 1st COPFDEC Conf, Columbo, March 1983.
12. Burcharth H F. "The lessons from recent breakwater failures, developments in breakwater design". Presented to Technical Congress, World Federation of Engineering Organisations, Vancouver, May 1987.
13. Port Sines Investigation Panel. "Failure of the breakwater at Port Sines, Portugal". American Society of Civil Engineers, New York, 1982.
14. Zwamborn J A. "Analysis of causes of damage to Sines breakwater". Proc Coastal Structures 79, Alexandria, ASCE, March 1979.
15. Bruun P (Ed). "Design and Construction of mounds for breakwaters and coast protection". Elsevier, Amsterdam, 1985.
16. Owen M W. "Design of seawalls allowing for wave overtopping". Report EX 924, Hydraulics Research, Wallingford, June 1980.
17. Owen M W. "The hydraulic design of sea wall profiles". Proc Conf Shoreline Protection, ICE, Southampton, September 1982.
18. Owen M W. "Overtopping of sea defences". Proc Conf Hydraulic Modelling of Civil Eng Structures, BHRA, Coventry, September 1982.
19. Steele A A J & Owen M W. "Prestatyn coast defence: prediction of discharge over a proposed seawall". Report EX 1335, Hydraulics Research, Wallingford, 1985.
20. Ahrens J P & Heimbaugh M S. "Irregular wave overtopping of sea walls". Proc Conf Oceans '86, IEEE, Washington, September 1986.
21. Allsop N W H. "Low crest breakwaters, studies in random waves". Proc Coastal Structures '83, ASCE Arlington, March 1983.
22. Jensen O J & Sorensen T. "Overspilling/ overtopping of rubble mound breakwaters. Results of studies, useful in design procedures". Coastal Eng Vol 3, No 1, Elsevier, Amsterdam, 1979.

23. Vera-Cruz D. "Overtopping of rubble mound breakwater with curtain wall". La Hoille Blanche, No 5, 1972.
24. Allsop N W H, Franco L & Hawkes P J. "Waves run-up on steep slopes: a literature review". Report SR 1, Hydraulics Research, Wallingford, March 1985.
25. Allsop N W H, Hawkes P J, Jackson F A & Franco L. "Wave run-up on steep slopes: model test under random waves". Report SR 2, Hydraulics Research, Wallingford, August 1985.
26. Tautenhaim E, Kohlase S & Partenscky H W. "Wave run-up at sea dikes under oblique wave approach". Proc 18th Coastal Eng Conf, Cape Town, 1982.
27. Allsop N W H. "Sea walls: a literature review". Report EX 1490, Hydraulics Research, Wallingford, September 1986.
28. Jensen O J. "Breakwater superstructures". Proc Conf Coastal Structures 83, ASCE, Arlington, March 1983.
29. Gravesen H & Sorensen T. "Stability of rubble mound breakwaters". 24th PIANC Congress, Leningrad, 1977.
30. Jensen O J. "A monograph on rubble mound breakwaters". Danish Hydraulic Institute, Horsholm, November 1984.
31. Gunbak A R & Gokce T. "Wave screen stability of rubble mound breakwaters". Athens Conf 1984.
32. Lundgren H. "Wave shock forces: An analysis of deformations and forces in the wave and in the foundation". Proc Symp Research on wave action, Delft, 1969.
33. Goda Y. "Random seas and design of maritime structures." University of Tokyo Press, Tokyo 1985.
34. Jensen O J & Juhl J. "Wave overtopping on breakwaters and sea dikes". Proc 2nd COPEDEC, Beijing, China, September 1987.
35. Bradbury A P & Allsop N W H. "Hydraulic effects of breakwater crown walls". Paper to breakwaters 88, ICE, Eastbourne, May 1988. [Also available as HR Conference Paper No 13].

36. Fukuda N, Uno T & Irie I. "Field observations of wave overtopping of wave absorbing revetments. Coastal Engineering in Japan, Vol 17, 1974.
37. Goda Y. "Expected rate of irregular wave overtopping of sea walls". Coastal Engineering in Japan, Vol 14, 1971.

TABLES.

TABLE 1 Test conditions

TEST	H_{si} (m)	T_p (s)	h(m) (Water depth at toe of test section)
1	0.09	1.20	0.50
2	0.16	1.20	0.50
3	0.12	1.40	0.50
4	0.16	1.40	0.50
5	0.09	1.60	0.50
6	0.12	1.60	0.50
7	0.16	1.60	0.50
8	0.20	1.60	0.50
9	0.16	1.80	0.50
10	0.20	1.80	0.50
11	0.16	2.00	0.50
12	0.16	1.20	0.40
13	0.15	1.40	0.40
14	0.13	1.60	0.40
15	0.16	1.60	0.40
16	0.19	1.60	0.40
17	0.16	1.80	0.40
18	0.18	1.80	0.40
19	0.16	2.00	0.40

TABLE 2 Test section construction

TEST SECTION	SLOPE TYPE (Cot $\alpha=2$)	SLOPE CREST LEVEL	WALL CREST LEVEL	R_c (m)	F_c (m)	A_c (m)	G_c (m)
1	SMOOTH	0.555	0.70	0.20	0.145	0.055	0.15
2	SMOOTH	0.700	0.70	0.20	0.000	0.200	0.00
3	SMOOTH	0.555	0.70	0.20	0.145	0.055	0.00
4	ARMOURED	0.555	0.70	0.20	0.145	0.055	0.15
5	ARMOURED	0.555	0.76	0.26	0.205	0.055	0.15
6	ARMOURED	0.555	0.64	0.14	0.085	0.055	0.15
7	ARMOURED	0.555	0.67	0.17	0.115	0.055	0.15
8	ARMOURED	0.555	0.64	0.14	0.040	0.100	0.15
9	ARMOURED	0.555	0.64	0.14	0.085	0.055	0.15
10	ARMOURED	0.555	0.64	0.14	0.000	0.140	0.15
11	ARMOURED	0.555	0.64	0.14	0.085	0.055	0.30
12	ARMOURED	0.555	0.68	0.18	0.000	0.180	0.15
13	ARMOURED	0.555	0.64	0.14	0.085	0.055	0.15

ALL LEVELS ARE RELATIVE TO THE TOE OF THE TEST SECTION (m)

TABLE 3 Summary of empirical coefficients for various crown wall configurations

Test Section	A	B	Correlation Coefficient R ²
1	5.0 x 10 ⁻⁷	-3.098	0.93
2	3.4 x 10 ⁻⁶	-2.033	0.81
3	1.4 x 10 ⁻⁵	-1.848	0.70
4	6.7 x 10 ⁻⁹	-3.457	0.81
5	3.6 x 10 ⁻⁹	-4.368	0.93
6	5.3 x 10 ⁻⁹	-3.514	0.84
7	1.8 x 10 ⁻⁹	-3.600	0.96
8	1.6 x 10 ⁻⁹	-3.182	0.84
9	1.3 x 10 ⁻⁸	-2.585	0.67
10	3.7 x 10 ⁻¹⁰	-2.920	0.73
11	1.0 x 10 ⁻⁹	-2.823	0.61
12	1.3 x 10 ⁻⁹	-3.817	0.80
13	5.9 x 10 ⁻¹⁰	-3.154	0.71

$$Q^* = A F^{*B}$$

TABLE 4 Results of comparative wave loading

SECTION NUMBER	IMPACT RATIO $IR = T_{imp}/T_m$	IR/IR 8f	ORDER OF INCREASING SEVERITY	5% EXCEEDENCE FILTERED PEAK FORCE (N/m run) F_{H5}	$F_{H5}/F_{H5\ 8f}$	ORDER OF INCREASING SEVERITY	MAXIMUM FILTERED PEAK FORCE F_{Hmax} (N/m run)	F_{Hmax}/F_{Hmax}	ORDER OF INCREASING SEVERITY
Test A, wave conditions: $H_s = 0.2m$, $T_m = 1.6s$, $d = 0.5m$									
4f	1.52	0.77	5	442	3.13	6	758	3.59	6
8f	1.98	1.00	4	141	1.00	3	211	1.00	3
10f	2.29	1.16	2	117	0.83	2	145	0.69	2
11f	2.05	1.04	3	169	1.20	4	260	1.23	4
12f	4.78	2.41	1	42	0.30	1	50	0.24	1
14f	1.41	0.71	6	222	1.57	5	375	1.78	5
Test B, wave conditions: $H_s = 0.2m$, $T_m = 1.8s$, $d = 0.5m$									
4f	2.06	1.04	4	553	3.14	6	849	3.52	6
8f	1.98	1.00	5	176	1.00	3	241	1.00	3
10f	2.27	1.15	2	108	0.61	2	149	0.62	2
11f	2.07	1.05	3	232	1.32	4	313	1.30	4
12f	3.72	1.88	1	48	0.27	1	65	0.27	1
14f	1.54	0.78	6	247	1.40	5	434	1.80	5

FIGURES.

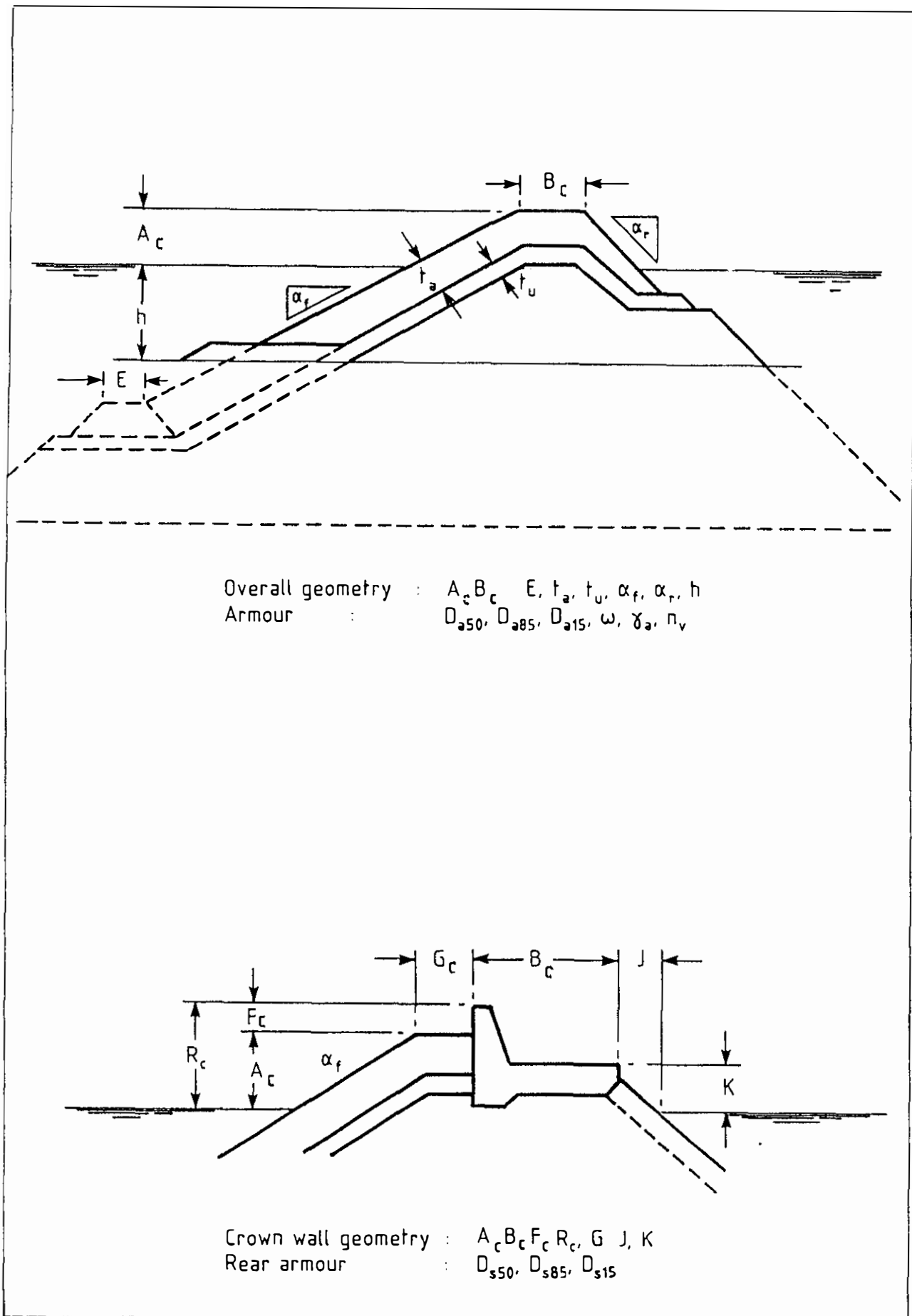


Fig 1 Geometry of breakwater cross sections

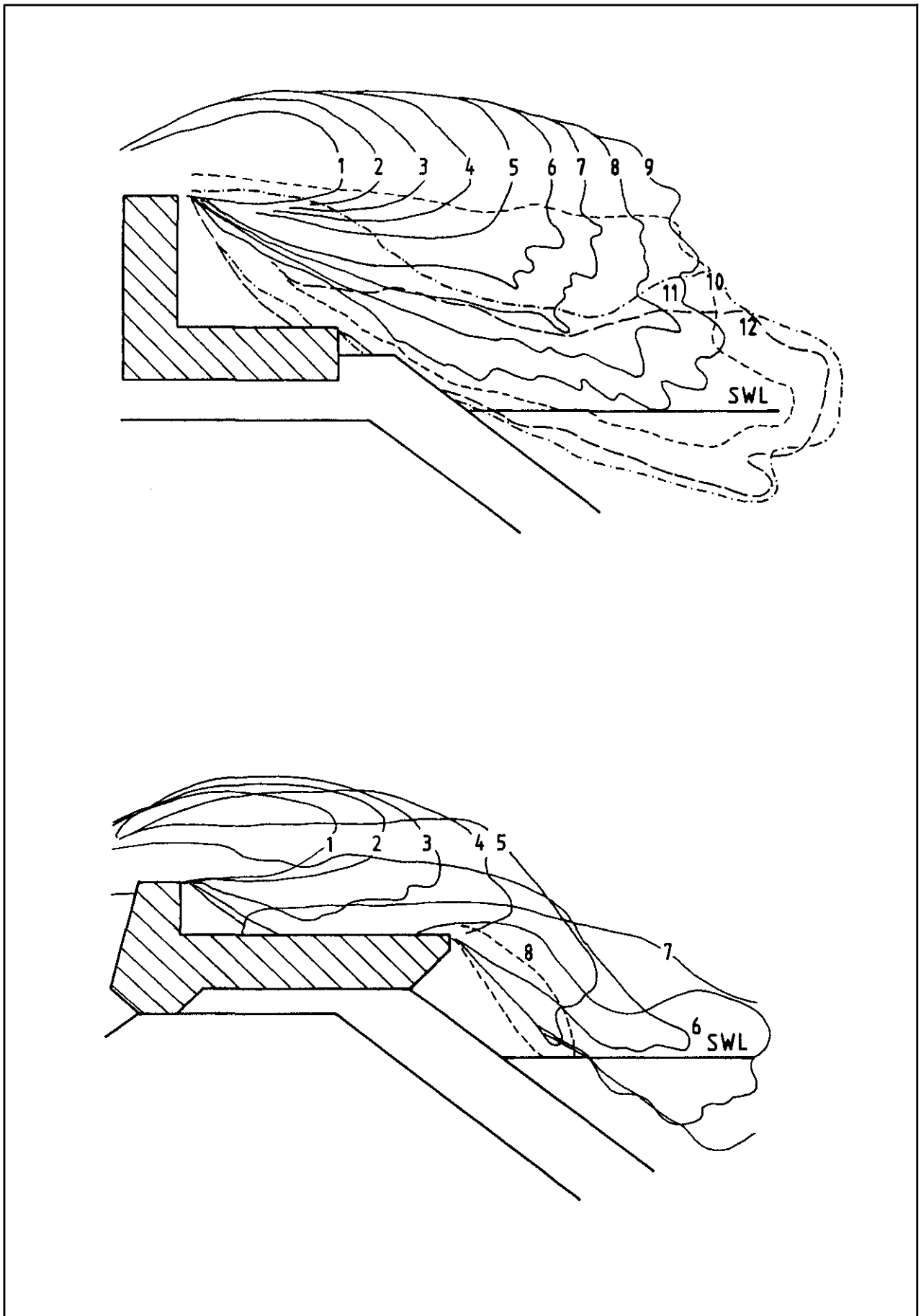


Fig 2 Overtopping of breakwater Crownwalls - after Gravesen et al

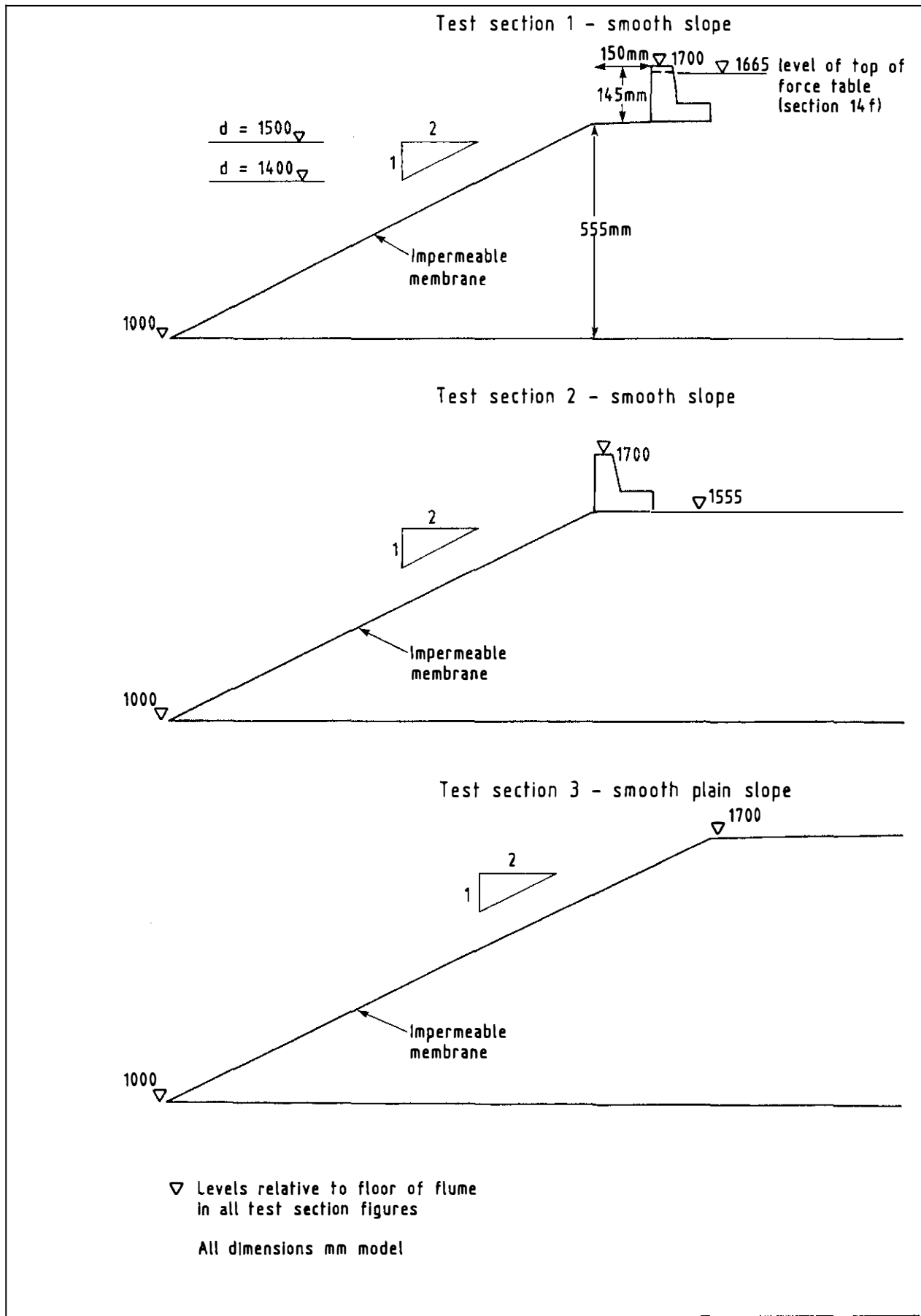


Fig 4 . Test sections 1, 2, 3 and 14 (smooth slopes)

Comparison of test sections 4 - 7
Variations of crown wall crest level

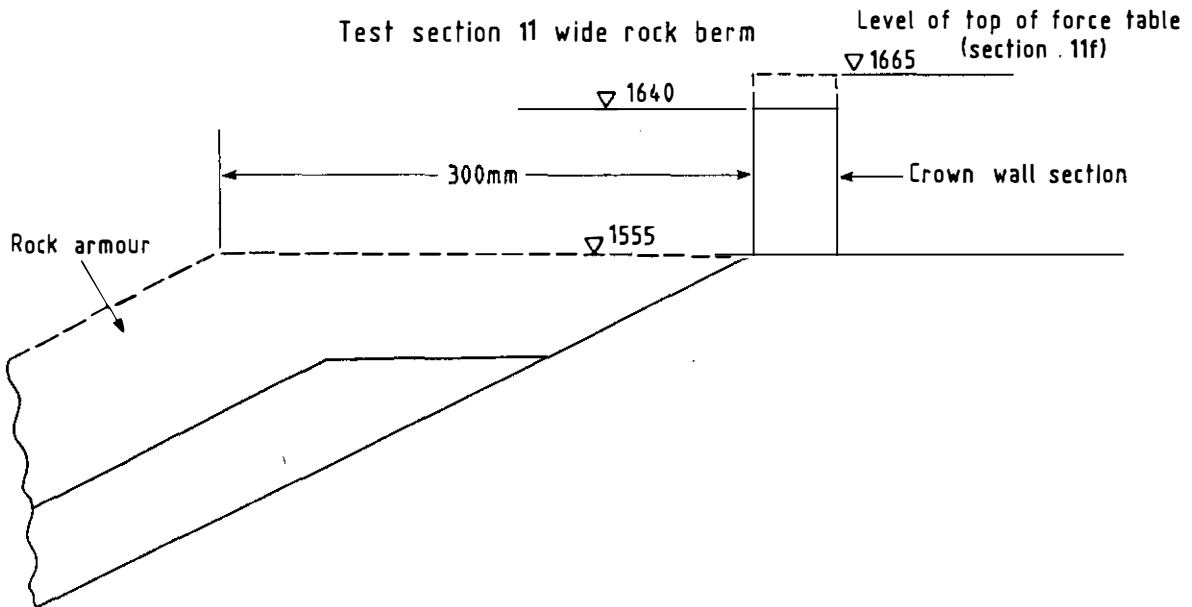
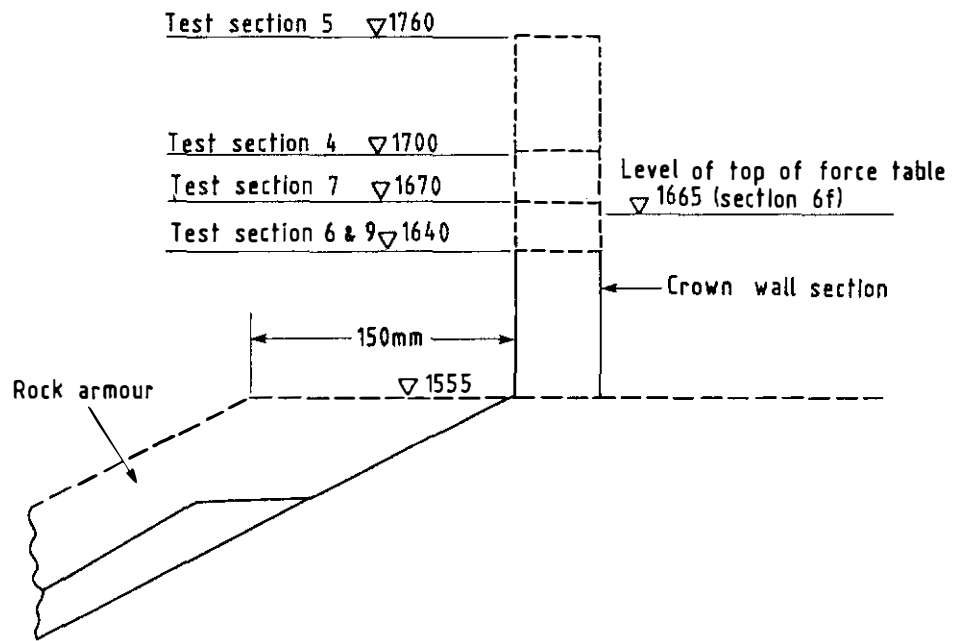


Fig 5 Test sections 4-7 and 11

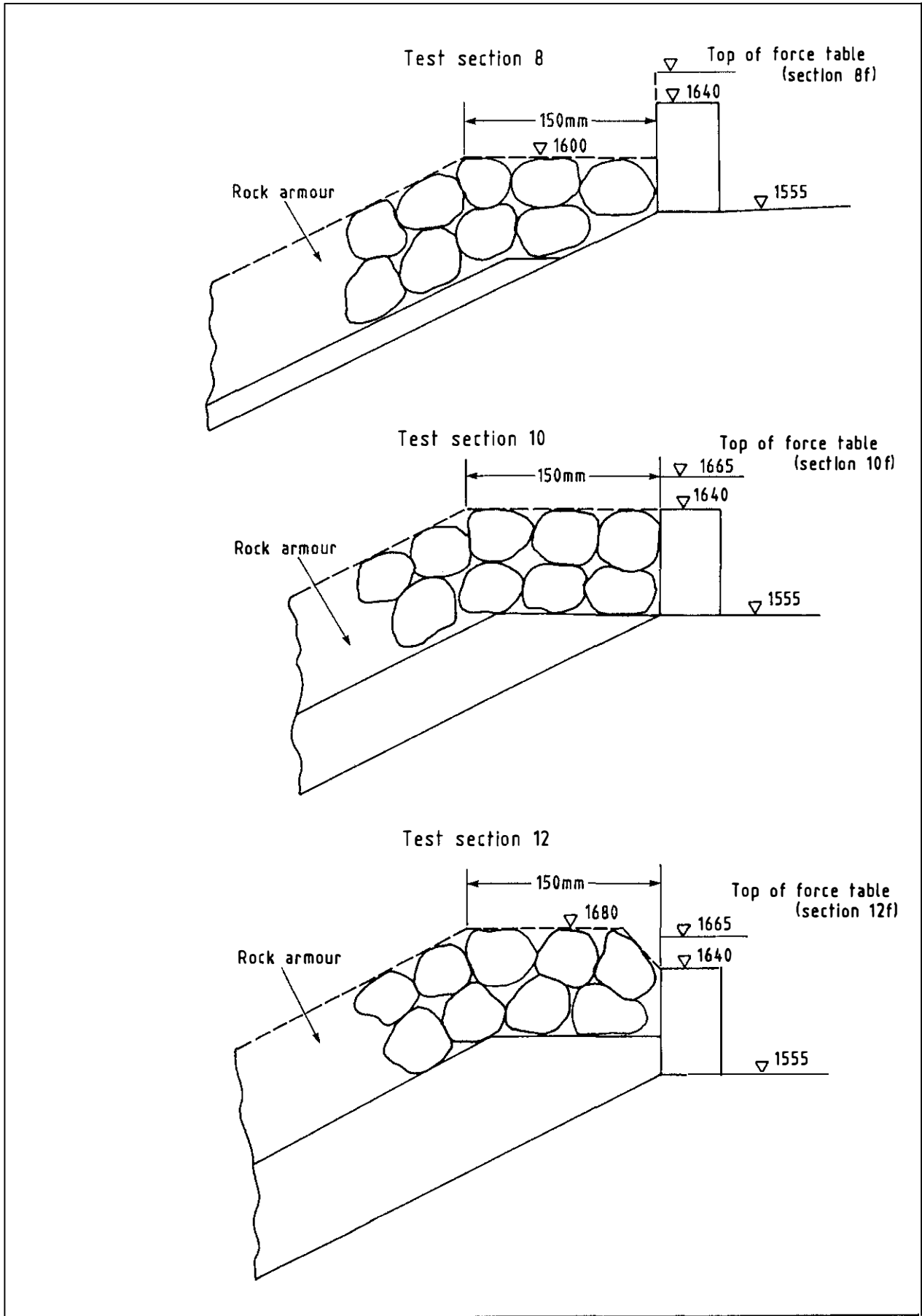


Fig 6 Comparison of armour configuration at crest

Test section 13 - recurved wall

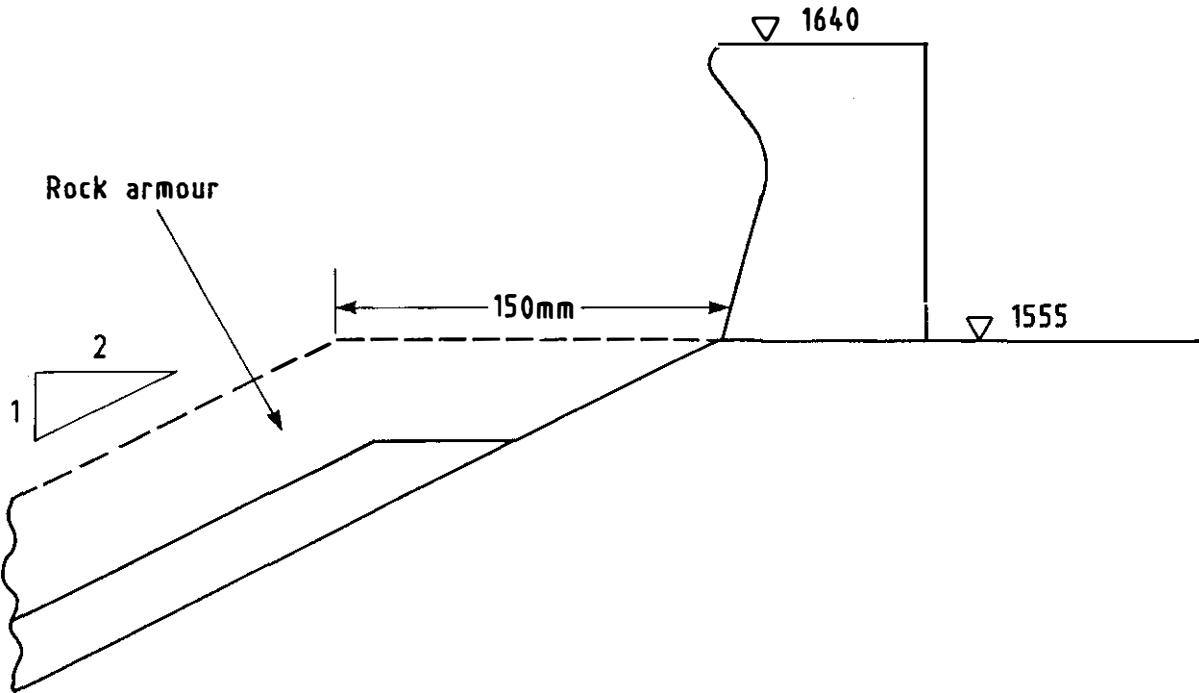


Fig 7 Test section 13 - recurved wall

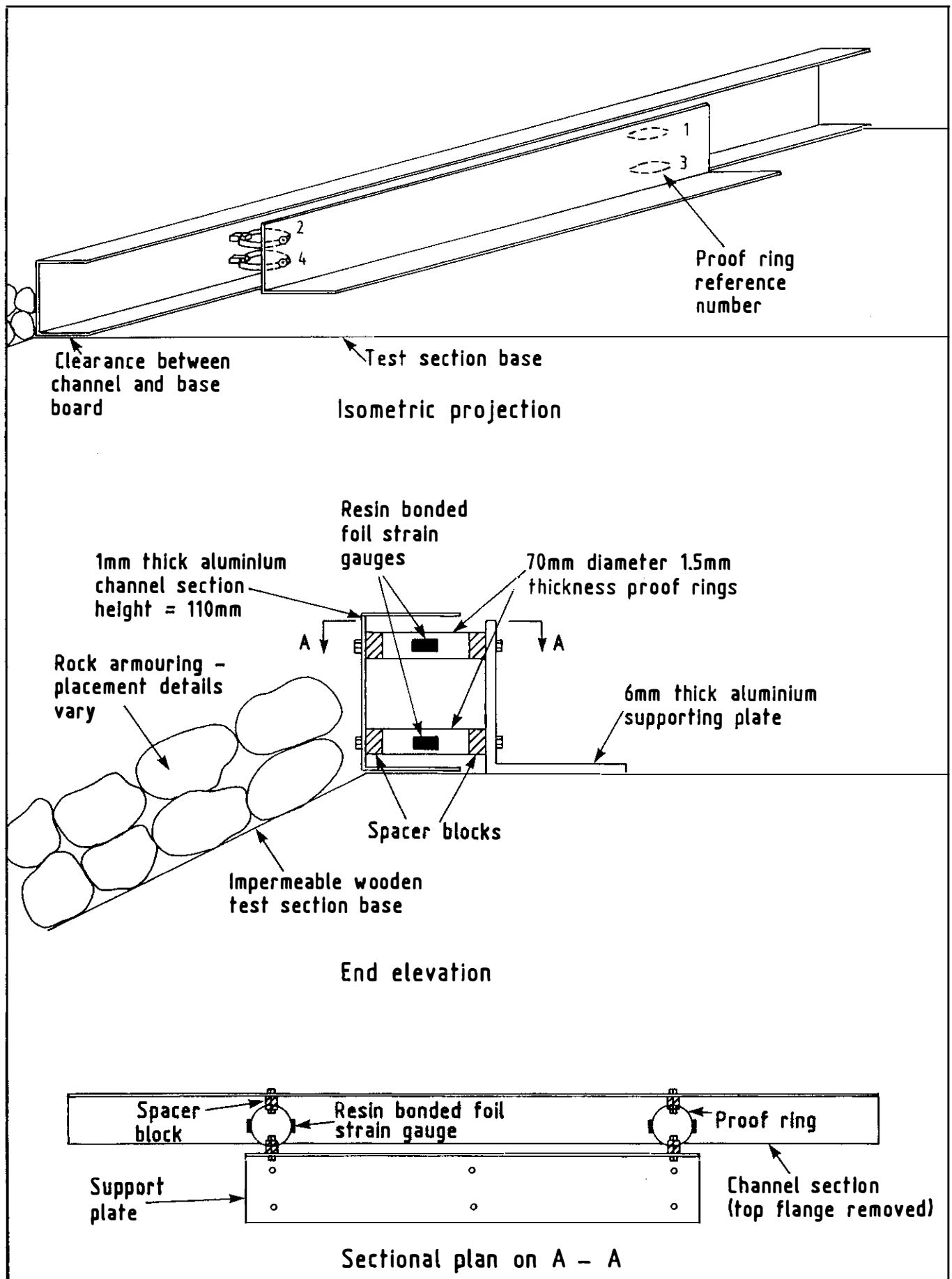


Fig 8 Force table

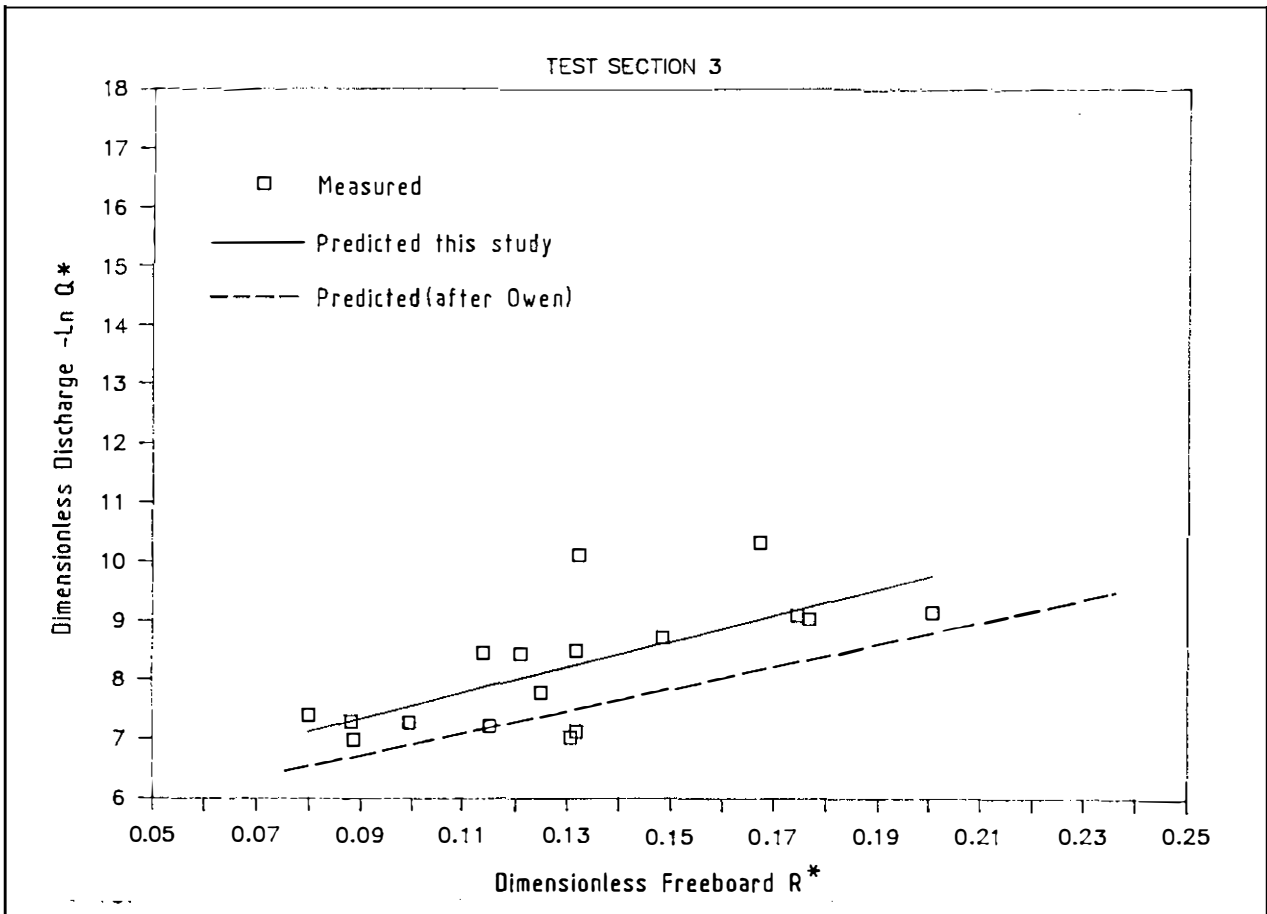


Fig 9 Test section 3 R^* vs $-\ln Q^*$

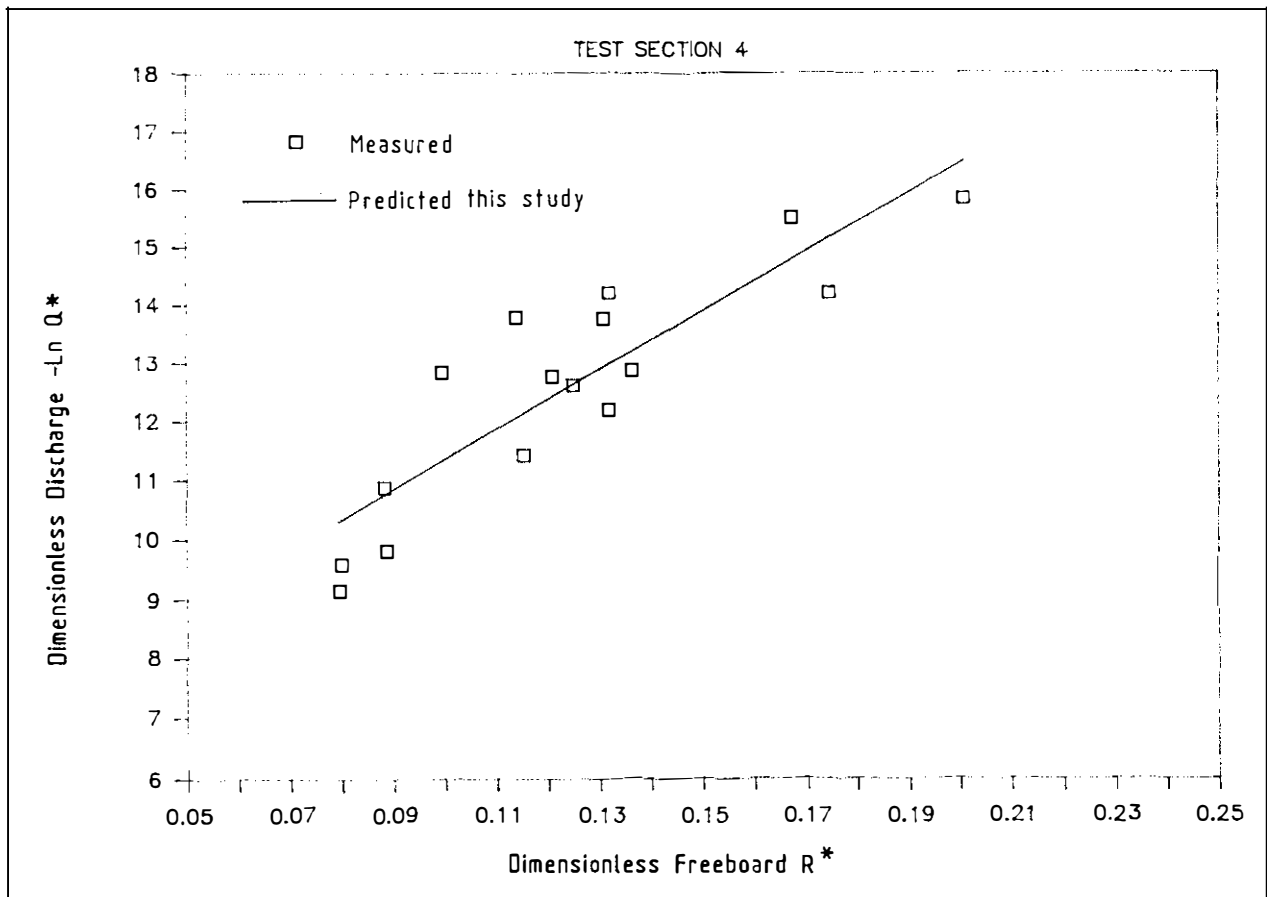


Fig 10 Test section 4 R^* vs $-\ln Q^*$

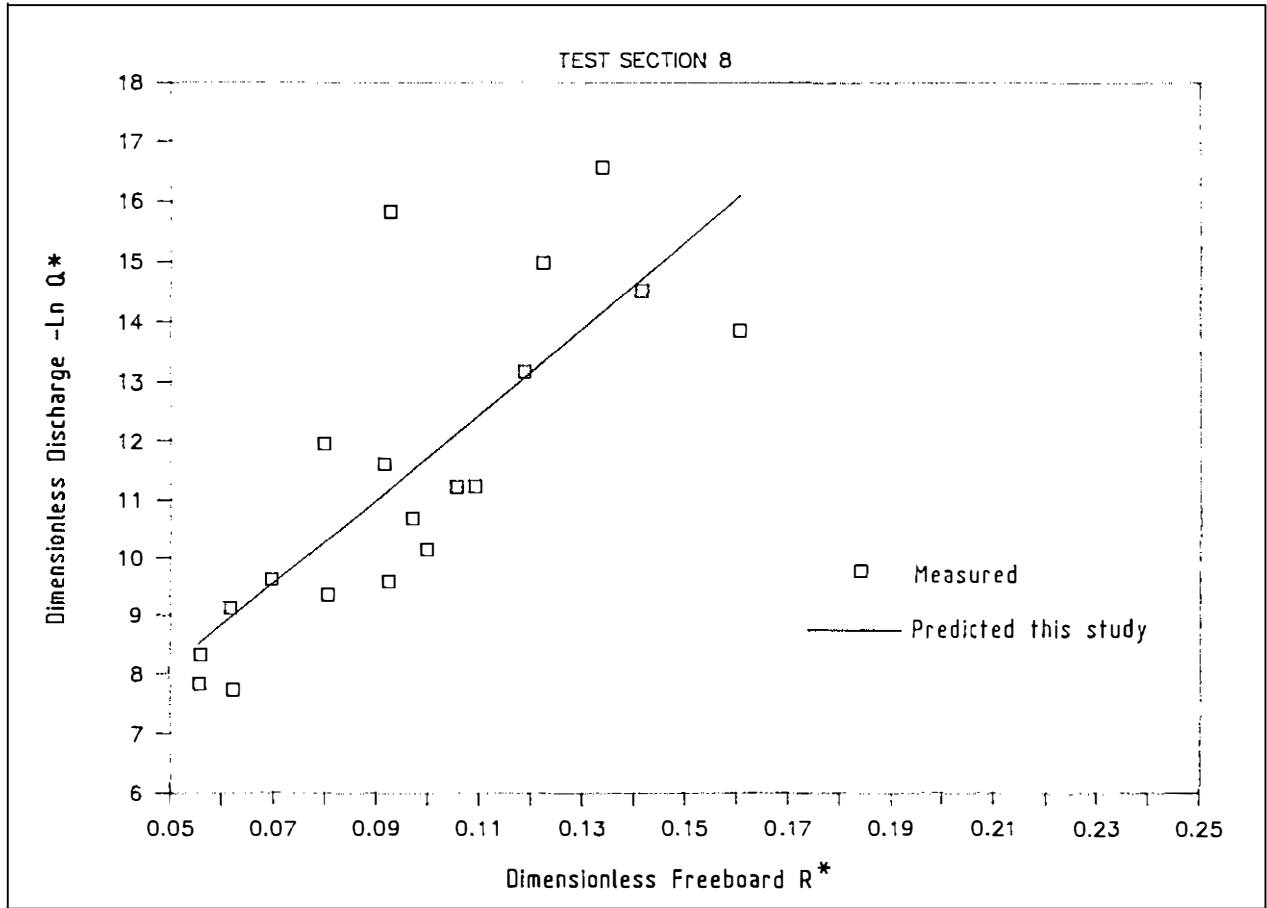


Fig 11 Test section 8 R^* vs $-\ln Q^*$

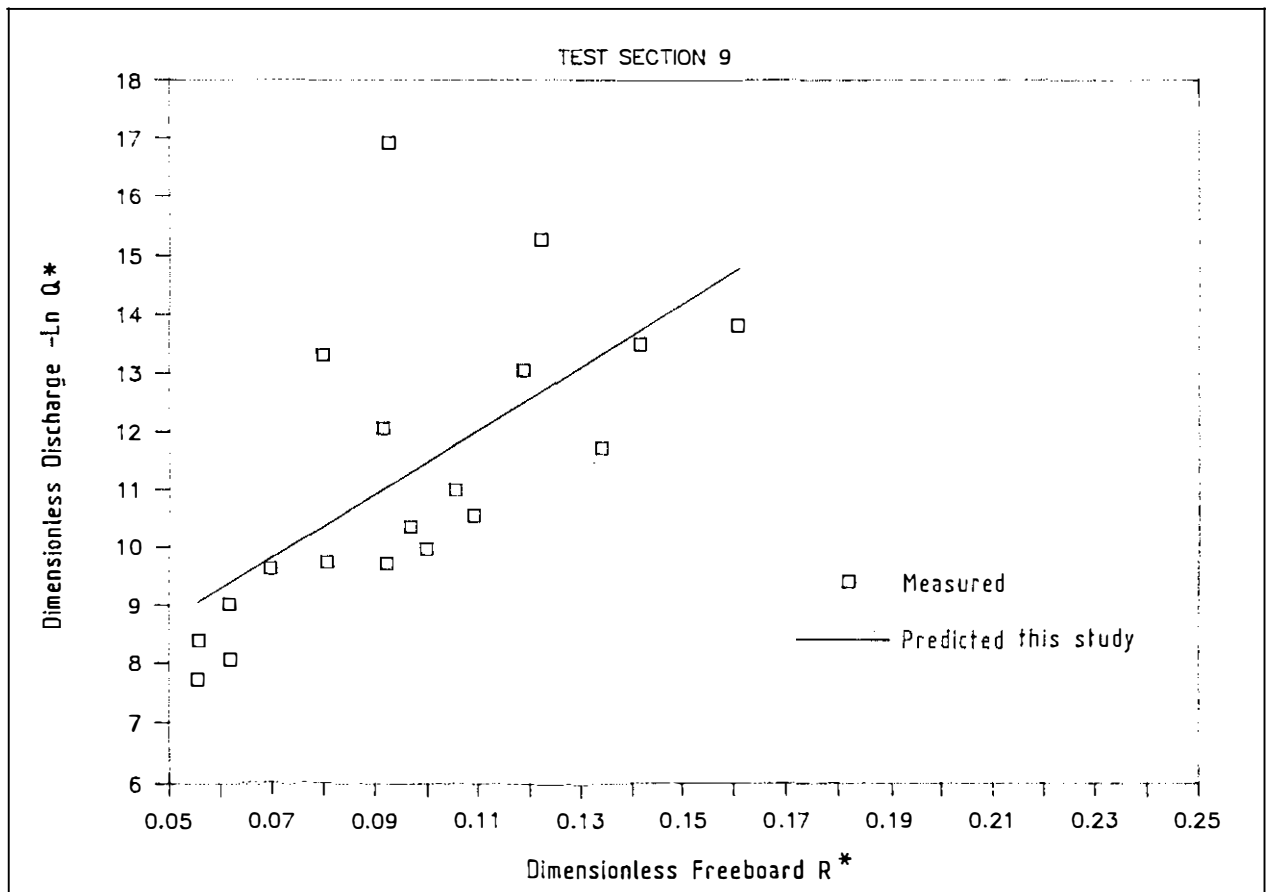


Fig 12 Test section 9 R^* vs $-\ln Q^*$

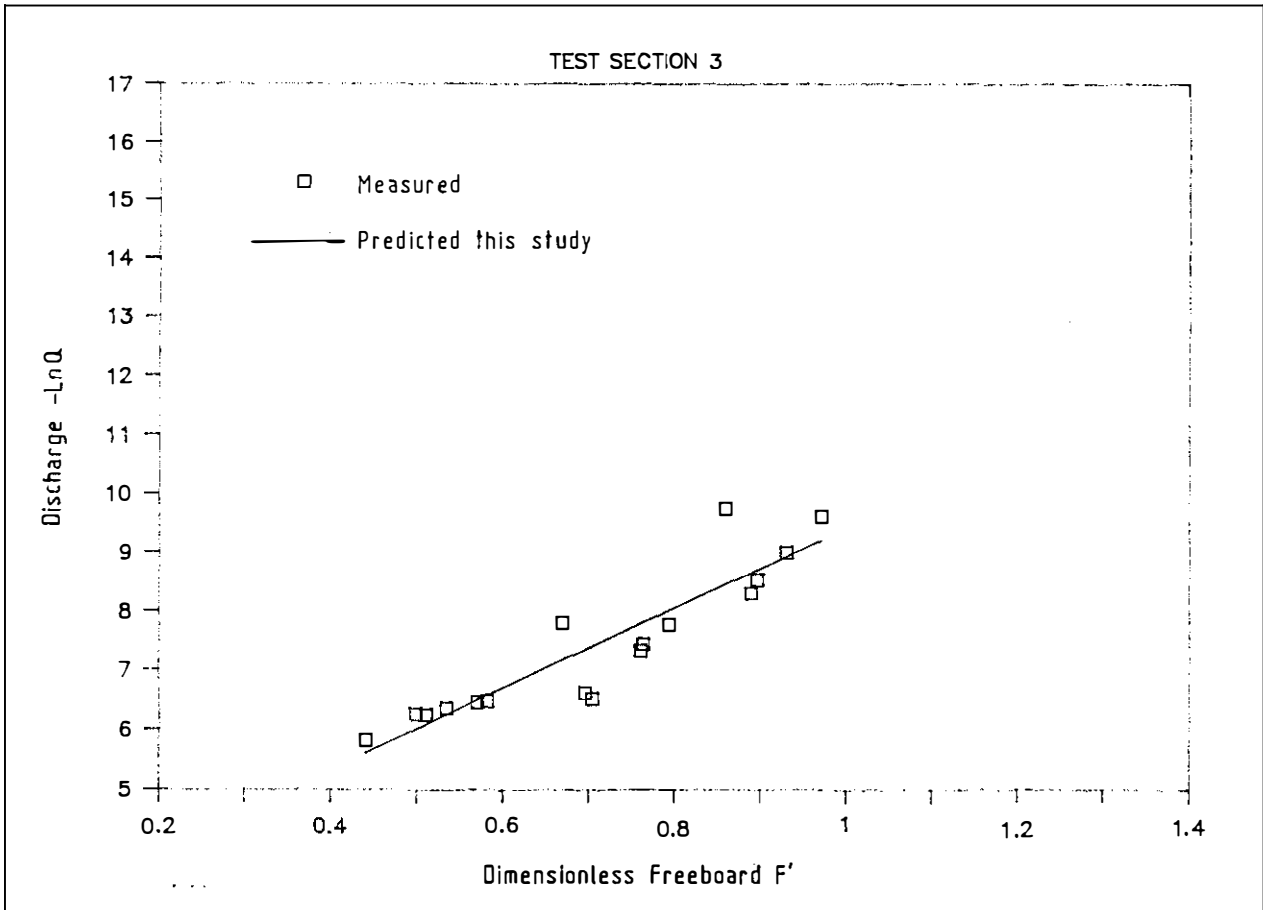


Fig 13 Test section 3 F' vs Q

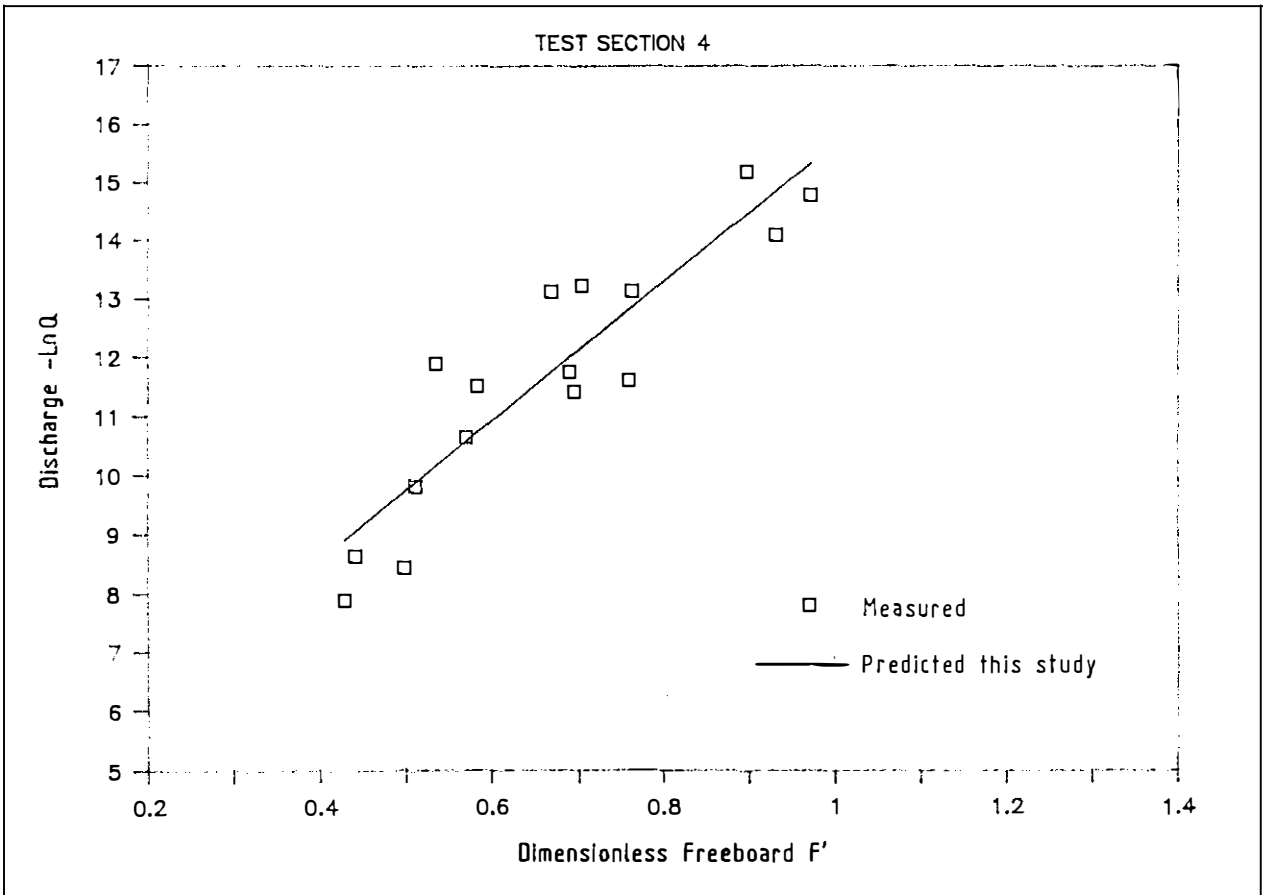


Fig 14 Test section 4 F' vs Q

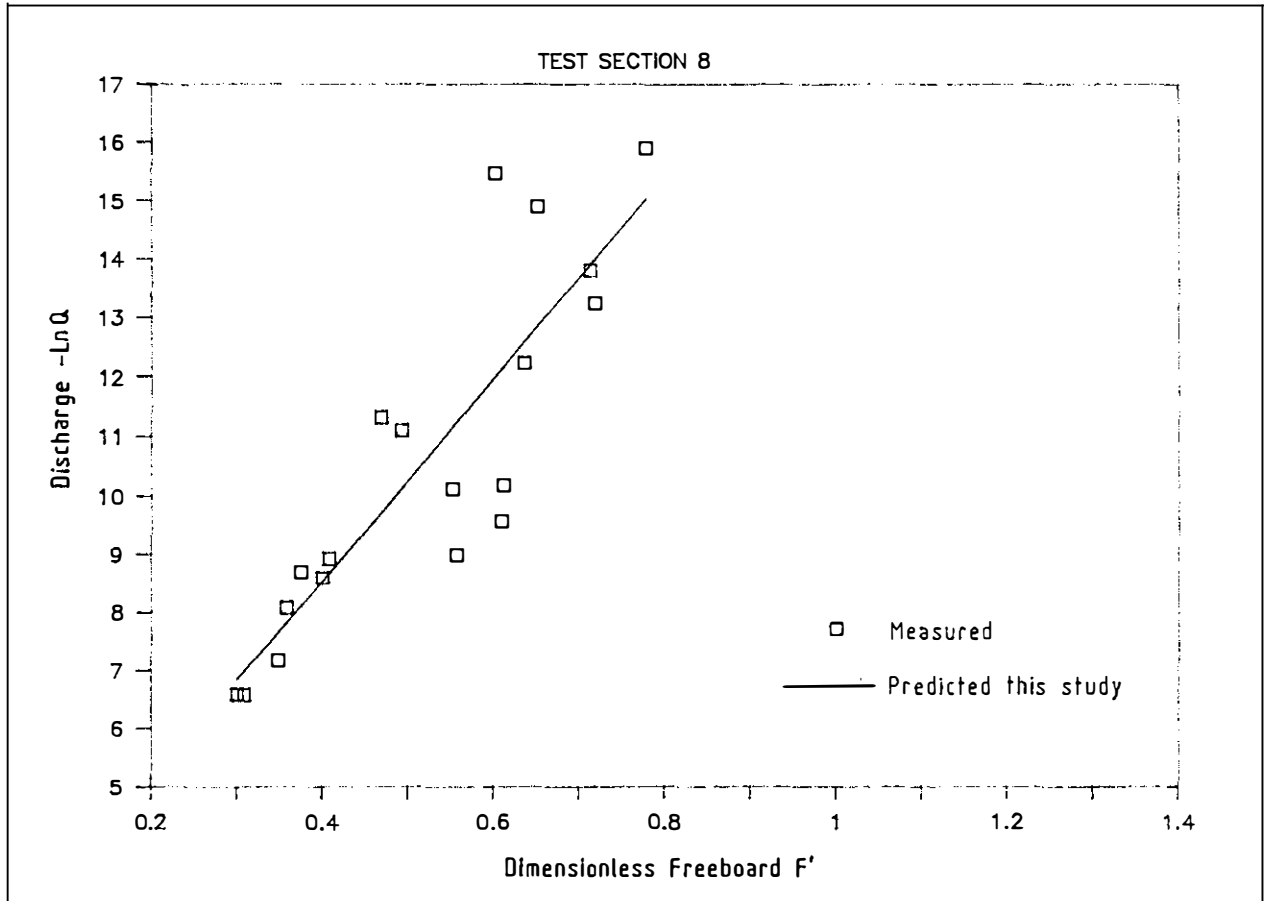


Fig 15 Test section 8 F' vs Q

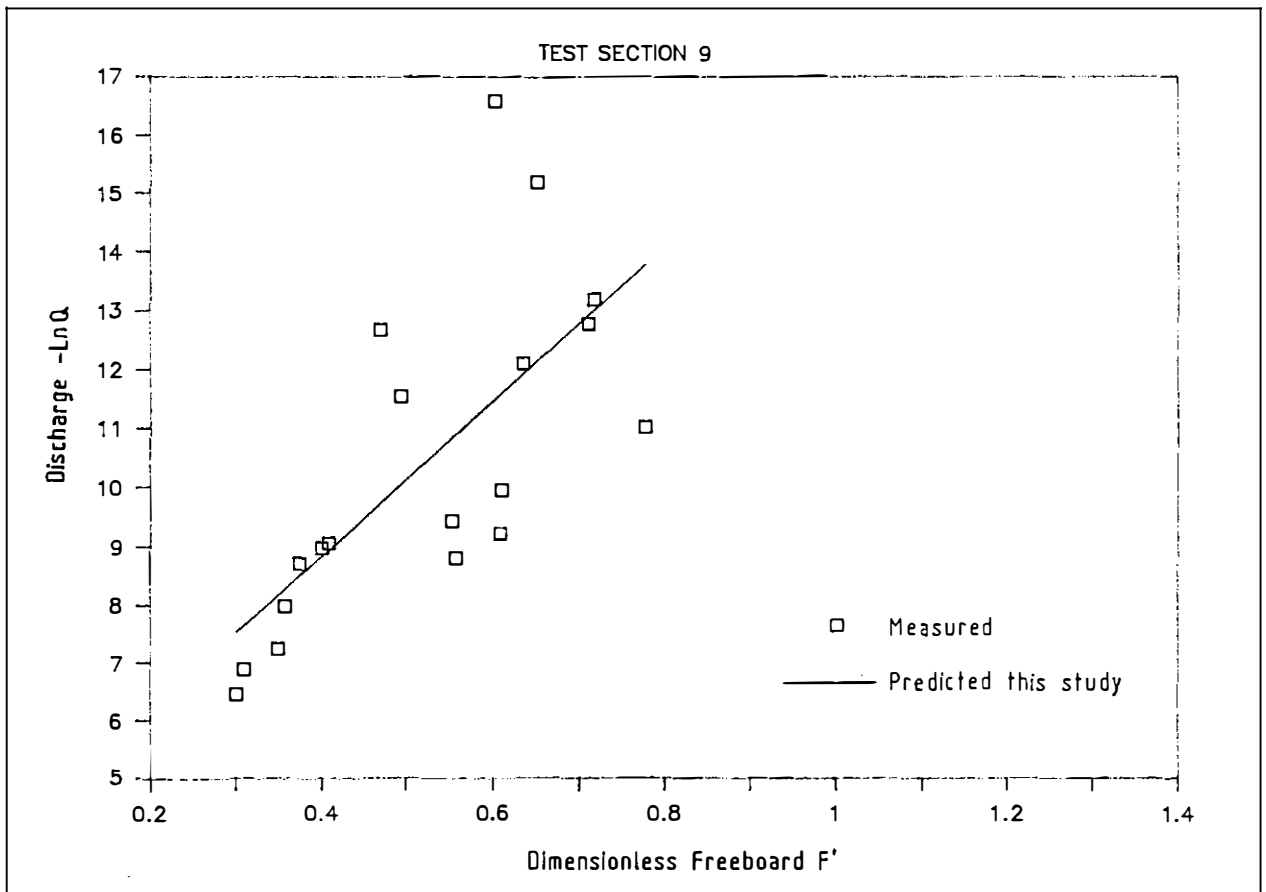


Fig 16 Test section 9 F' vs Q

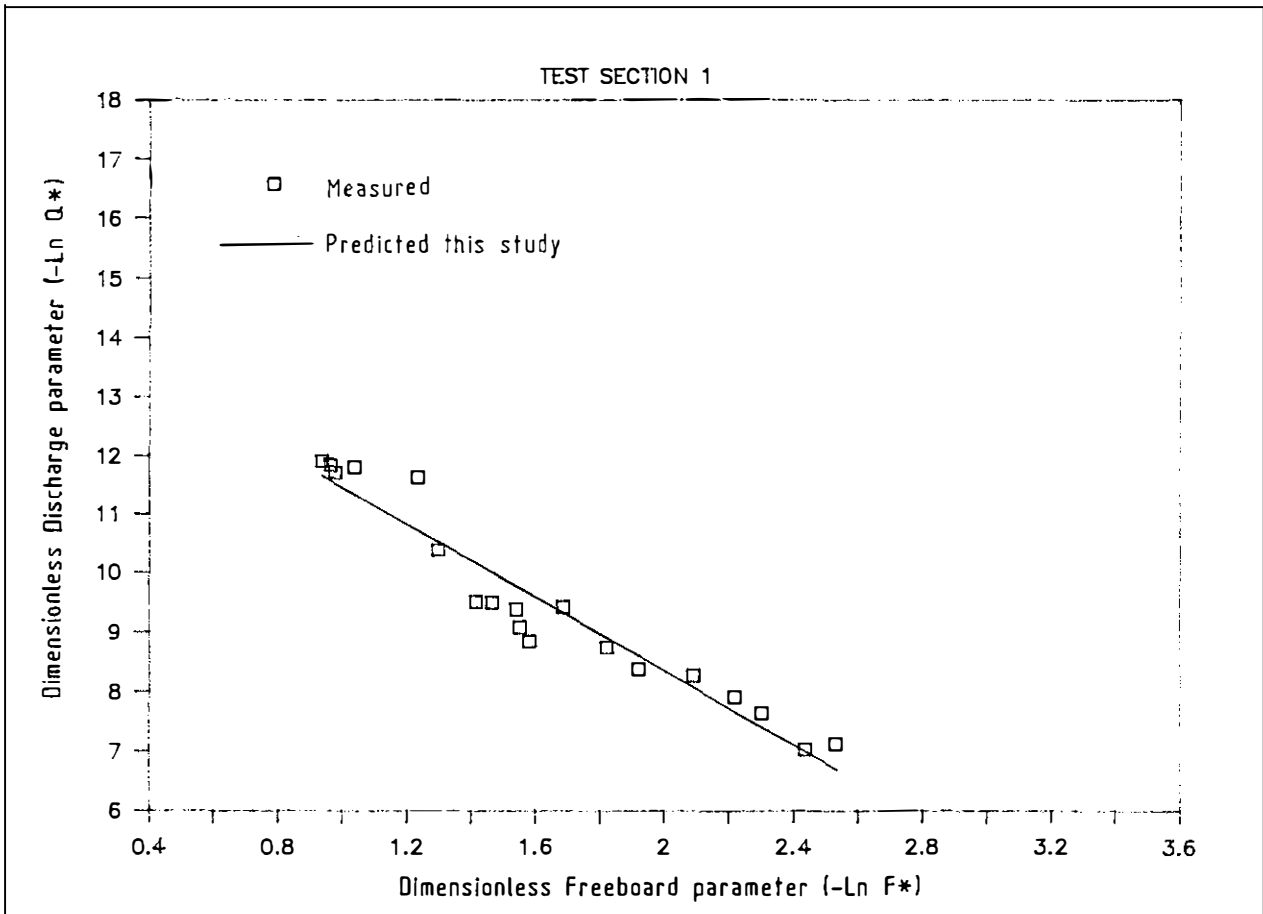


Fig 17 Test section 1 $-\ln F^*$ vs $-\ln Q^*$

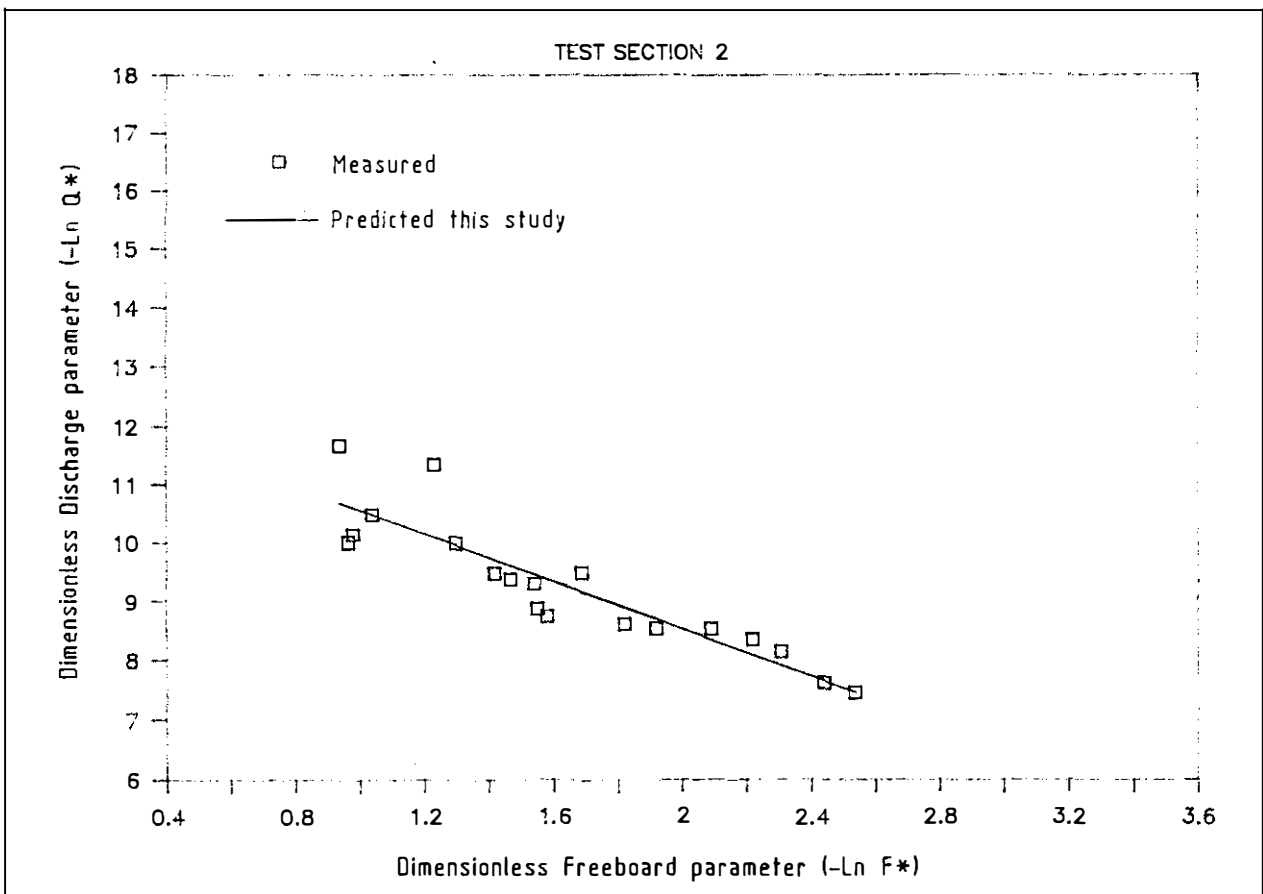


Fig 18 Test section 2 $-\ln F^*$ vs $-\ln Q^*$

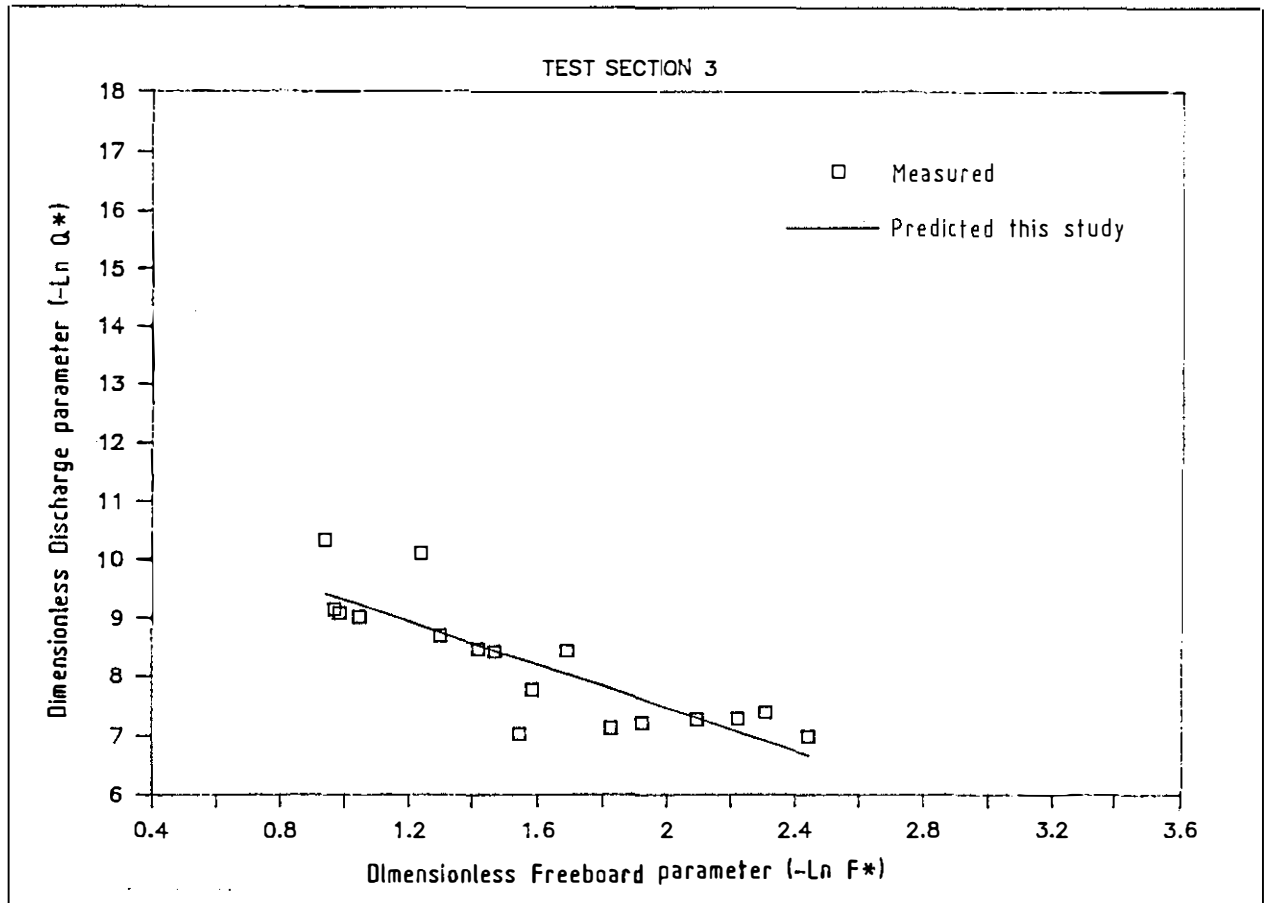


Fig 19 Test section 3- $-\ln F^*$ vs $-\ln Q^*$

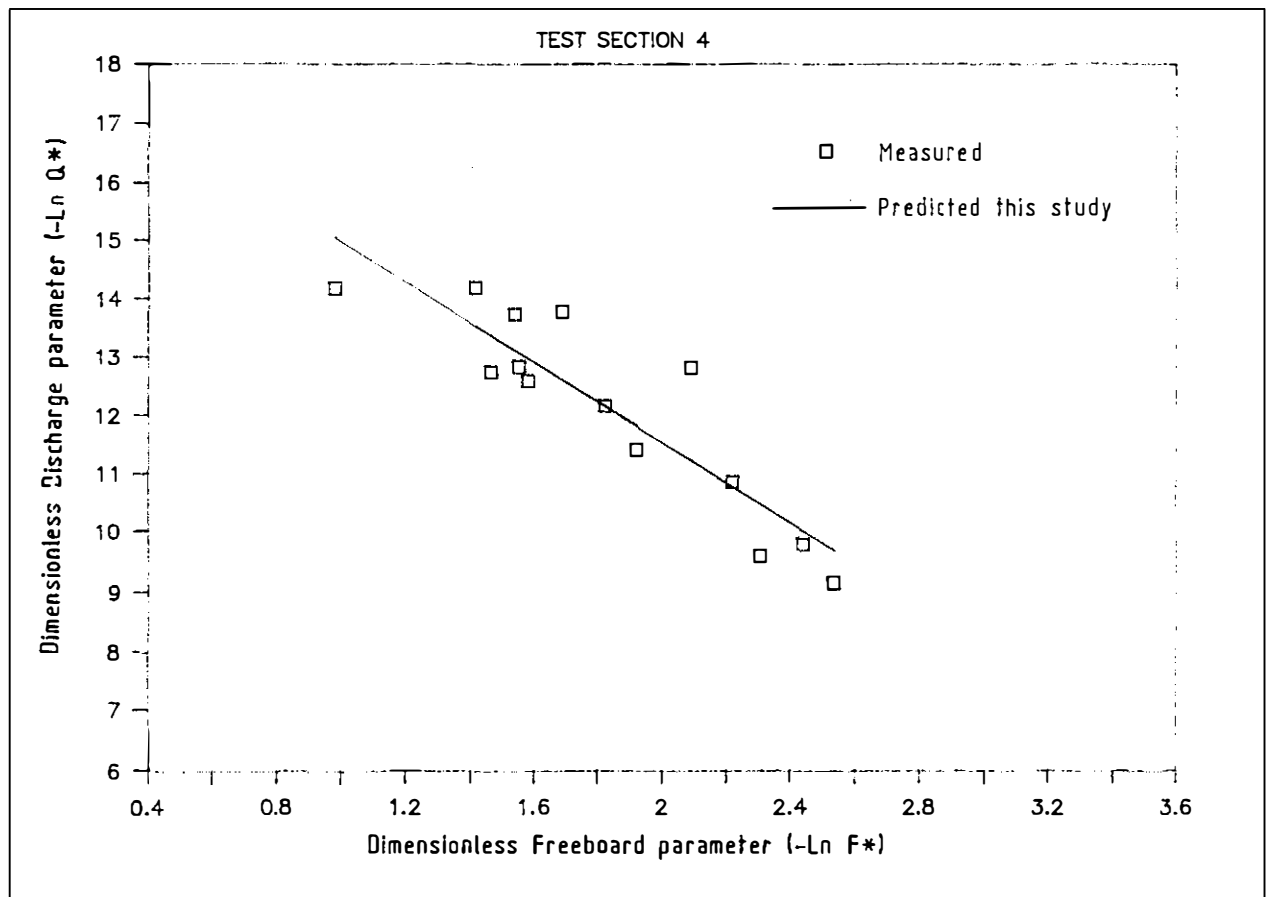


Fig 20 Test section 4 $-\ln F^*$ vs $-\ln Q^*$

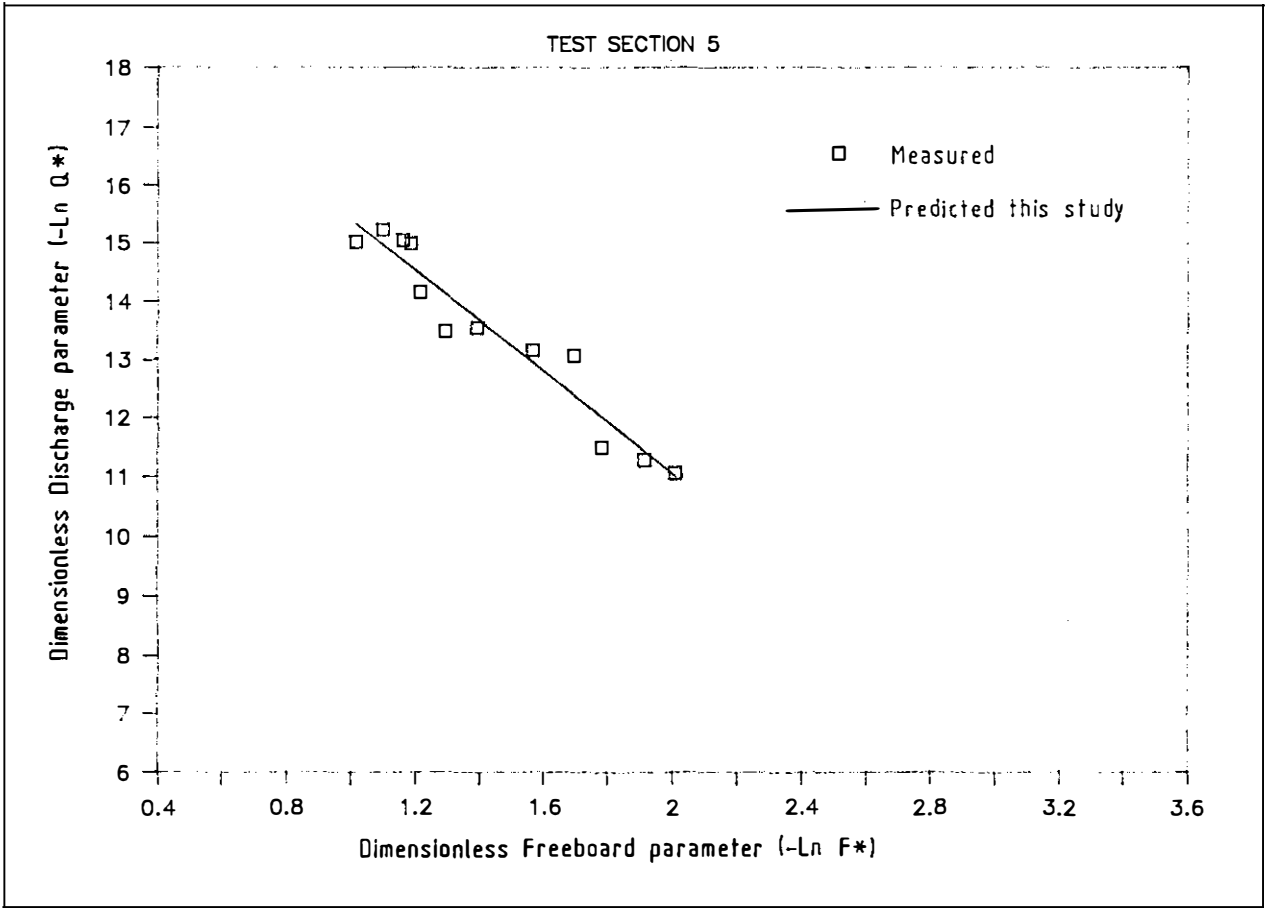


Fig 21 Test section 5 $-\ln F^*$ vs $-\ln Q^*$

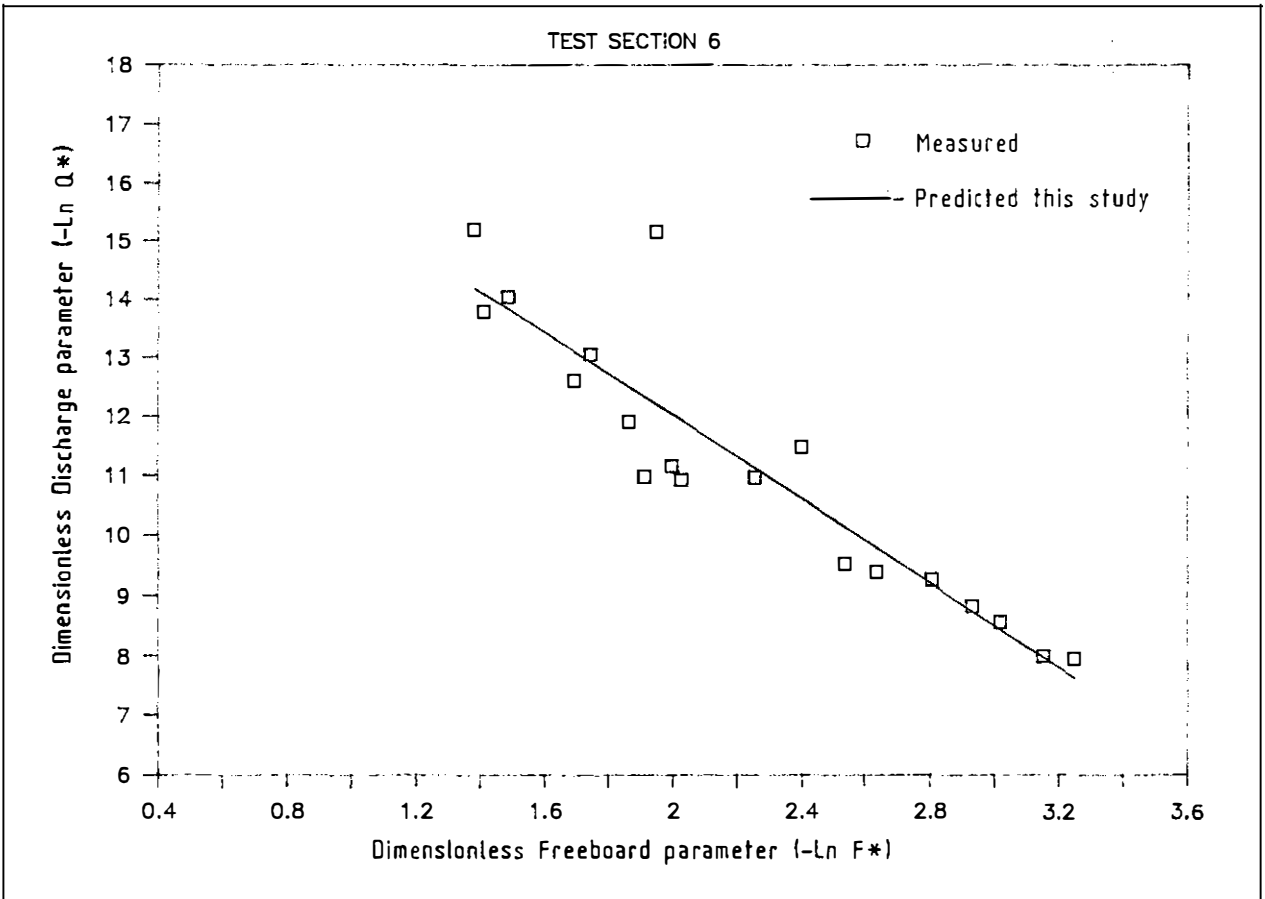


Fig 22 Test section 6 $-\ln F^*$ vs $-\ln Q^*$

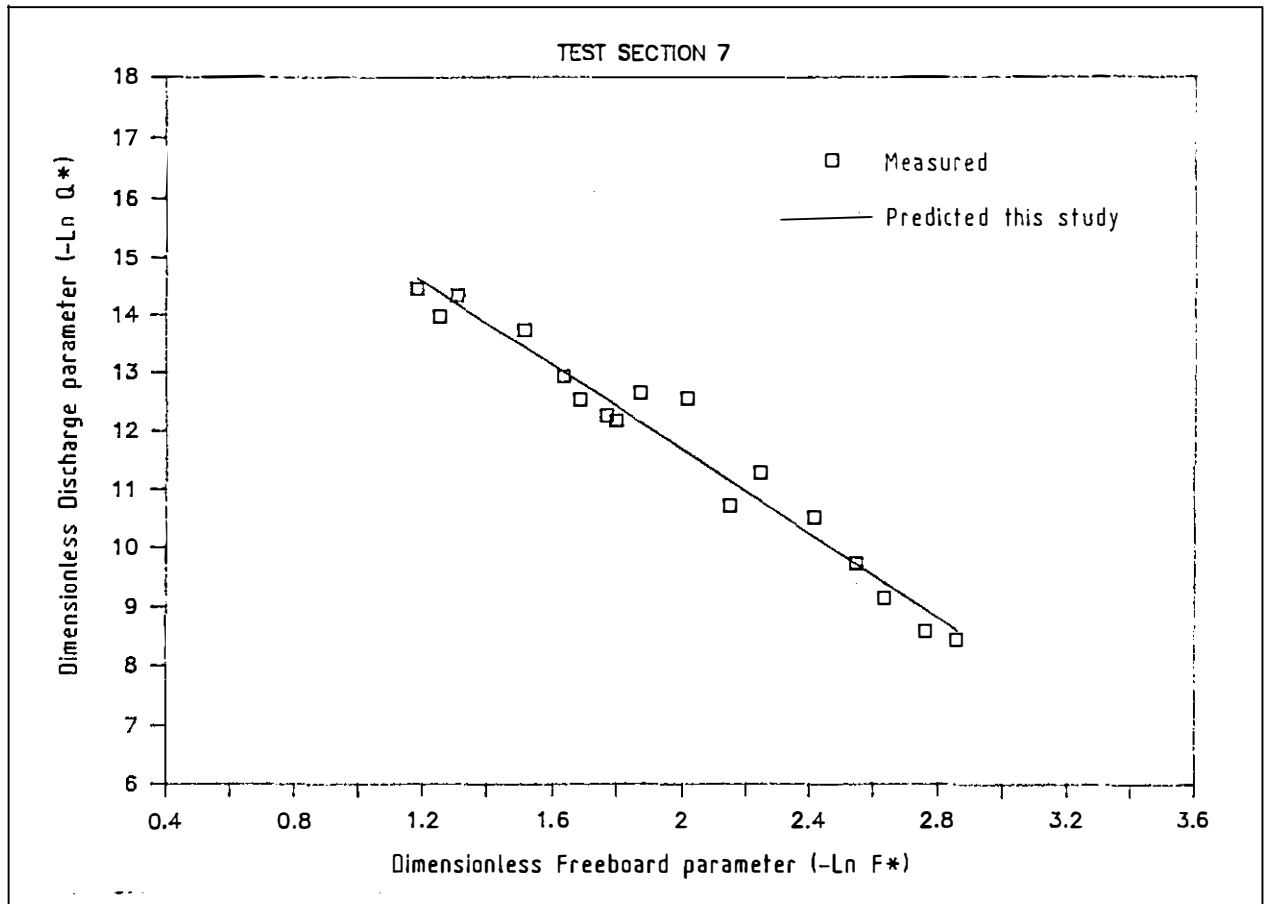


Fig 23 Test section 7 $-\ln F^*$ vs $-\ln Q^*$

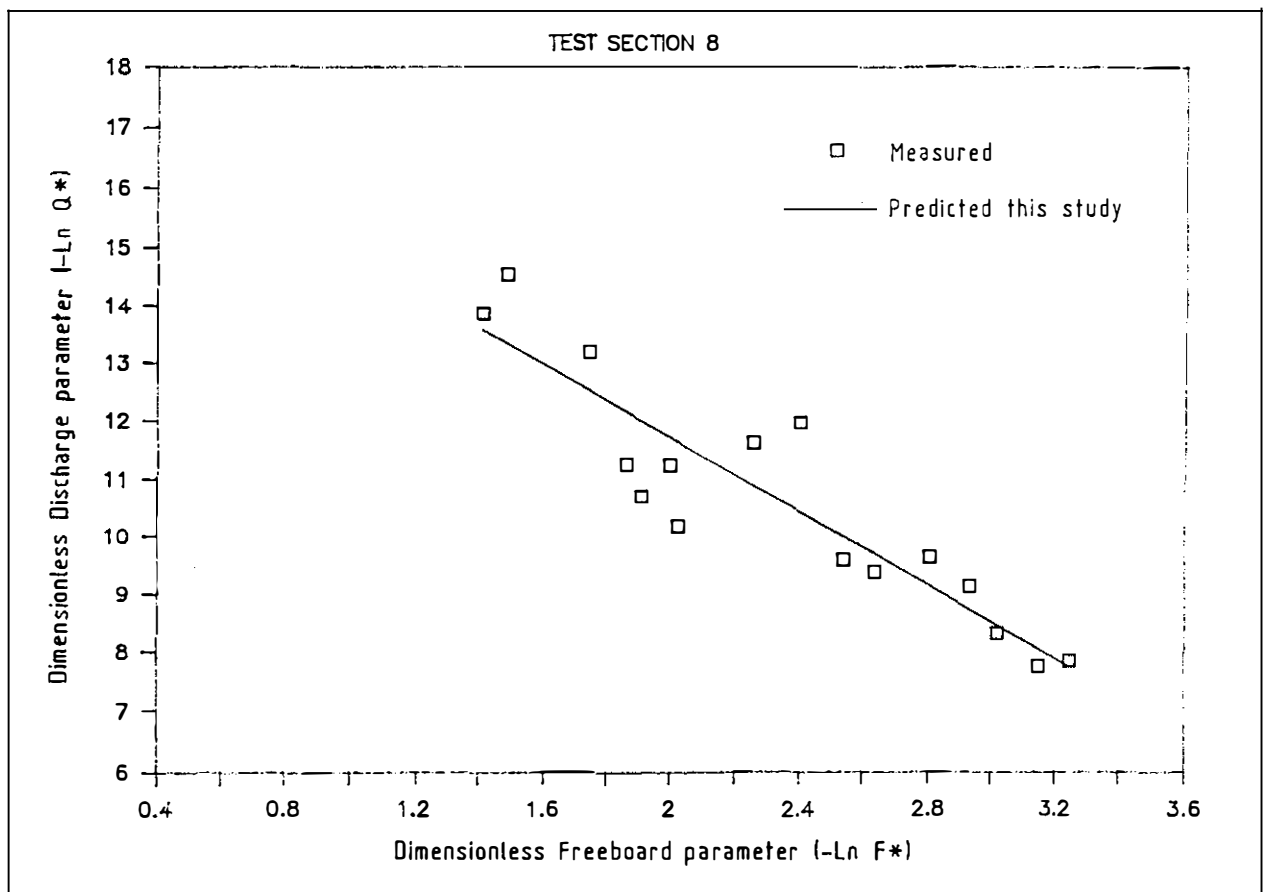


Fig 24 Test section 8 $-\ln F^*$ vs $-\ln Q^*$

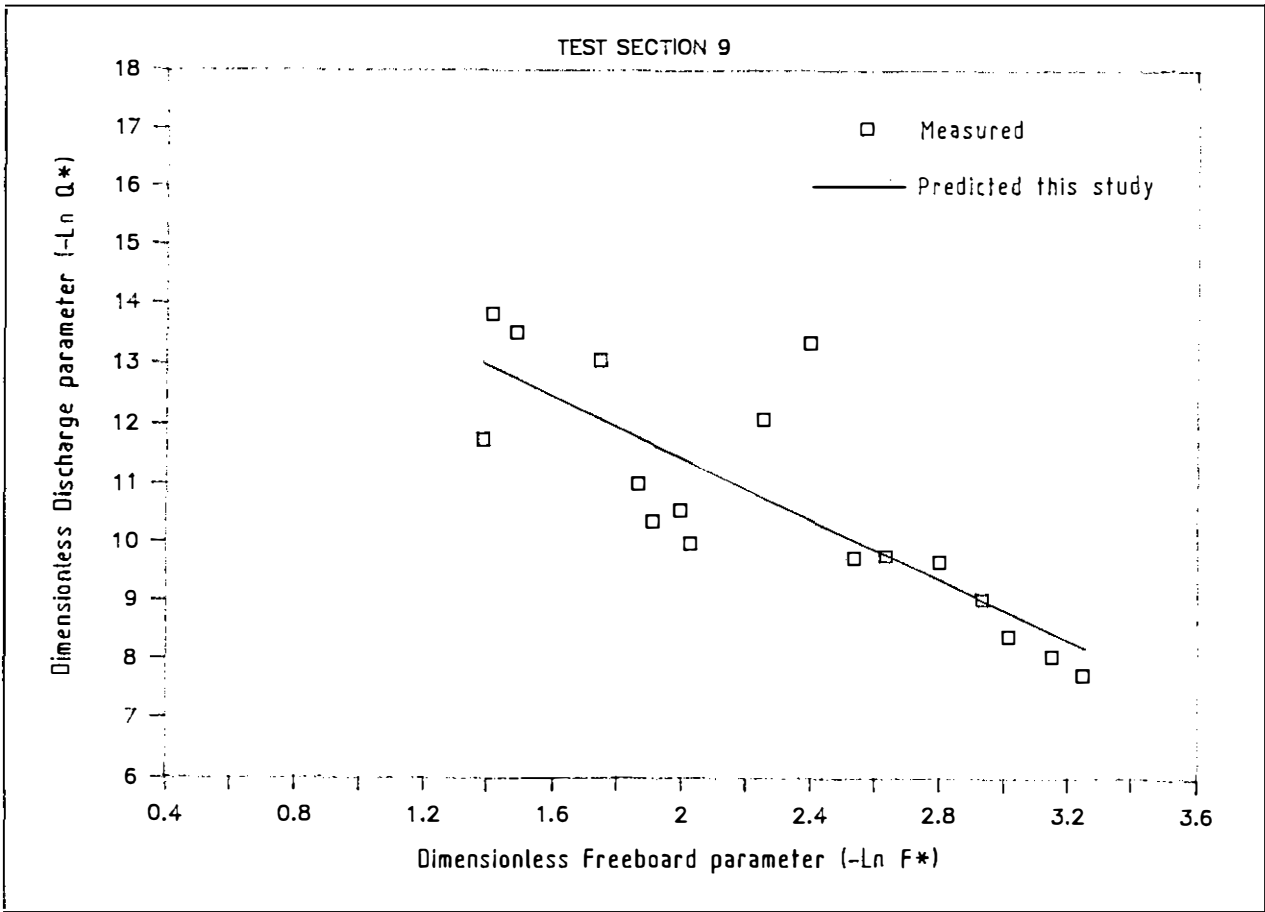


Fig 25 Test section 9 $-\ln F^*$ vs $-\ln Q^*$

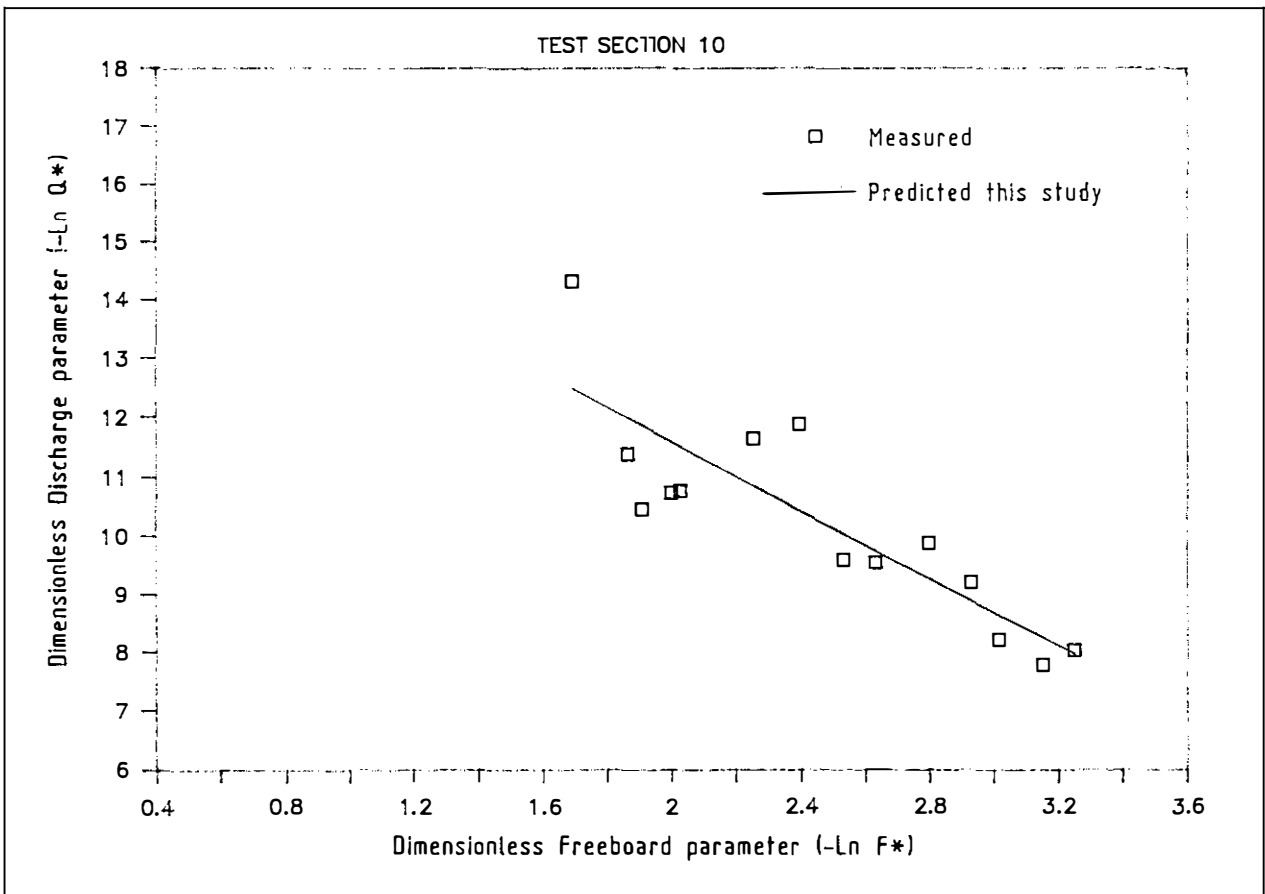


Fig 26 Test section 10 $-\ln F^*$ vs $-\ln Q^*$

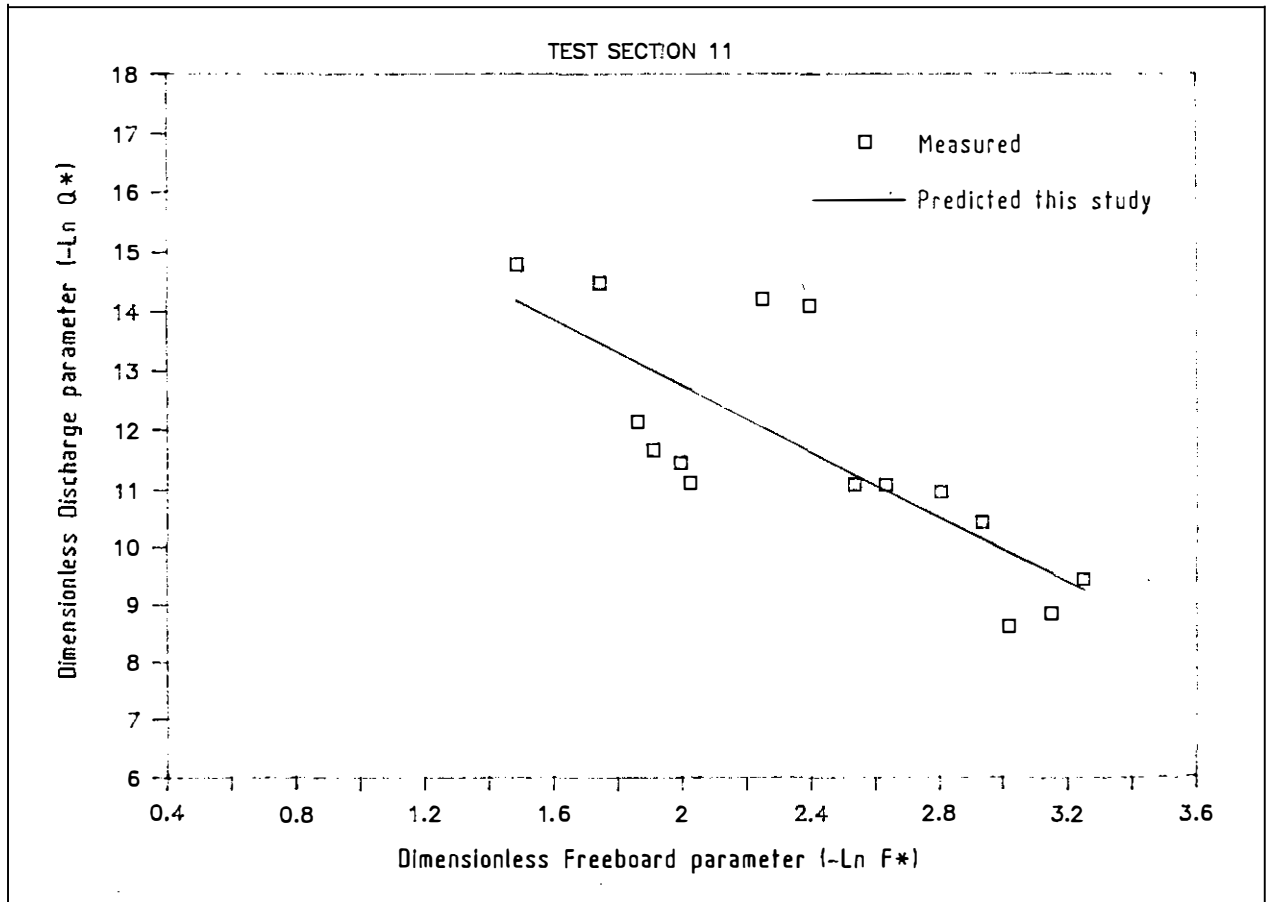


Fig 27 Test section 11 $-\ln F^*$ vs $-\ln Q^*$

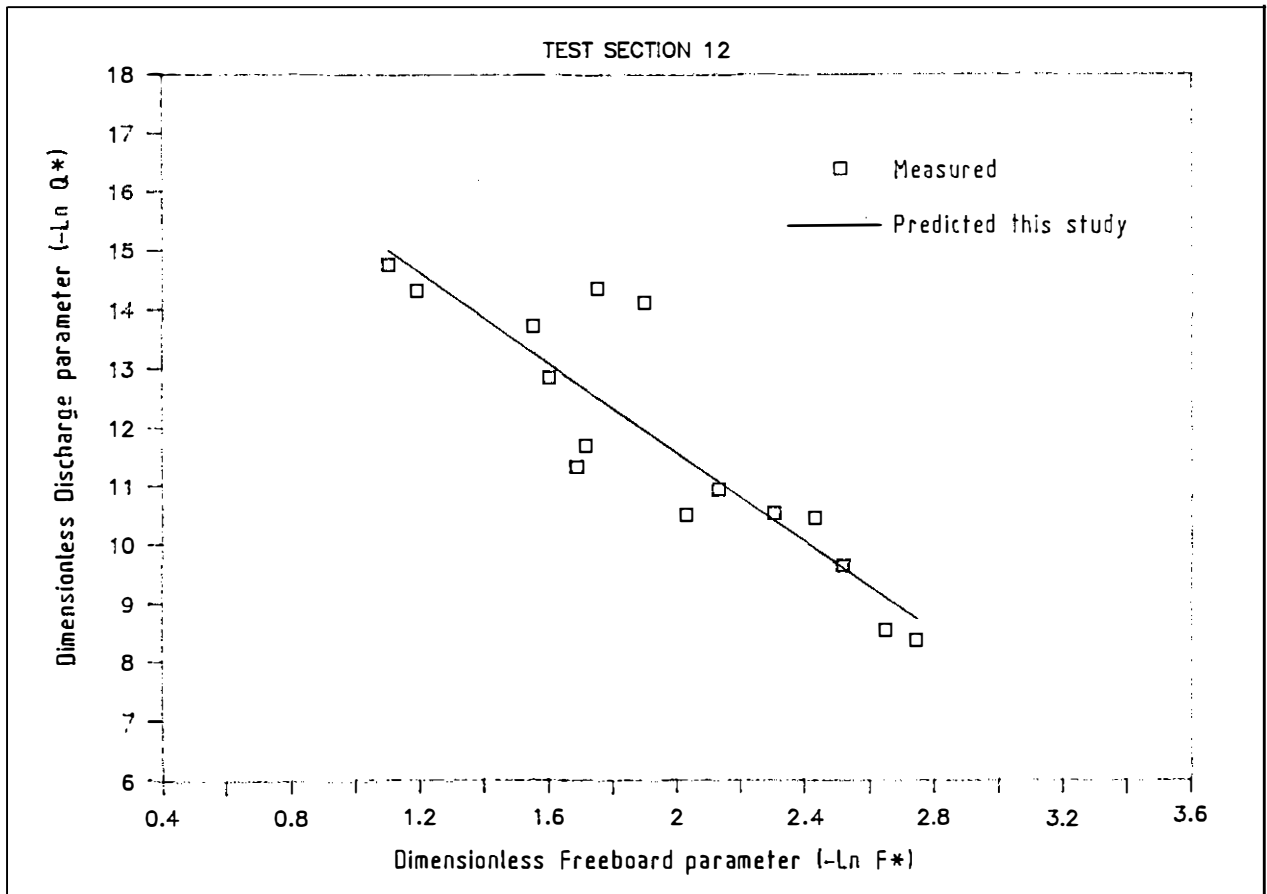


Fig 28 Test section 12 $-\ln F^*$ vs $-\ln Q^*$

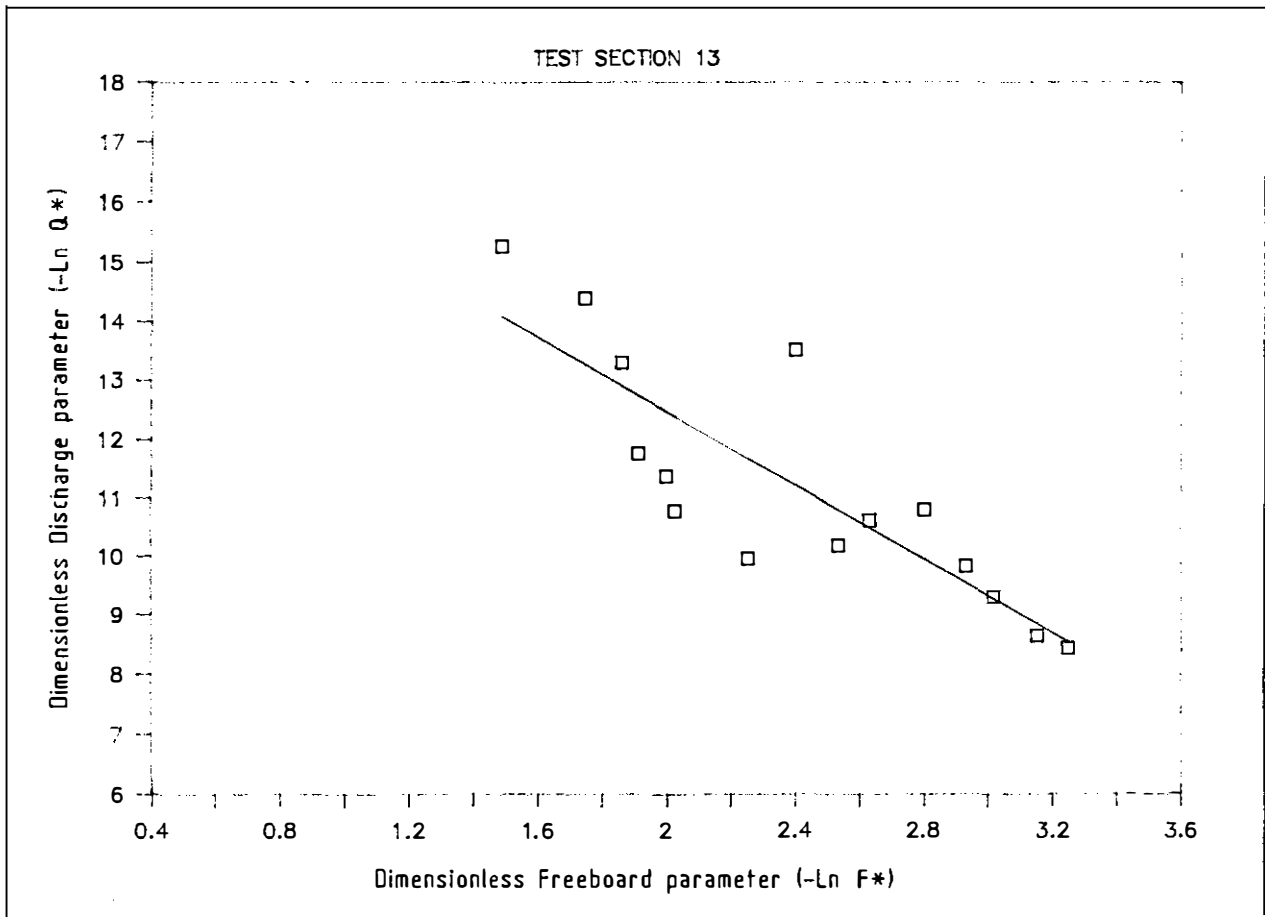


Fig 29 Test section 13 $-\ln F^*$ vs $-\ln Q^*$

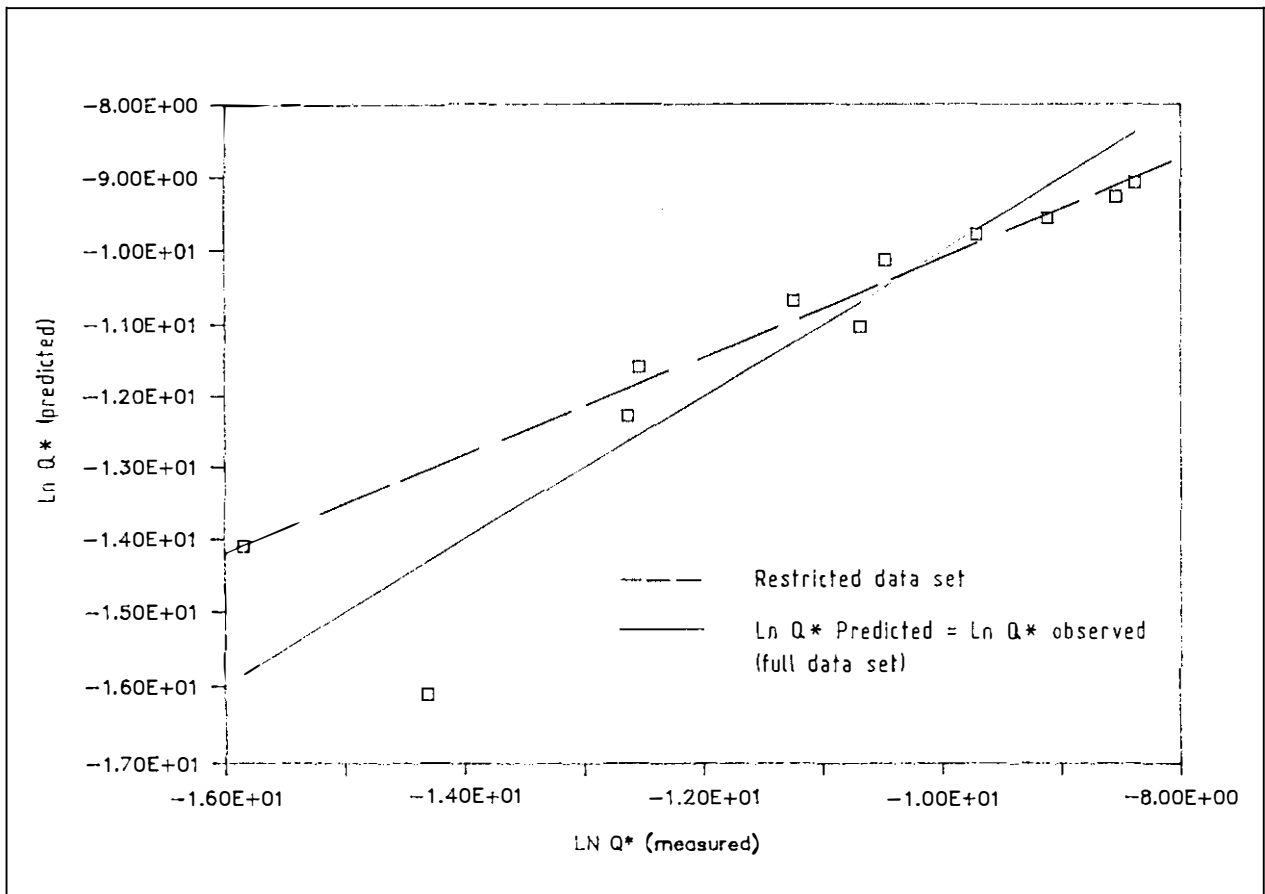
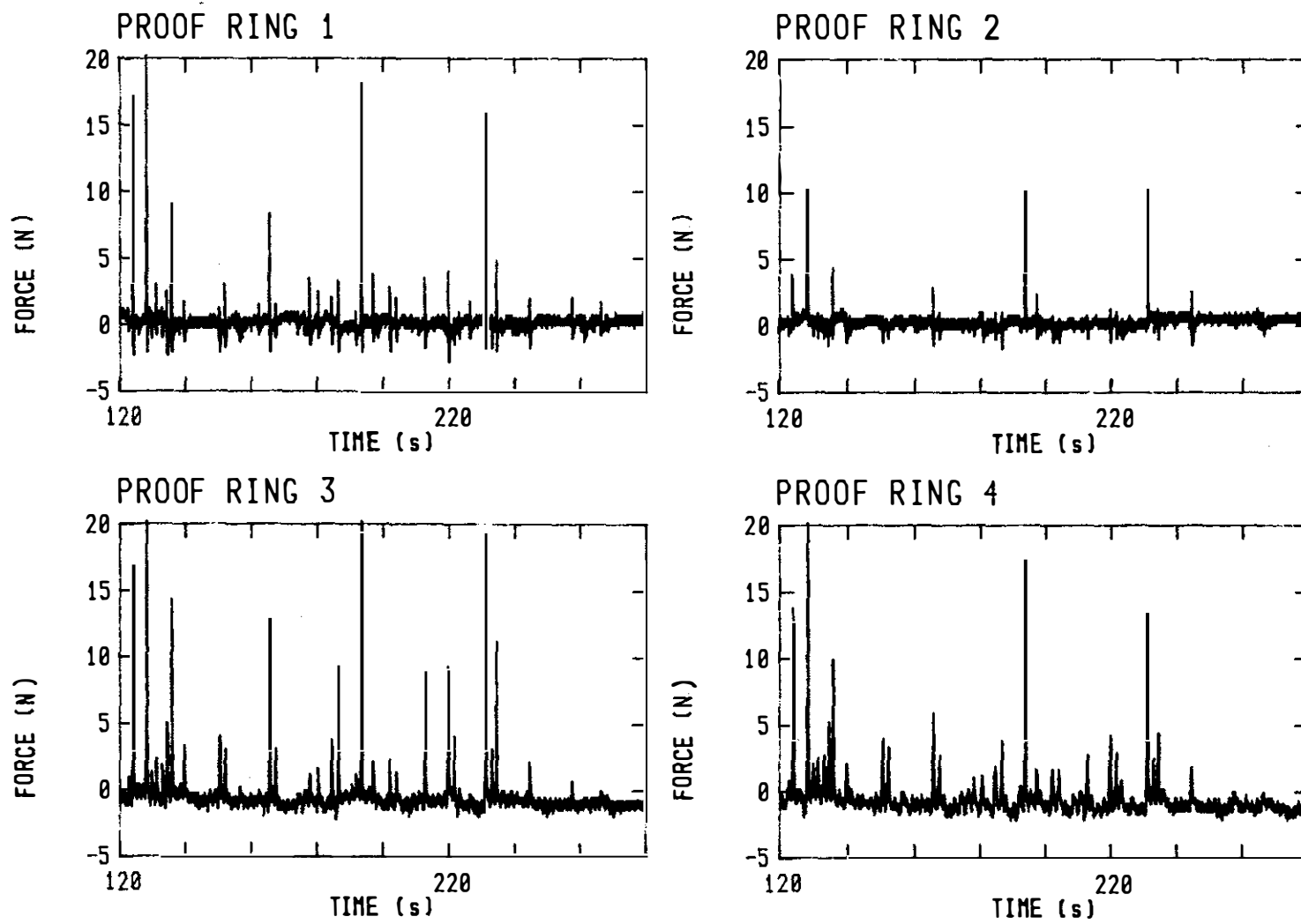


Fig 30 Comparison of measured and predicted discharges

Fig 31 Example of force table output signals



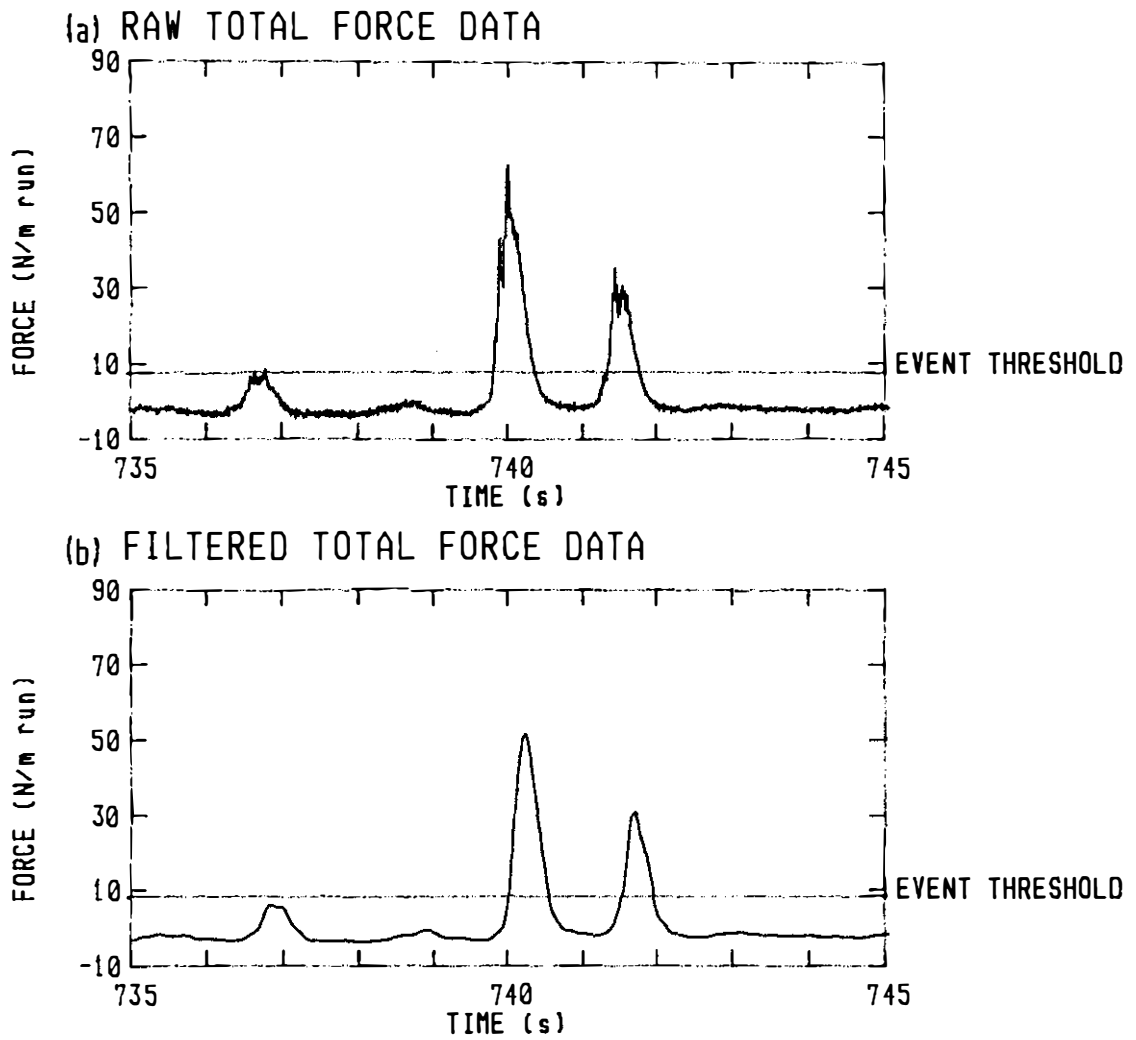


Fig 32 Example of derived total force time series

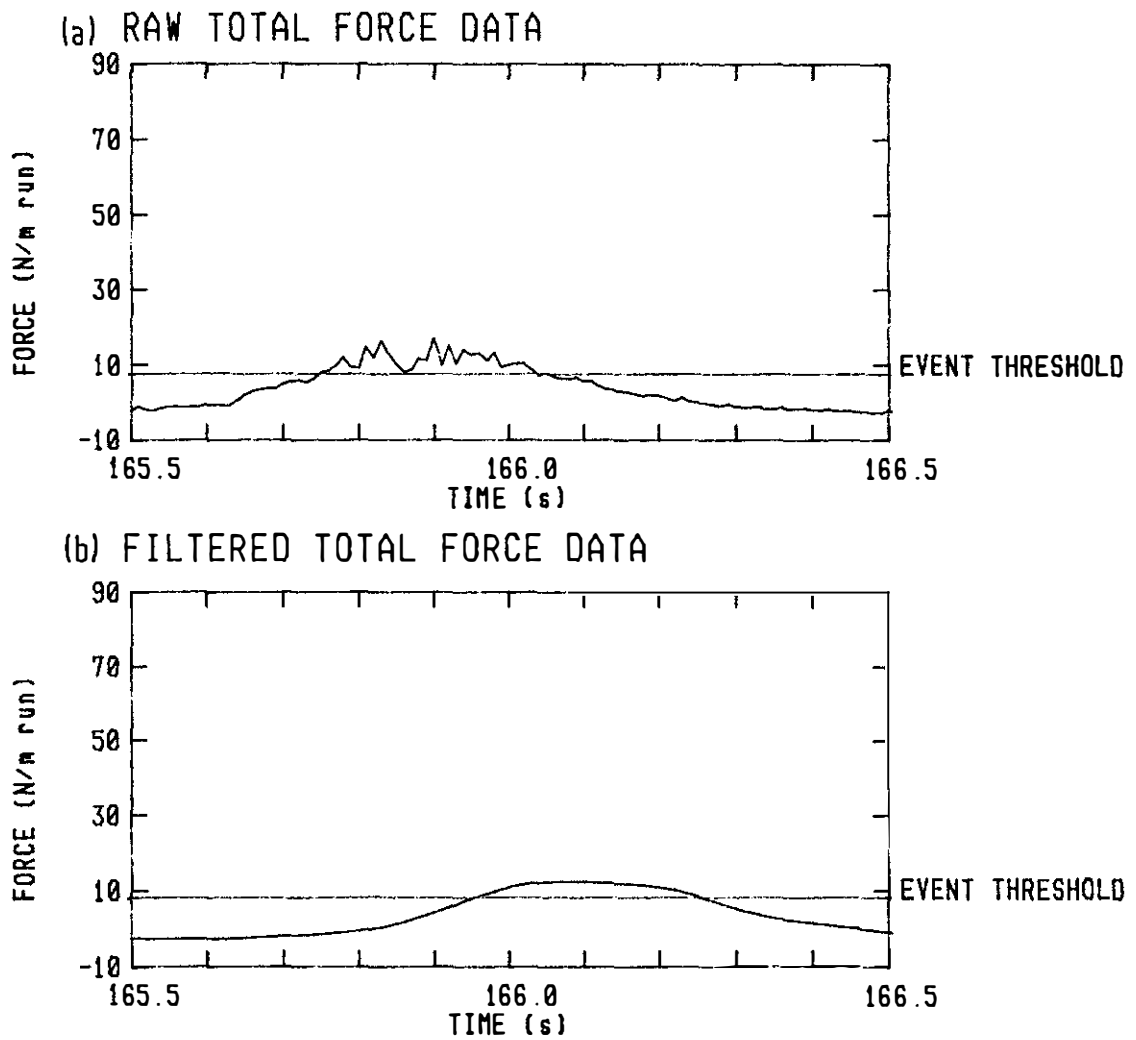


Fig 33 Example of multiple threshold crossing with raw data

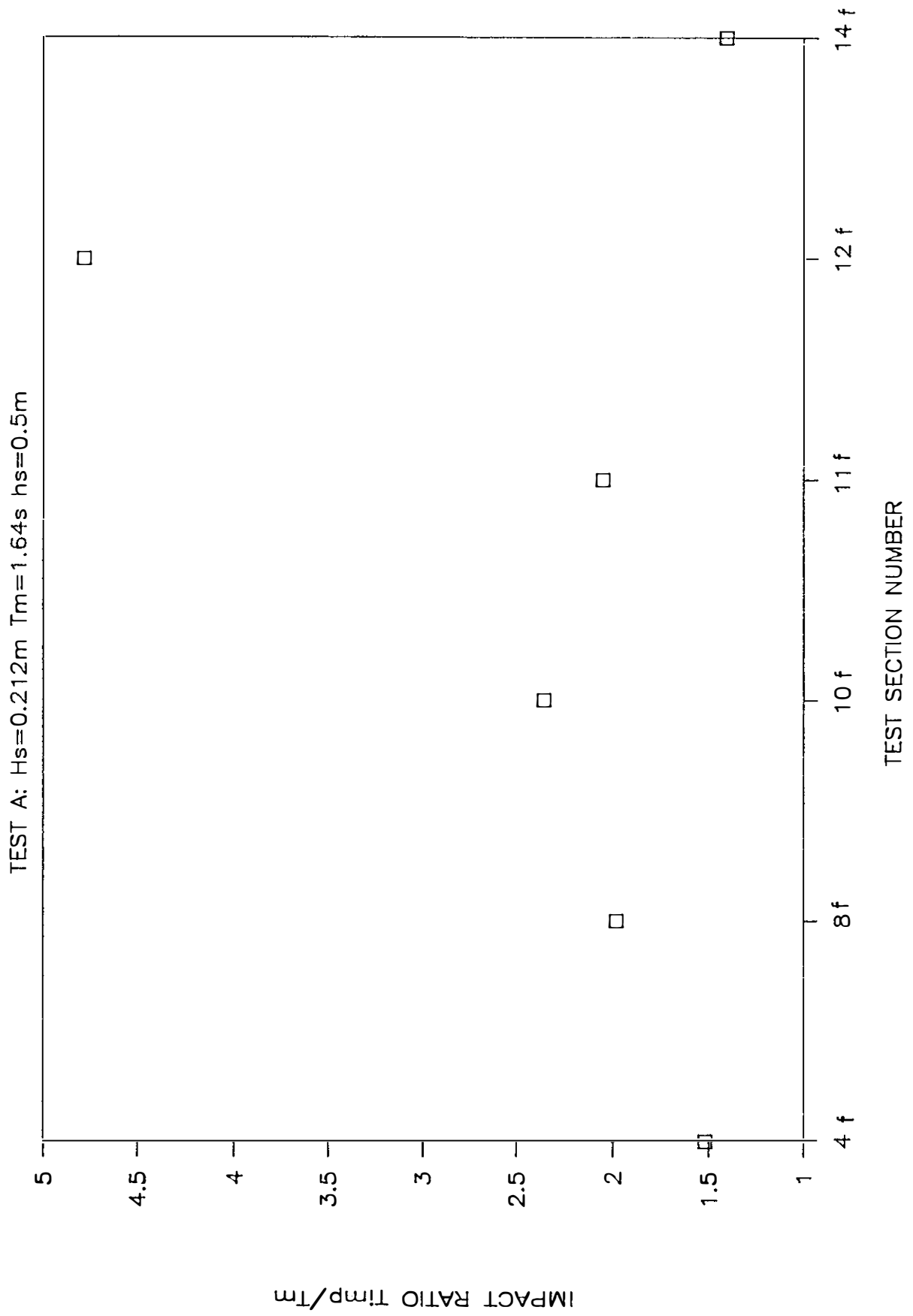


Fig 34 Influence of section geometry on impact ratio

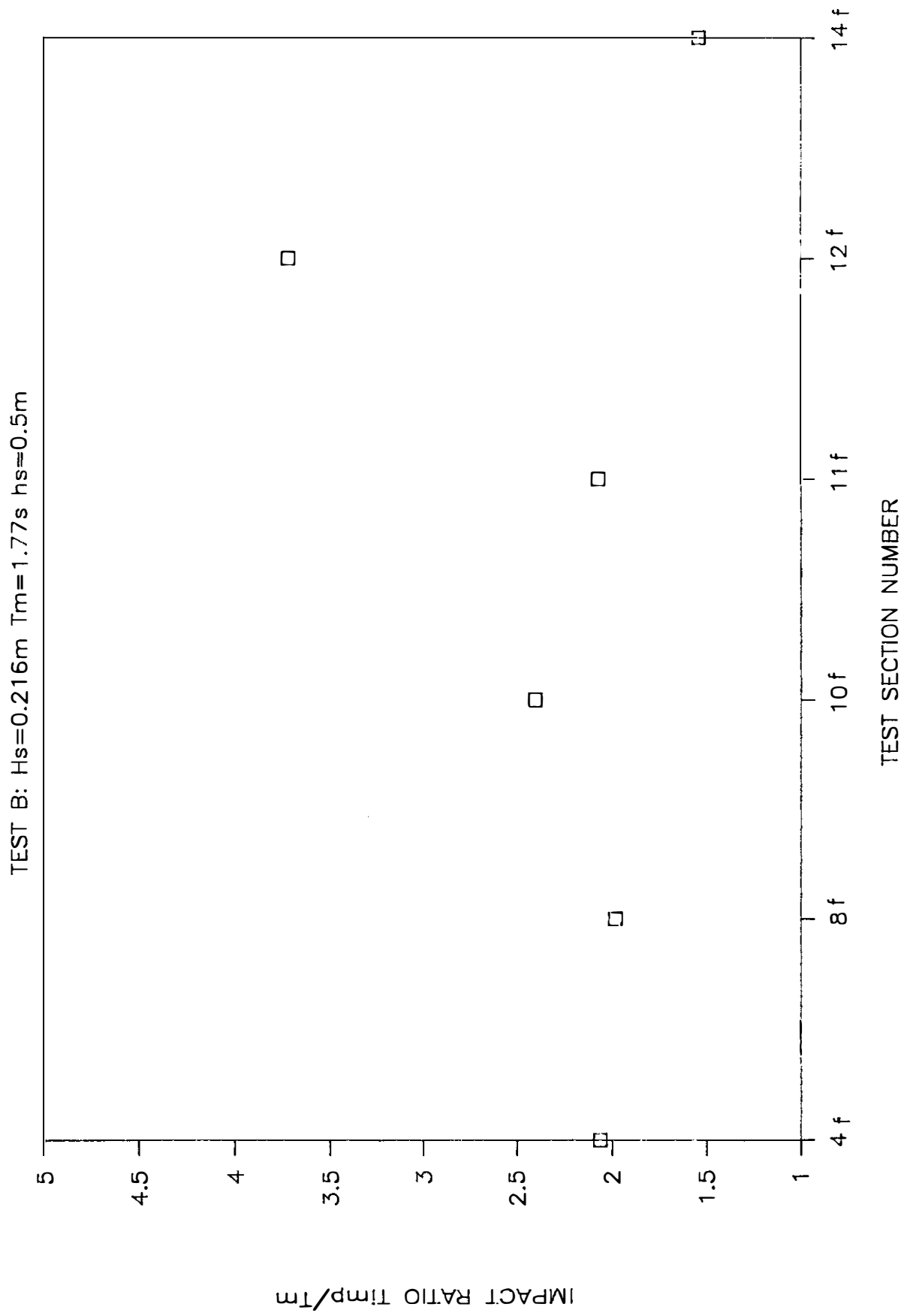


Fig 35 Influence of section geometry on impact ratio

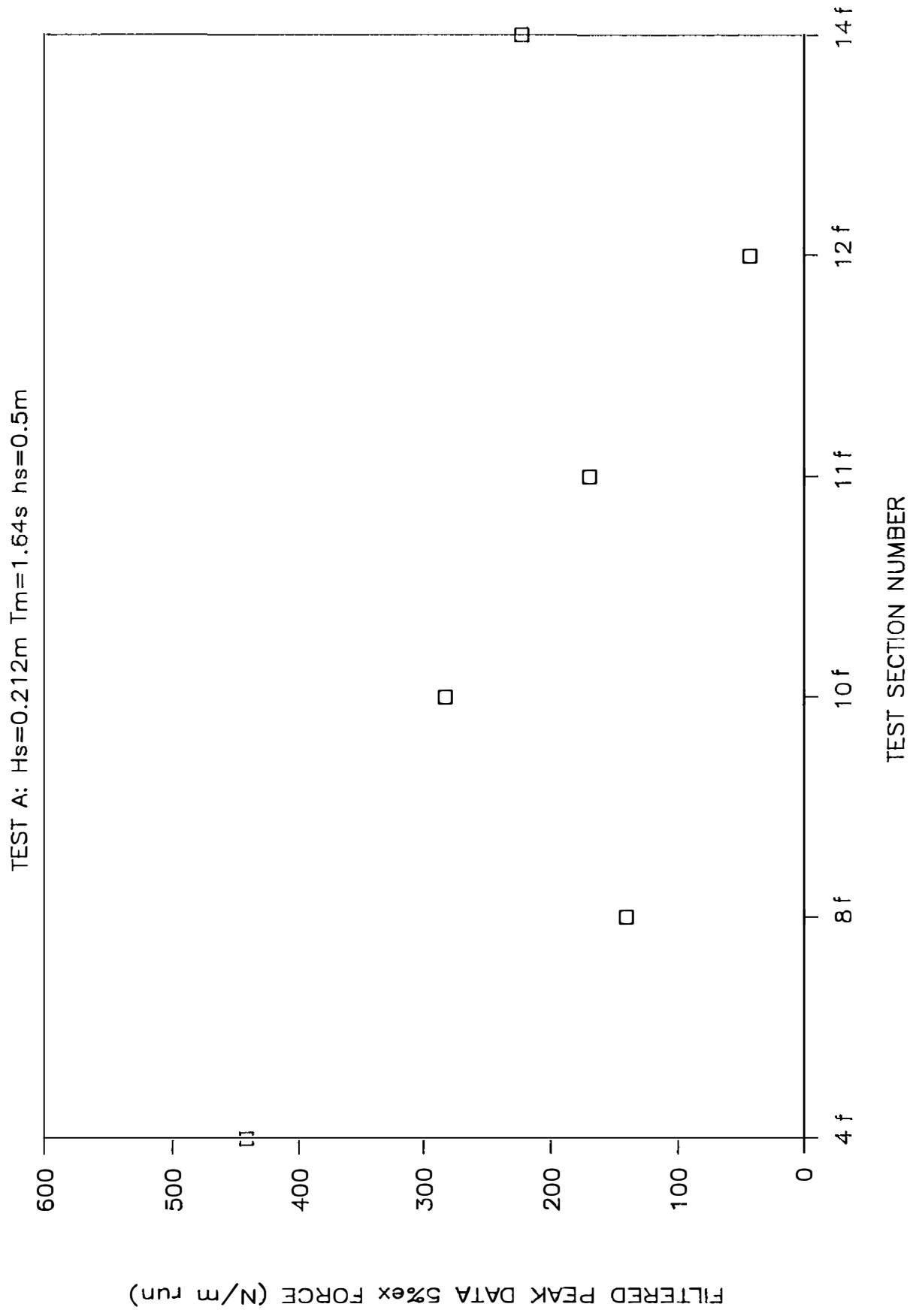


Fig 36 Influence of section geometry on filtered 5% exceedence force

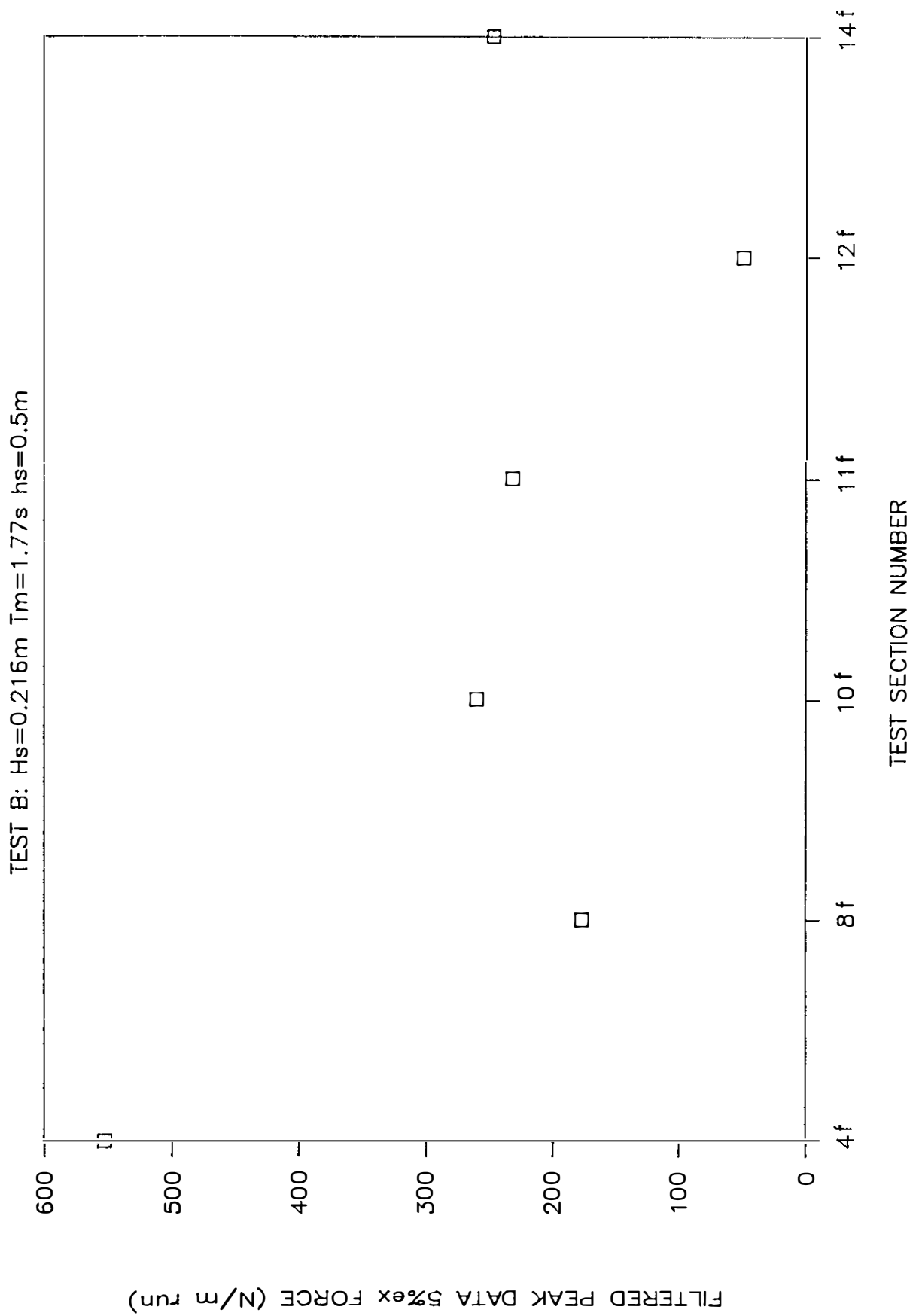


Fig 37 Influence of section geometry on filtered 5% exceedence force

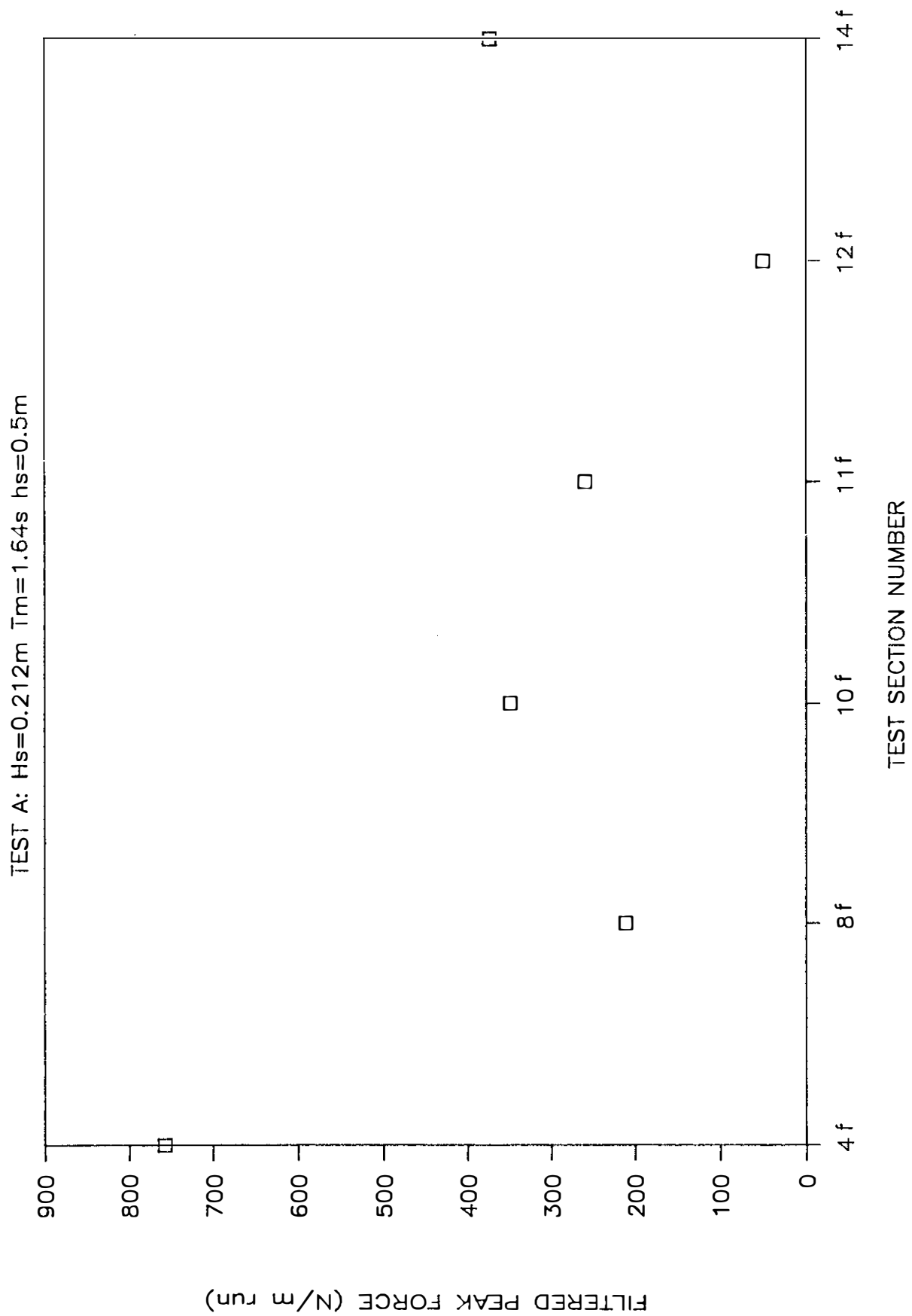


Fig 38 Influence of section geometry on filtered maximum force

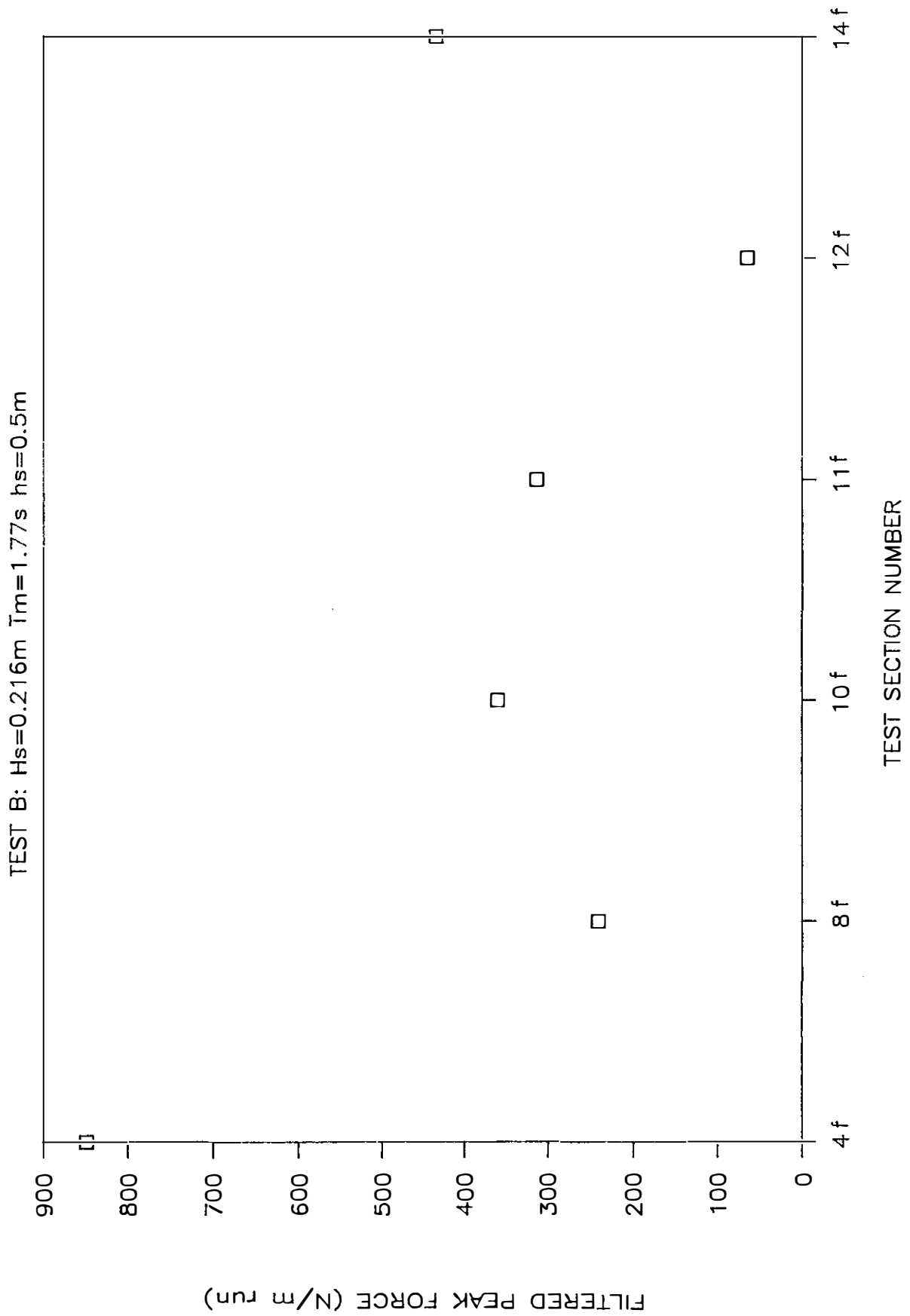


Fig 39 Influence of section geometry on filtered maximum force

Fig 40 Influence of T_m on filtered maximum force – constant H_s

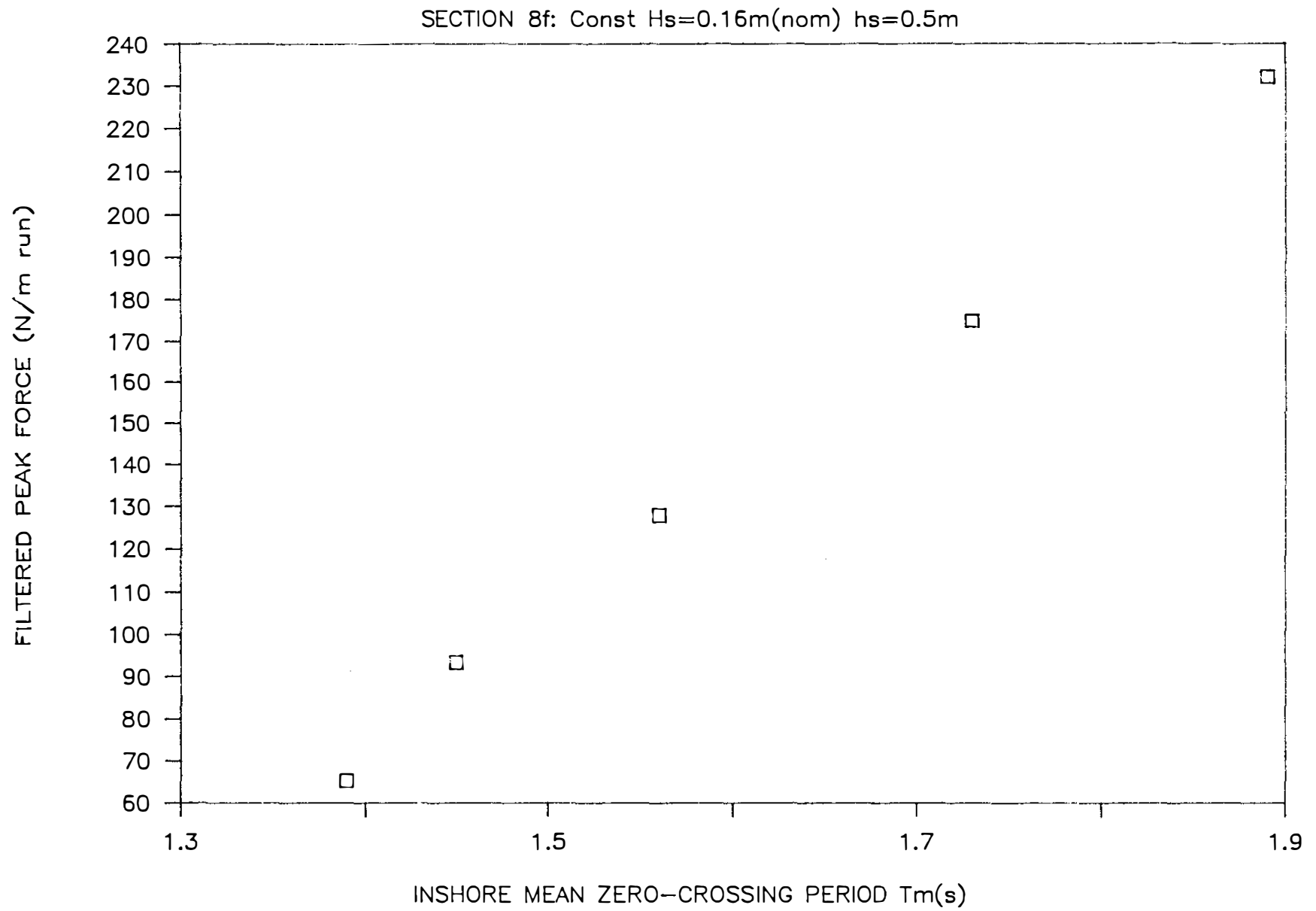


Fig 4.1 Influence of T_m on impact ratio - constant H_s

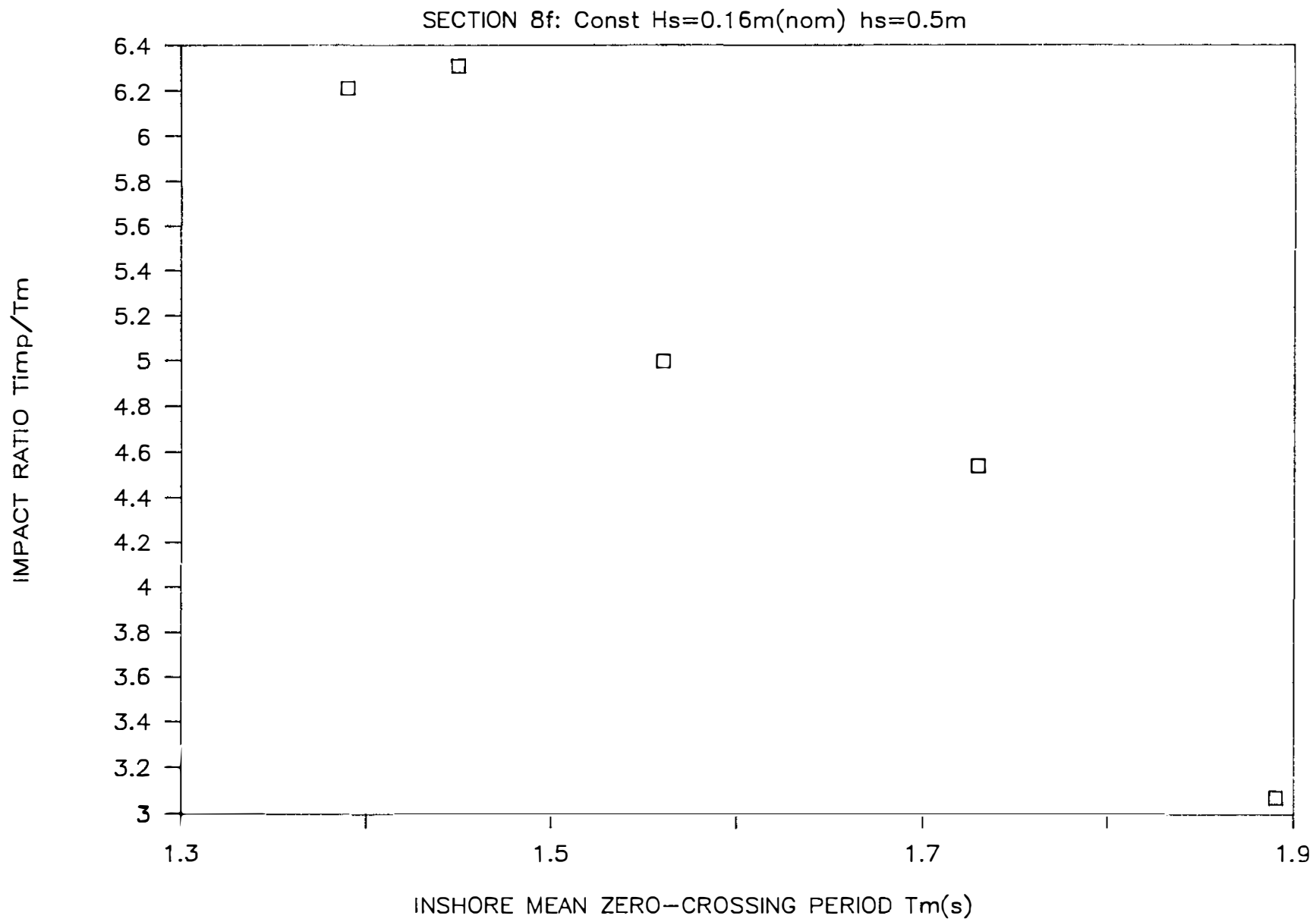


Fig 42 Influence of H_s on filtered maximum force - constant T_m

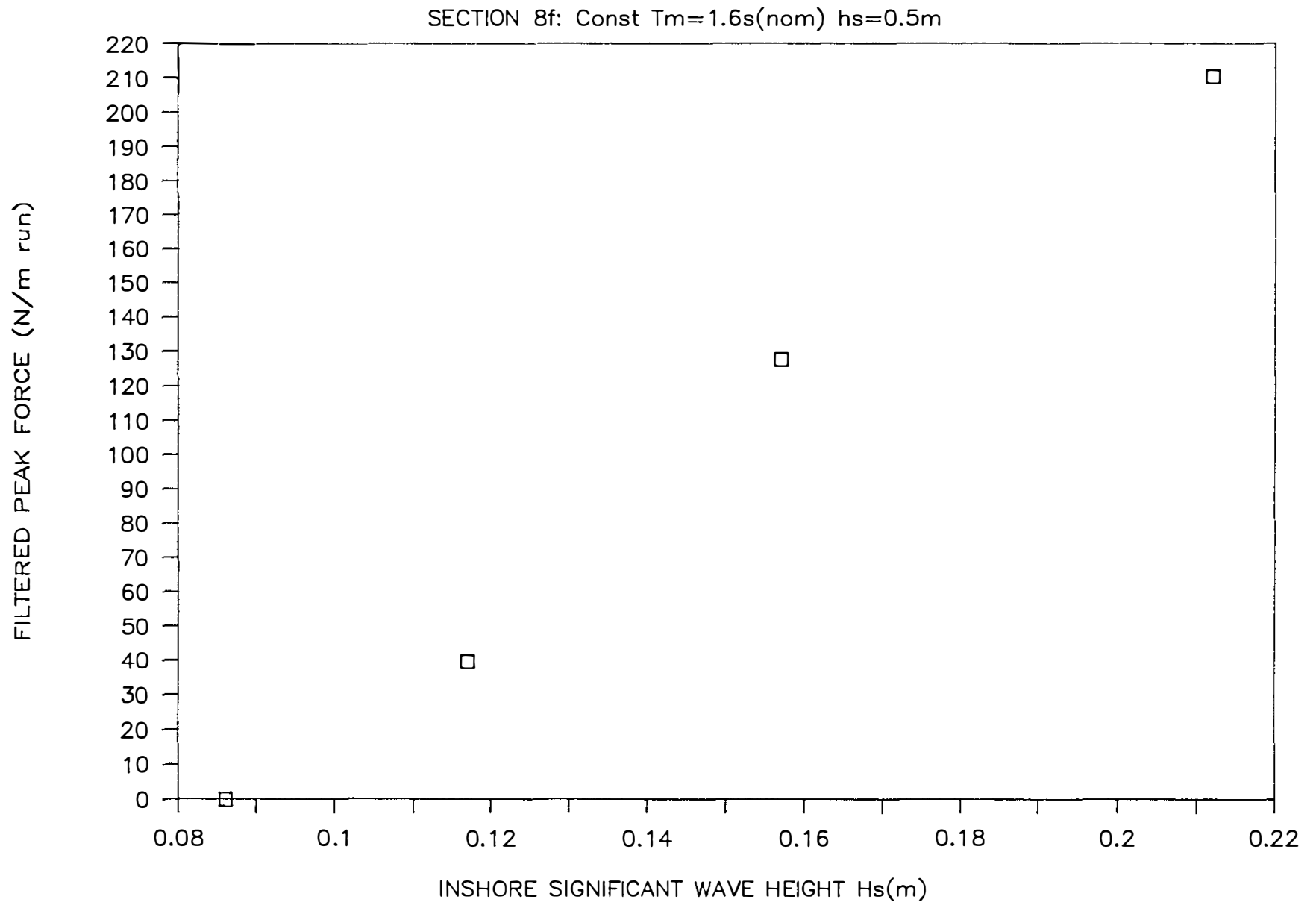


Fig 43 Influence of H_s on impact ratio - constant T_m

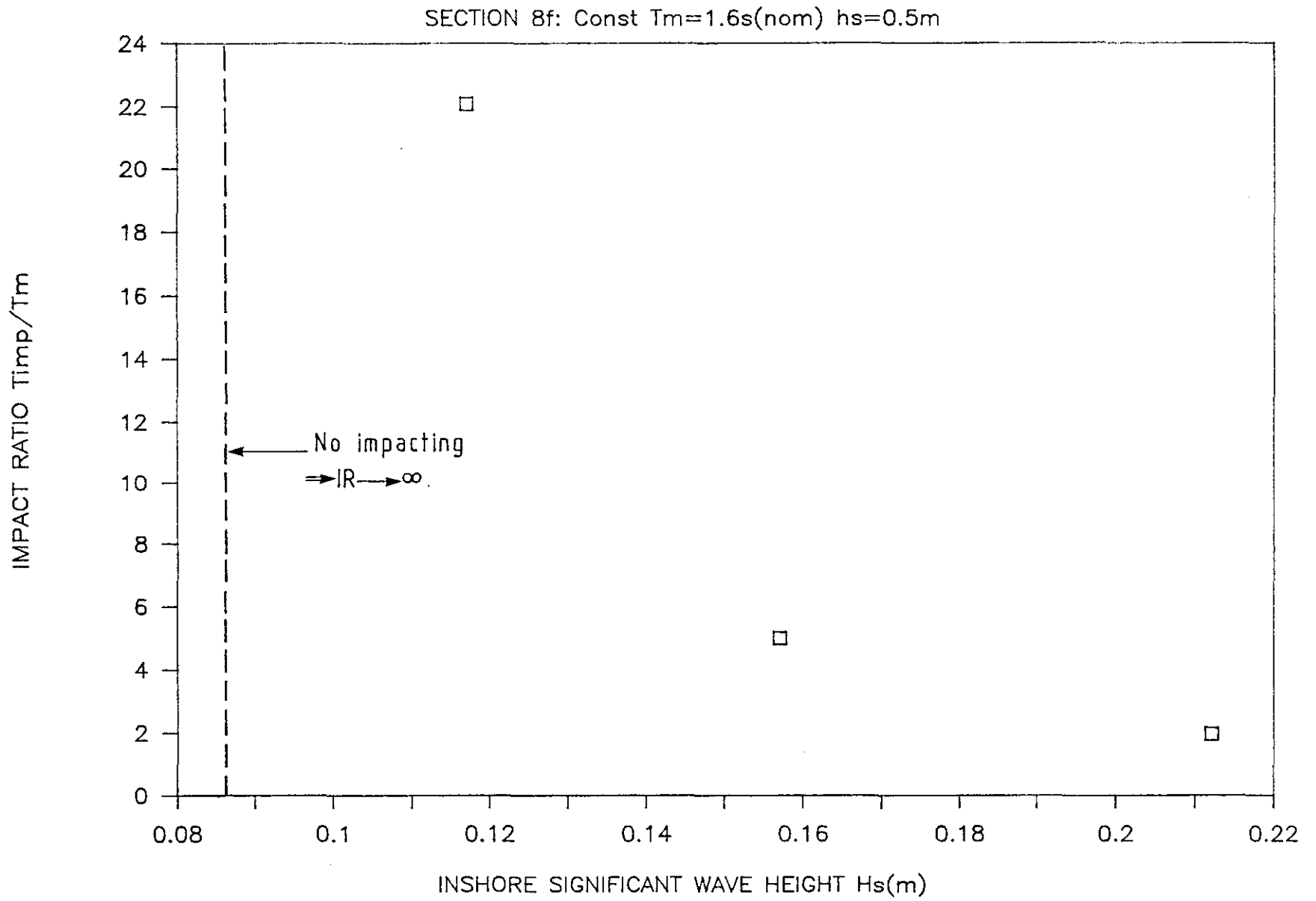
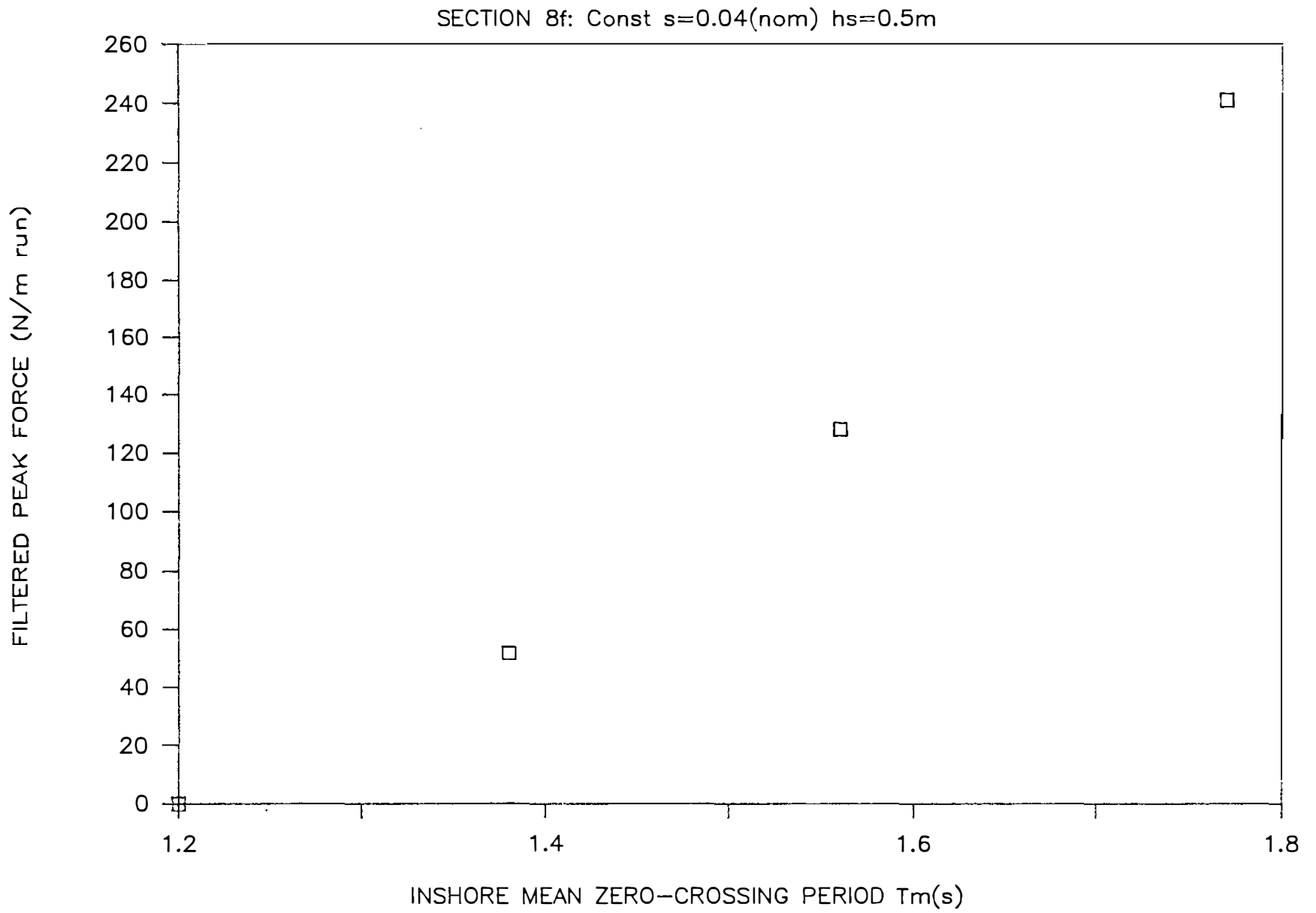


Fig 44 Influence of T_m on filtered maximum force - constant s



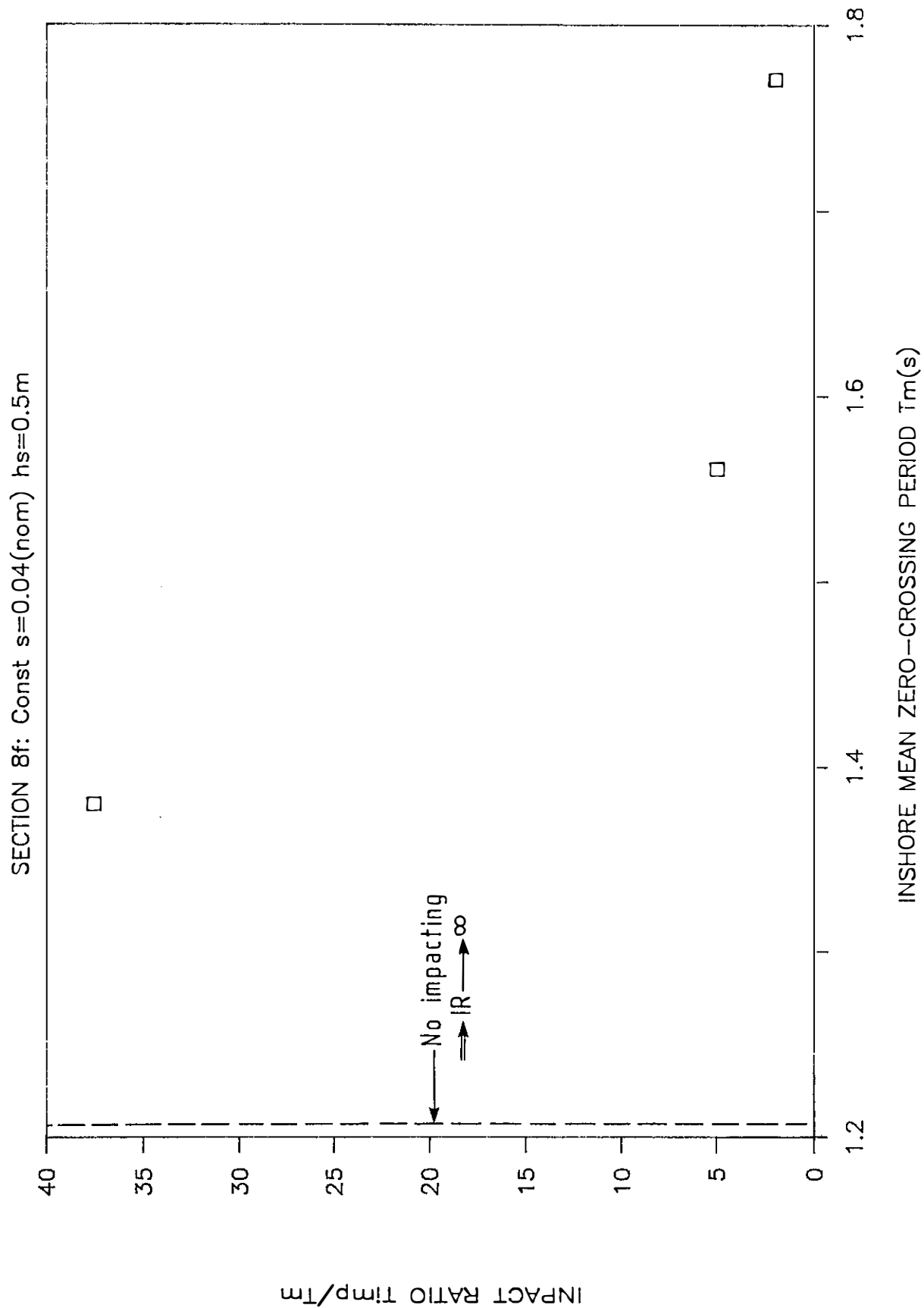


Fig 45 Influence of T_m on impact ratio - constant s

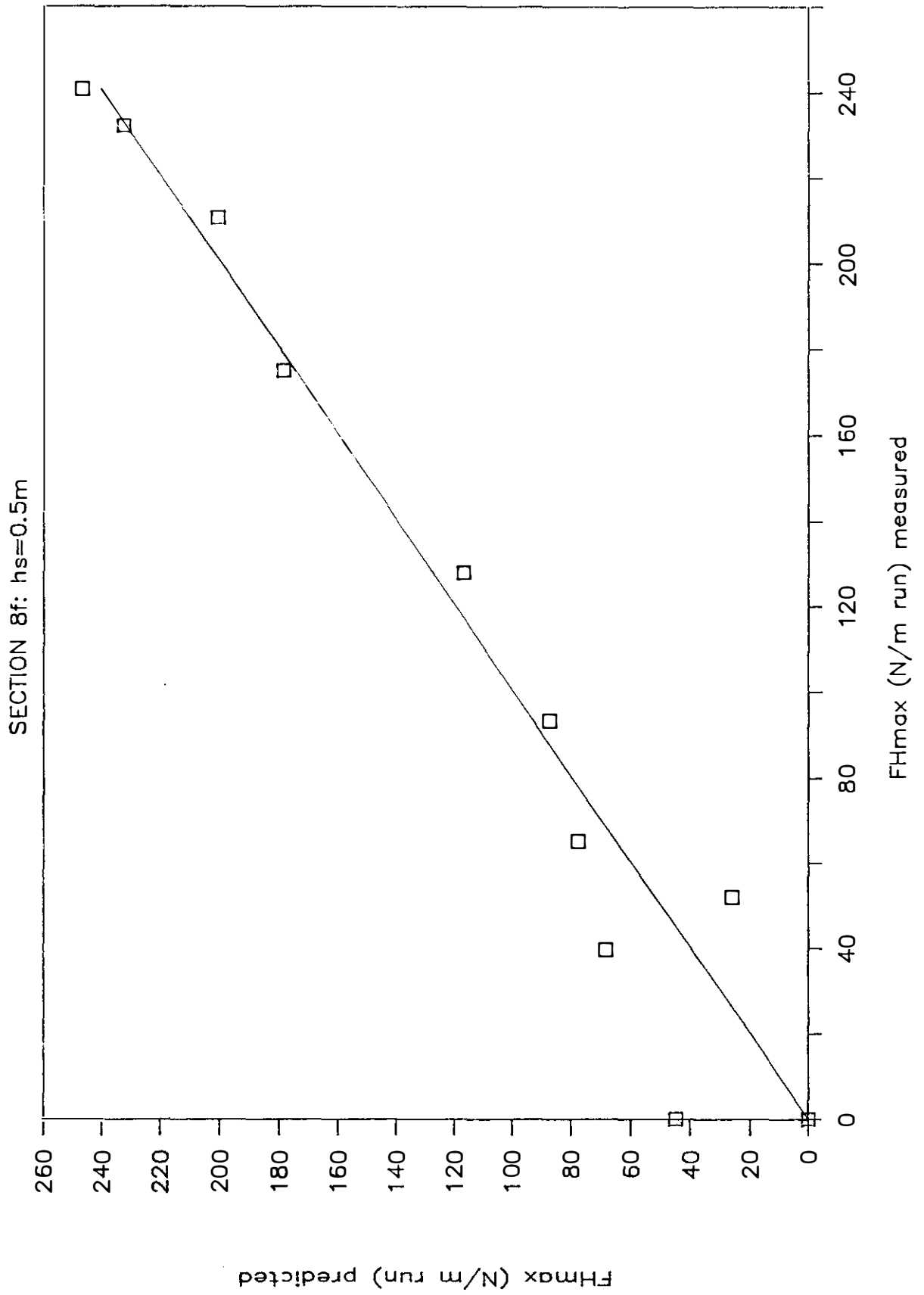


Fig 46 Comparison between measured forces and those predicted

SECTION 8f: $h_s=0.5m$ $A_c=0.1m$ $h_f=0.11m$

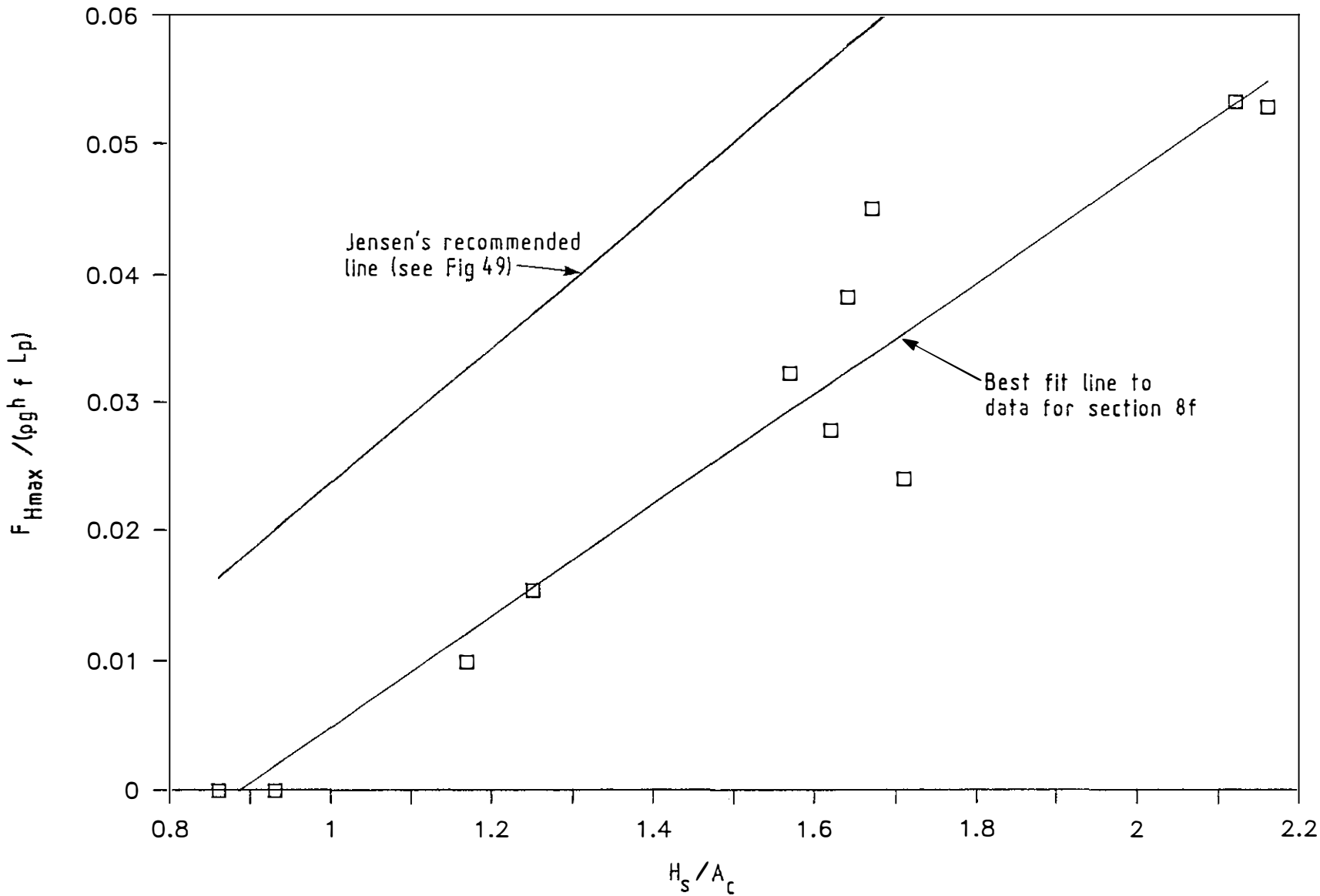


Fig 47 Measured forces presented in the form proposed by Jensen

SECTION 8f: $h_s=0.5m$ $A_c=0.1m$ $h_f=0.11m$

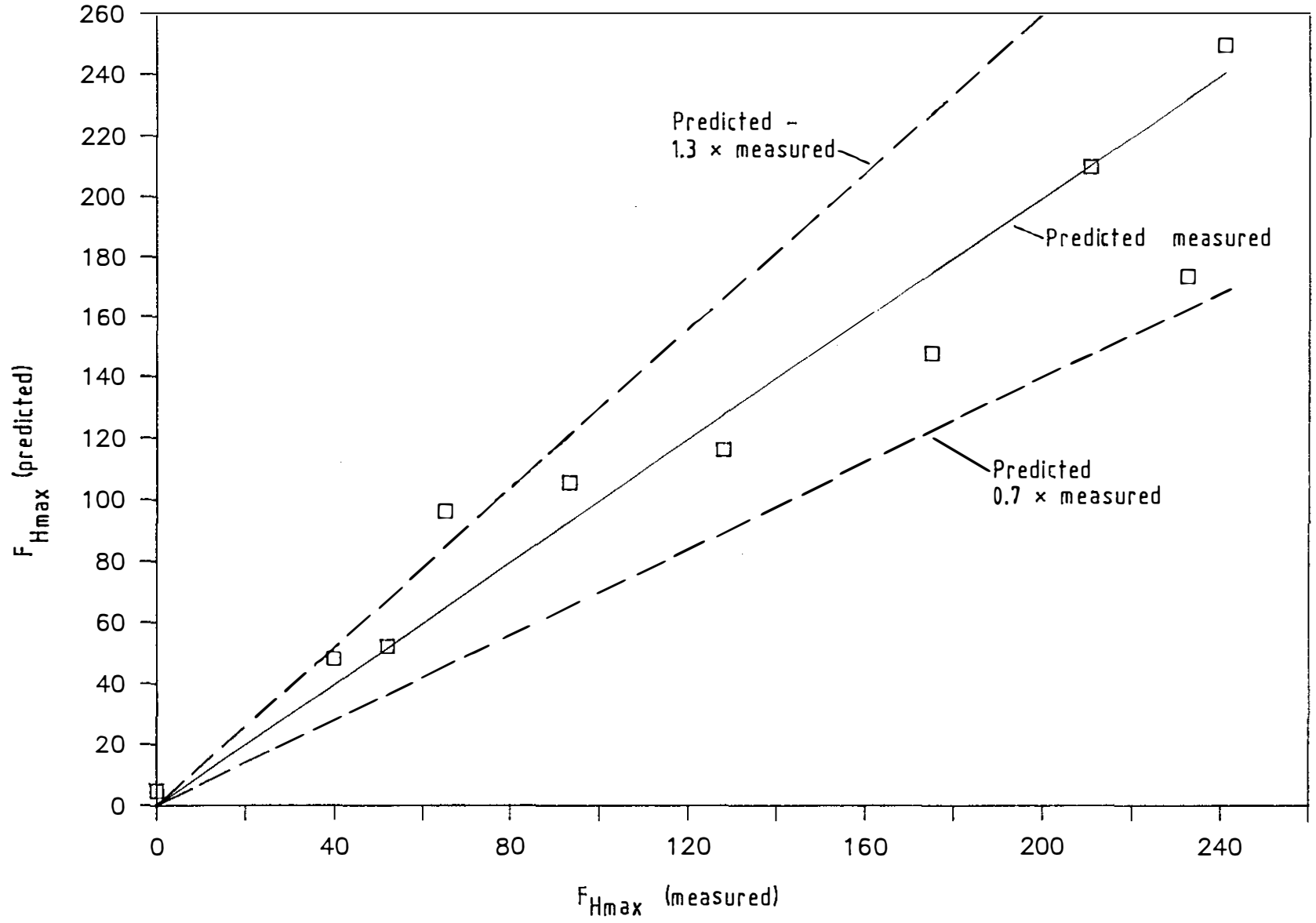
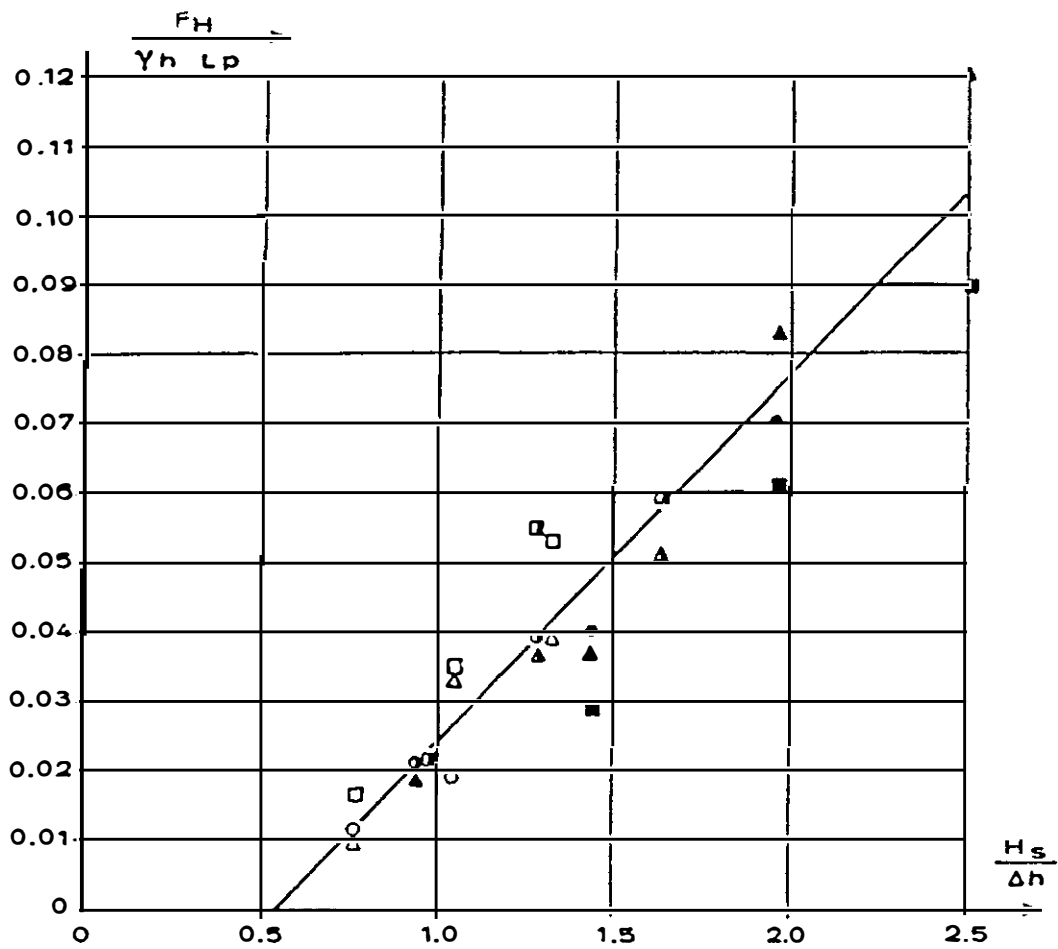


Fig 48 Comparison between measured forces and predicted forces using Jensen's best fit line



LEGEND:

WATER LEVEL (m)	PEAK WAVE PERIOD T_p (s)		
	14	16	18
+ 5.3	●	▲	■
+ 2.3	○	△	□
+ 0.3	○	△	□

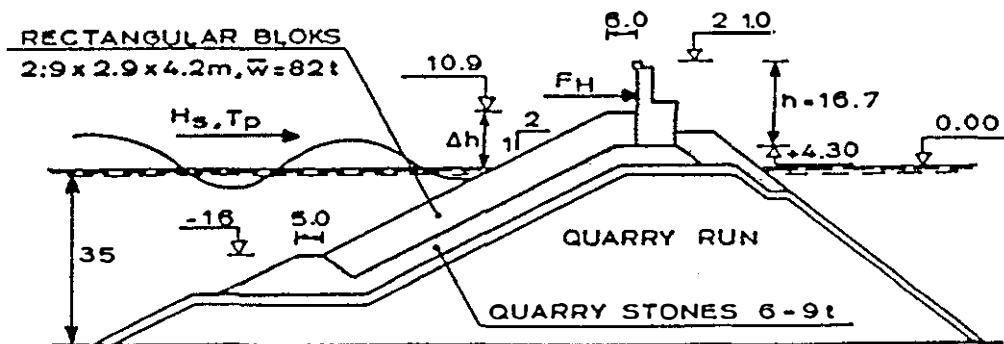


Fig 49 Force data presented by Jensen (Ref 28)

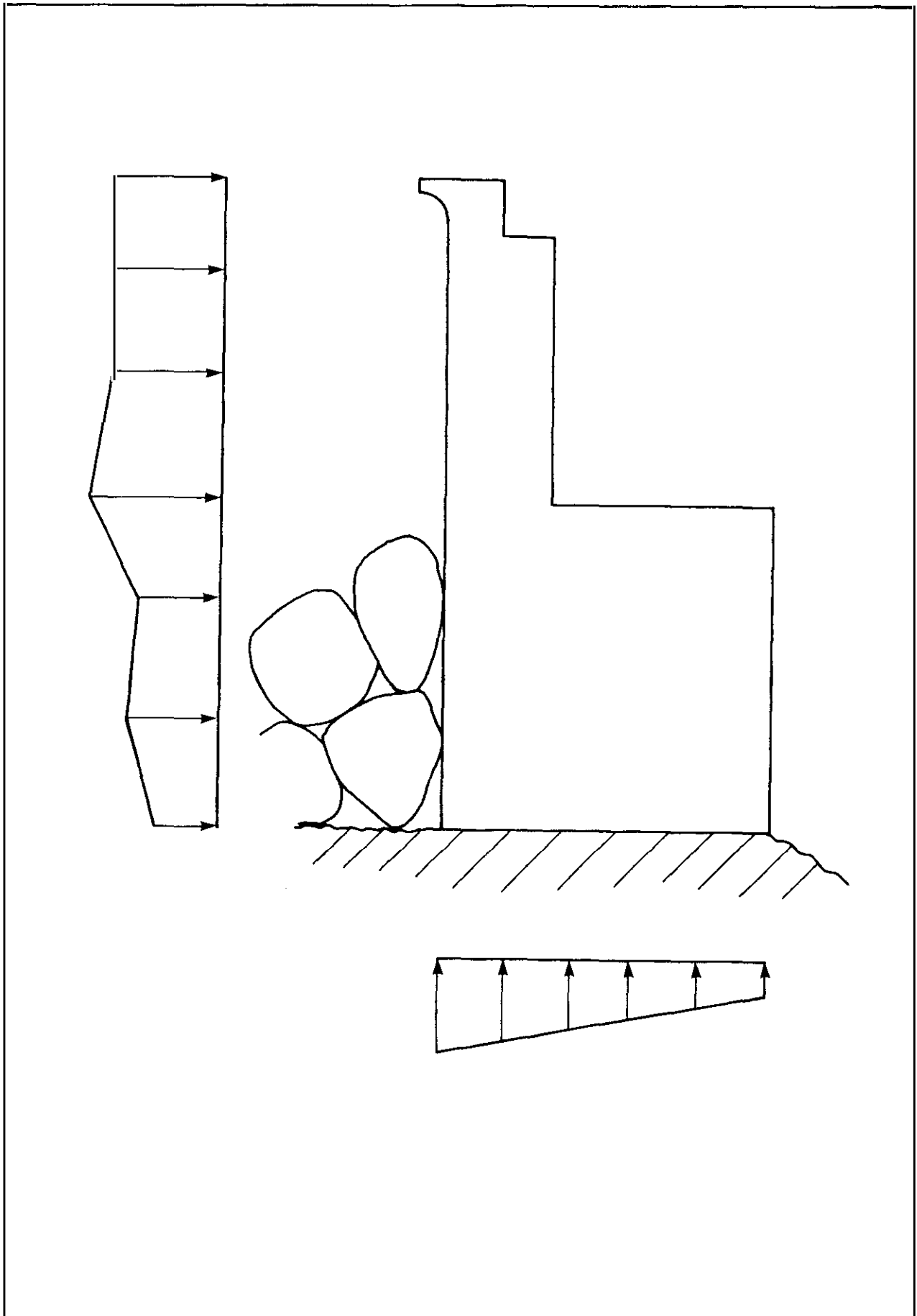


Fig 50 Spatial distribution of maximum wave pressure on Crownwall - after Jensen

PLATE.

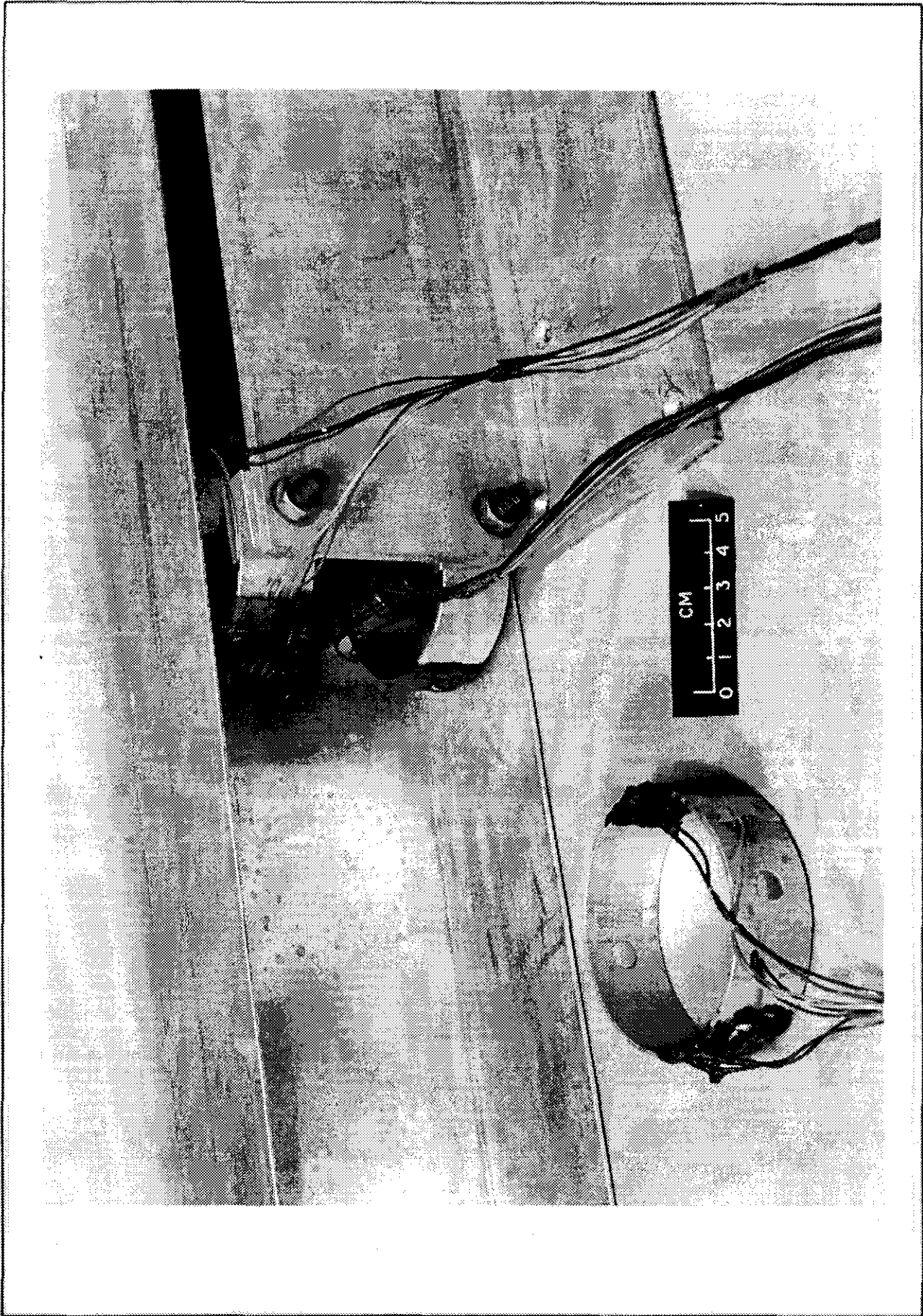


Plate 1 Force table showing proof ring details.

APPENDIX.

APPENDIX A

Analysis of crown wall force data

A least squares regression analysis was applied to the results for section 8f to approximate the measured maximum wave forces by the equation:

$$F_{Hmax} = A H_s + B T_m + C \quad (A1)$$

Where A, B and C are dimensional constants. The forces predicted from the derived relationship are plotted against the respective measured forces in Figure 46. Clearly, the relationship fits well, especially for the larger forces. The mean magnitude of discrepancy between measured and predicted forces for section 8f was 11.5N/m run. For section 8f at water depth $h_s = 0.5m$, the derived coefficients for equation A1 are:

$$A = 1061 \text{ N/m}^2$$

$$B = 318 \text{ N/s/m}$$

$$C = -546 \text{ N/m}$$

It should be noted that the characteristic linear relationships between force, F_m , and wave height, H_s , and between F_m and wave period, T_m , shown in Figures 40 and 42 are only valid at model scale. The linearity will become distorted when the data is scaled to prototype terms.

It has not been possible to derive a satisfactory dimensionless relationship from the data. However, the model results could be applied to a prototype problem of similar geometric configuration using Froude model scaling laws. Hence, if d_p is a characteristic prototype dimension such as crown wall height or water depth, and d_m is the corresponding dimension from test section 8f, then we can define $\lambda = d_p/d_m$.

The prototype maximum horizontal force in Newtons per metre run may then be estimated from:

$$F_{Hmax} (\text{Prototype}) = \lambda A H_s + \lambda^{1.5} B T_m + \lambda^2 C \quad (A2)$$

Where H_s and T_m are prototype wave parameters and A, B and C are the coefficient values tabulated above. Where predicted forces are less than zero, incident waves would not be expected to reach the crown wall. The above procedure may tentatively be extrapolated to other armour slope configurations for which force measurements were made, by multiplying the resulting

force from equation A2 by the appropriate value of armour coefficient $F_{H_{max}}/F_{H_{max} 8f}$ from Table 4. It should be borne in mind that these factors are each only strictly valid for a single random wave condition.

Further work is required to substantiate the formulae proposed above and to examine fully their range of validity. At present, only a single water depth has been investigated. For satisfactory use of the proposed formula, it is necessary to include a term for structural freeboard, and also to define more rigorously the scale factor λ in equation A2. This has not been possible within the scope of the present study.